NASA/TM-2008-214637

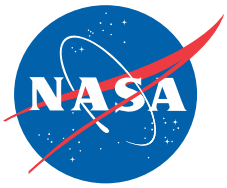

Tests and Techniques for Characterizing and Modeling X-43A Electromechanical Actuators

Yohan Lin and Ethan Baumann
NASA Dryden Flight Research Center
Edwards, California

David M. Bose and Roger Beck
Analytical Mechanics Associates
Hampton, Virginia

Gavin Jenney
Dynamic Controls, Inc.
Dayton, Ohio

December 2008

NASA STI Program ... in Profile

Since its founding, NASA has been dedicated to the advancement of aeronautics and space science. The NASA scientific and technical information (STI) program plays a key part in helping NASA maintain this important role.

The NASA STI program is operated under the auspices of the Agency Chief Information Officer. It collects, organizes, provides for archiving, and disseminates NASA's STI. The NASA STI program provides access to the NASA Aeronautics and Space Database and its public interface, the NASA Technical Report Server, thus providing one of the largest collections of aeronautical and space science STI in the world. Results are published in both non-NASA channels and by NASA in the NASA STI Report Series, which includes the following report types:

- TECHNICAL PUBLICATION. Reports of completed research or a major significant phase of research that present the results of NASA programs and include extensive data or theoretical analysis. Includes compilations of significant scientific and technical data and information deemed to be of continuing reference value. NASA counterpart of peer-reviewed formal professional papers but has less stringent limitations on manuscript length and extent of graphic presentations.

- TECHNICAL MEMORANDUM. Scientific and technical findings that are preliminary or of specialized interest, e.g., quick release reports, working papers, and bibliographies that contain minimal annotation. Does not contain extensive analysis.

- CONTRACTOR REPORT. Scientific and technical findings by NASA-sponsored contractors and grantees.

- CONFERENCE PUBLICATION. Collected papers from scientific and technical conferences, symposia, seminars, or other meetings sponsored or cosponsored by NASA.

- SPECIAL PUBLICATION. Scientific, technical, or historical information from NASA programs, projects, and missions, often concerned with subjects having substantial public interest.

- TECHNICAL TRANSLATION. English-language translations of foreign scientific and technical material pertinent to NASA's mission.

Specialized services also include creating custom thesauri, building customized databases, and organizing and publishing research results.

For more information about the NASA STI program, see the following:

- Access the NASA STI program home page at *http://www.sti.nasa.gov*

- E-mail your question via the Internet to help@sti.nasa.gov

- Fax your question to the NASA STI Help Desk at (301) 621-0134

- Phone the NASA STI Help Desk at (301) 621-0390

- Write to:
  NASA STI Help Desk
  NASA Center for AeroSpace Information
  7115 Standard Drive
  Hanover, MD 21076-1320

NASA/TM-2008-214637

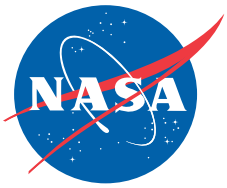

Tests and Techniques for Characterizing and Modeling X-43A Electromechanical Actuators

Yohan Lin and Ethan Baumann
NASA Dryden Flight Research Center
Edwards, California

David M. Bose and Roger Beck
Analytical Mechanics Associates
Hampton, Virginia

Gavin Jenney
Dynamic Controls, Inc.
Dayton, Ohio

National Aeronautics and
Space Administration

Dryden Flight Research Center
Edwards, California 93523-0273

December 2008

ACKNOWLEDGEMENTS

The authors would like to offer their gratitude to the following people for their contributions to the X-43A actuation test program: Brian Strovers (Analytical Mechanics Associates); William Talley, Bruce Raymond (Dynamic Controls, Inc); Fred Lallman (NASA LaRC); Charlie Nichols (Dyncorp); Randy Wagner, John Kelly, Matt Redifer, Jeanette Le, Mark Stephenson, Carrie Rhoades, Tom Horn, Mark Nunnelee (NASA DFRC); Paul Lundstrom (Spiral Technology Inc); Steve Thomas, Art Younger (Analytical Services & Materials); Mike Mashburn (ATK GASL); Tom Cimato (Moog, Inc.); Gary Sjoberg (KADAN, Inc.). Special acknowledgement and thanks to everyone at Dynamic Controls, Inc., for more than 35 years of dedicated service to the advancement of actuation technology. Additional thanks to the NASA DFRC engineers and technicians at the Flight Loads Laboratory for their support during the compliance and hysteretic damping tests.

NOTICE

Use of trade names or names of manufacturers in this document does not constitute an official endorsement of such products or manufacturers, either expressed or implied, by the National Aeronautics and Space Administration.

Available from:

NASA Center for AeroSpace Information
7115 Standard Drive
Hanover, MD 21076-1320
(301) 621-0390

CONTENTS

ABSTRACT

A series of tests were conducted on the electromechanical actuators of the X-43A research vehicle in preparation for the Mach 7 and 10 hypersonic flights. The tests were required to help validate the actuator models in the simulation and acquire a better understanding of the installed system characteristics. Static and dynamic threshold, multichannel crosstalk, command-to-surface timing, free play, voltage regeneration, calibration, frequency response, compliance, hysteretic damping, and aircraft-in-the-loop tests were performed as part of this effort. This report describes the objectives, configurations, and methods for those tests, as well as the techniques used for developing second-order actuator models from the test results. When the first flight attempt failed because of actuator problems with the launch vehicle, further analysis and model enhancements were performed as part of the return-to-flight activities. High-fidelity models are described, along with the modifications that were required to match measurements taken from the research vehicle. Problems involving the implementation of these models into the X-43A simulation are also discussed. This report emphasizes lessons learned from the actuator testing, simulation modeling, and integration efforts for the X-43A hypersonic research vehicle.

NOMENCLATURE

A	area of hysteresis loop, in•lb
AIL	aircraft-in-the-loop
ATP	acceptance test program
C	hysteretic damping coefficient
DAU	data acquisition unit
deg	degree
DFRC	Dryden Flight Research Center
EMA	electromechanical actuator
EMAC	electromechanical actuator controller
EMF	electromagnetic field
F	load, lb
FAS	fin actuation system
FMU	flight management unit
FORTRAN	formula translation
FS	full scale
Gr	gear ratio
h	hysteretic damping constant, lb/in.
h_m	hinge moment
HOAC	high-order actuator continuous
HOAD	high-order actuator discrete

HOALM	high-order actuator linear model
HXLV	Hyper-X Launch Vehicle
HXRV	Hyper-X Research Vehicle
IS	surface inertia, in•lb•s^2
K	gear train stiffness, lb/in.
Kb	slope of calibration error equation, deg/deg
Kbs	backup structure stiffness, lb/in.
K_{CE}	command error gain, 1 + Kb
K_{CP}	compliance correction gain
Kf	gain, $(\omega_n)^2$, 1/s^2
K_{HM}	hinge moment gain, deg/in•lb•s^2
$K2$	slope of rate curve with respect to load, deg/(s•lb)
LOAC	low-order actuator continuous
LOADA	low-order actuator discrete auto-code
LOADF	low-order actuator discrete FORTRAN
LOES	low-order equivalent system
LVDT	linear variable differential transformer
marm	moment arm
O-scope	oscilloscope
PID	parameter identification
P_K	peak amplitude of deflection, in.
PWM	pulse width modulation
rl	unloaded rate limit
scramjet	supersonic combustion ramjet
SLOAC	simplified low-order actuator continuous
$V_{p\text{-}p}$	volt peak to peak
X	actuator position, in.
$1/s$	Laplace integrator
6-DOF	six-degree-of-freedom
ΔV	difference in velocity, ft/s
$\Delta\theta$	difference in angle (roll, pitch, yaw), deg
ζ	damping ratio
Ω	electrical resistance (ohm)
ω	frequency, rad/s or 1/s
ω_n	natural frequency, rad/s or 1/s

1.0 INTRODUCTION

Actuators that are installed on aerospace vehicles typically exhibit performance and operating characteristics that differ from uninstalled units. Such differences can be attributed to signal command quantization, calibration errors, system free play, linkage compliance (elastic deformation), hysteretic damping, and time delay effects. Using actuator models derived from the uninstalled configuration in a simulation may provide inaccurate or misleading results. For example, a vehicle with marginal control system design in conjunction with inaccurate actuator models may yield simulation results with high stability margins, when in reality the design may not be adequate to fulfill mission requirements. With higher fidelity models, the results may show that the vehicle is unstable, indicating that the control system should be improved or redesigned to increase its robustness.

1.1 Purpose and Scope of Report

This report identifies the tests required to adequately characterize and model an installed electromechanical actuation system, using experience and knowledge acquired from the hypersonic X-43A project. It also describes how the test data were used for constructing accurate linear and nonlinear simulation models and how they were used for mission analyses. Problems involving model implementation into source code and their integration into the X-43A simulation are also discussed.

The tests that were conducted on the X-43A electromechanical actuators (EMAs) include static and dynamic threshold; multichannel crosstalk; command-to-surface timing; free play; voltage regeneration; surface calibration; step, frequency, Schroeder, and ramp response; compliance; hysteretic damping; and aircraft-in-the-loop (AIL) tests. These tests were designed to measure the performance and characteristics of the system as installed on the vehicle.

Methods of constructing second-order models are found in section 3.1. Nonlinear elements such as command errors, free play, and compliance are included in the buildup of the models. Following this topic is a discussion on the X-43A EMA high-fidelity model and how it was modified to reflect the true compliance and hysteretic damping of the onboard system.

This report also provides a brief description of the NASA six-degree of freedom (6-DOF) nonlinear simulation and the different types of EMA models that were used for the mission analyses. The second-order and high-order models were implemented in the continuous and discrete domains using a number of techniques to further refine their fidelity and make them useable in the 6-DOF simulation. The techniques are explained in detail, along with problems that were encountered when the models were integrated into the simulation.

The model frequency response and command response performance are compared with flight data in subsequent sections. Lessons learned from the modeling and simulation efforts are also presented. A summary of the testing, modeling, and simulation work conducted on the X-43A EMA system concludes this report.

1.2 Applicability

The tests and techniques presented can be applied to any vehicle or system that uses EMAs. In addition, vehicles that are modified for use outside their traditional operational envelope should include a thorough analysis of actuator models to ensure that the modified control system is robust enough to manage the uncertainty associated with the new application. Accurate predictions acquired from better actuator models could potentially improve the mission success of a program. Most of the tests and techniques described can be modified and applied to hydraulic actuation systems, with the exception of crosstalk and regenerative voltage tests.

1.3 Project Overview

The Hyper-X program was developed to research and advance the field of hypersonics and bring it into the flight test arena (ref. 1). The X-43A project was part of the Hyper-X program. Its primary objective was to demonstrate the operation of an airframe integrated scramjet engine at Mach 7 and 10 flight conditions. Figure 1 shows the X-43A Hyper-X Research Vehicle (HXRV, Alliant Techsystems, Inc., Tullahoma Tennessee). In this report, the terms “X-43A” and “HXRV” are used interchangeably.

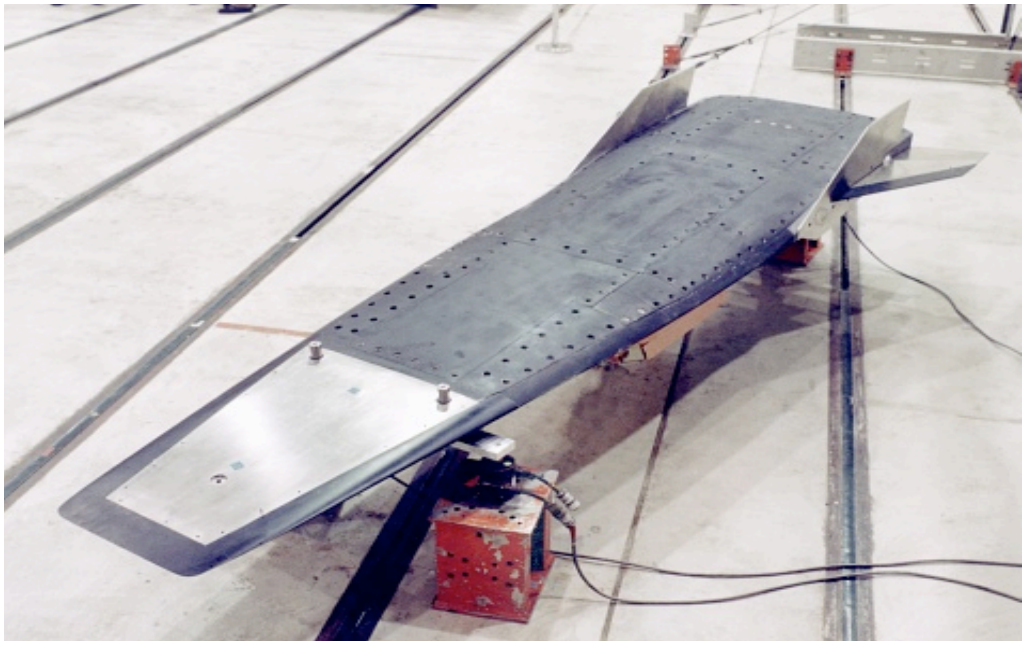

EC 99-45265-22

Figure 1. Hyper-X Research Vehicle.

The HXRV was attached to the Hyper-X Adapter and Hyper-X Launch Vehicle (HXLV, Orbital Sciences Corporation, Chandler, Arizona) in a stack configuration (fig. 2). The stack was carried by the NASA B-52B aircraft (The Boeing Company, Chicago, Illinois) to a launch site west of Point Mugu Naval Warfare Center, California. Upon launch the stack was boosted to an altitude of 94,000 ft (109,000 ft for Mach 10). After target flight conditions were achieved, ejection

pistons were used to separate the HXRV from the adapter and booster stack, allowing the vehicle to perform its free-flight mission. The engine cowl door opened and the scramjet experiment was conducted for approximately 10 s, using gaseous hydrogen as the fuel, silane as the ignitor, and air as the oxidizer. Following the experiment, the vehicle performed a set of parameter identification (PID) maneuvers, which were used to estimate aerodynamic performance including stability and control derivatives. Once these secondary objectives had been accomplished, the vehicle continued to fly autonomously along a preplanned trajectory until it impacted the Pacific Ocean.

Figure 2. The X-43A stack carried by the B-52B aircraft.

The HXRV was originally designed by NASA Langley Research Center (Hampton, Virginia) and Boeing Phantom Works. The concept vehicle was 202 ft long but was scaled down to approximately 12 ft to minimize project costs. Figure A1 in Appendix A shows the dimensions of the HXRV. The airframe and subsystems were manufactured by Alliant Techsystems-General Applied Scientific Laboratory (ATK-GASL) in Tullahoma, Tennessee. The engine and fuel systems were designed and built by ATK-GASL in Ronkonkoma, New York. Boeing North American (Huntington Beach, California) was responsible for the aerodynamics, systems, and structural design, as well as flight software development. A total of three HXRVs were built. Each vehicle weighed approximately 2800 lb. Before the first flight, the actuator threshold, crosstalk, timing, free play, voltage regeneration, calibration, frequency response, and AIL tests were performed on the HXRV so that the EMA system could be characterized and modeled for mission simulation and analysis. These tests were part of the standard verification and validation requirements for each research vehicle.

The HXLV was derived from the Pegasus® launch vehicle (Orbital Sciences Corporation, Chandler, Arizona), which is a commercial platform that is air launched from a carrier aircraft to deliver a payload into orbit. For control, the HXLV had a fin actuation system (FAS), which consisted of one rudder and two elevon fins that were actuated by three EMAs and a controller.

The project goal was to perform two flights at Mach 7 and one flight at Mach 10. On June 2, 2001, the first flight attempt at Mach 7 was unsuccessful and resulted in the loss of the Hyper-X stack. During the pitchup maneuver of the boost phase, approximately 11.5 s after launch, the HXLV started to experience diverging roll oscillations. Approximately 1.5 s later, the HXLV rudder EMA stalled, causing the vehicle to sideslip approximately 8°. This divergence led to structural damage of the HXLV starboard elevon. The stack began to lose control and the flight eventually had to be terminated. The mishap investigation team concluded, "The HXLV failed because the vehicle control system design was deficient for the trajectory flown due to inaccurate analytical models which overestimated the system margins" (ref.2). The major contributors of the mishap included inaccurate modeling of the HXLV FAS, inaccurate aerodynamic models, inaccurate mass properties, and insufficient parametric uncertainty analyses. Individually these contributors might not have caused the loss of the stack, but their combined effects were significant enough to cause this unfortunate event.

After the mishap investigation concluded, a number of return-to-flight activities based on the findings were conducted. The HXLV FAS system was redesigned to provide approximately 50 percent more torque margin for each control surface, and compliance and hysteretic damping tests were added to provide better characterization data for use in the HXLV simulation. Other improvements were made, such as obtaining better wind tunnel data and increasing the fidelity of the FAS models. Although the HXRV system operation did not contribute to the mishap, the project felt that the compliance and hysteretic damping tests should be included as part of the standard suite of actuator tests for the remaining HXRV vehicles. These tests provided further verification of actuator performance, as well as data for HXRV actuator model enhancement.

The second flight at Mach 7 was successfully conducted on March 27, 2004 (fig. 3). The HXRV accelerated to a maximum Mach number of 6.83, and approximately 11 s of scramjet data were acquired. Primary and secondary mission objectives were achieved. On November 16, 2004, the third HXRV flew and reached cruise conditions at Mach 9.68 (fig. 4). Approximately 10 s of scramjet data were acquired.

Figure 3. The first free flight of a scramjet vehicle; aft view of Hyper-X Research Vehicle 2 separating from the adapter.

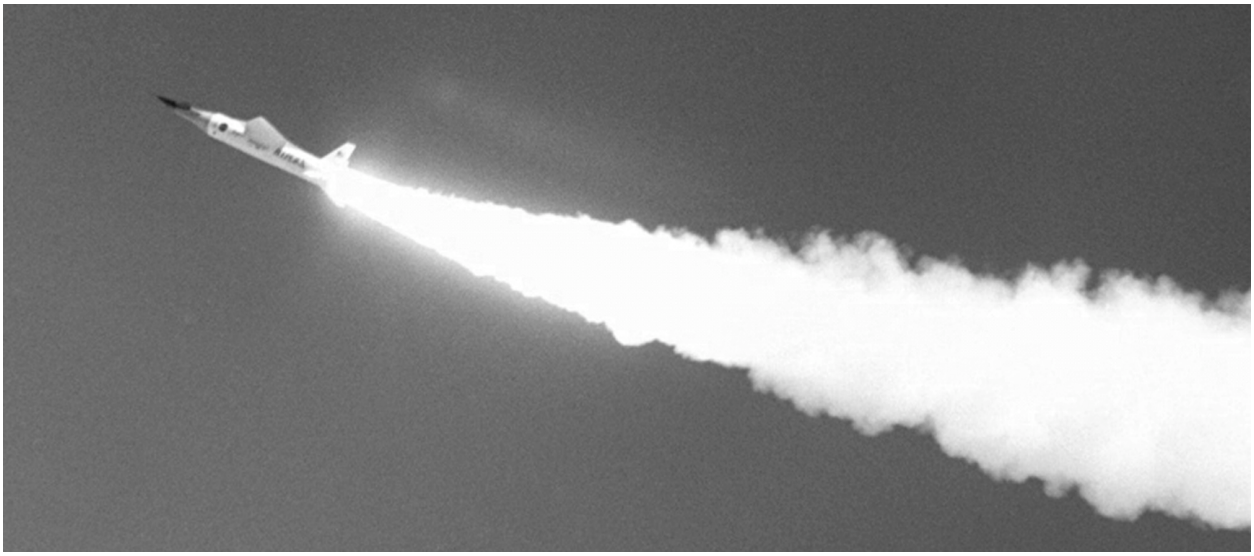

Image processed by Steve Parcel

(a) Stack during boost.

Figure 4. X-43A Mach 10 flight.

Image processed by Steve Parcel

(b) Separation.
Figure 4. Concluded.

1.4 Description of the X-43A Electromechanical Actuation System

The HXRV has a total of five EMAs. They are used to move two wings, two rudders, and one engine cowl door (figs. 5, 6). All actuators are identical with the exception of the cowl door EMA, which has a longer wire bundle, oblique tail stock, and modified housing to accommodate the volume constraints of the vehicle. Each EMA has a three-phase brushless direct current motor that provides 2500 lbf of load capability and requires 150 Vdc for operation. All actuators are controlled by the electromechanical actuator controller (EMAC) shown in figure 7. The EMAC electronics system requires 28 Vdc power for operation and has five actuator controller channels, one for each EMA. The EMAs and controllers were manufactured by Moog, Inc. (East Aurora, New York).

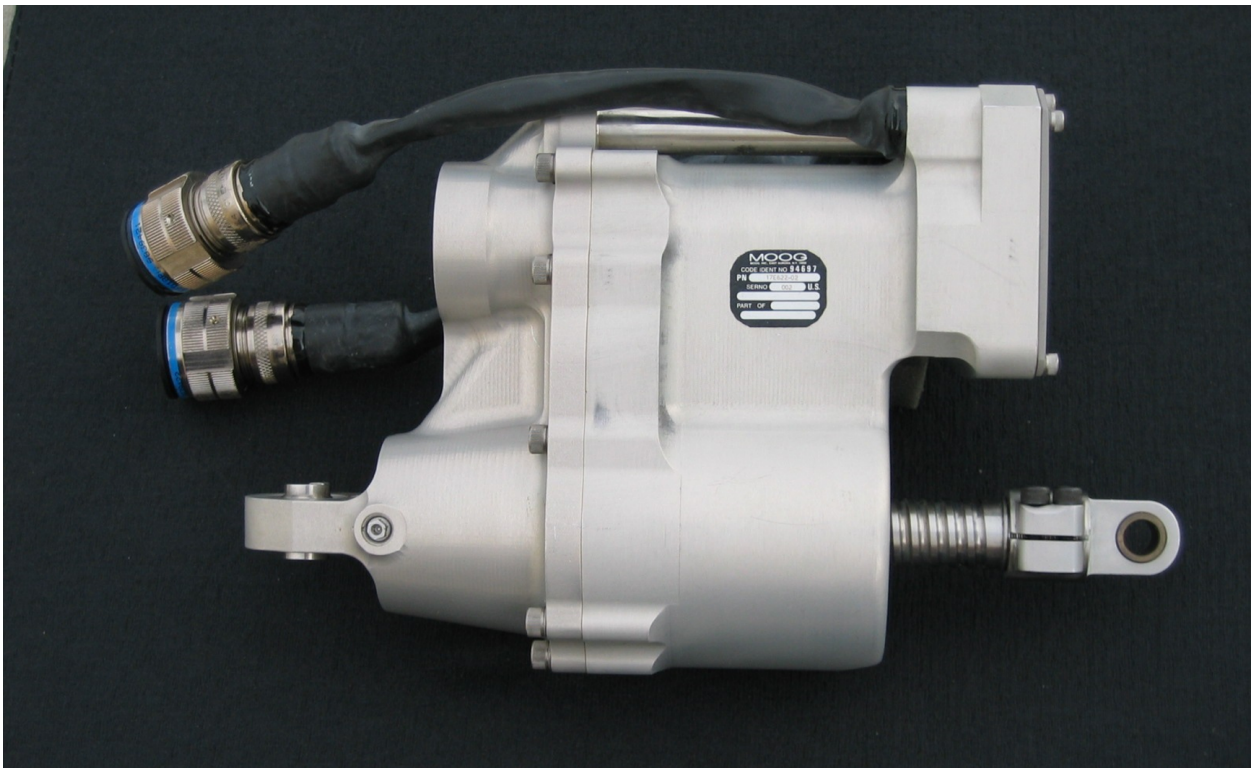

Photo courtesy of Yohan Lin

Figure 5. The X-43A electromechanical actuator.

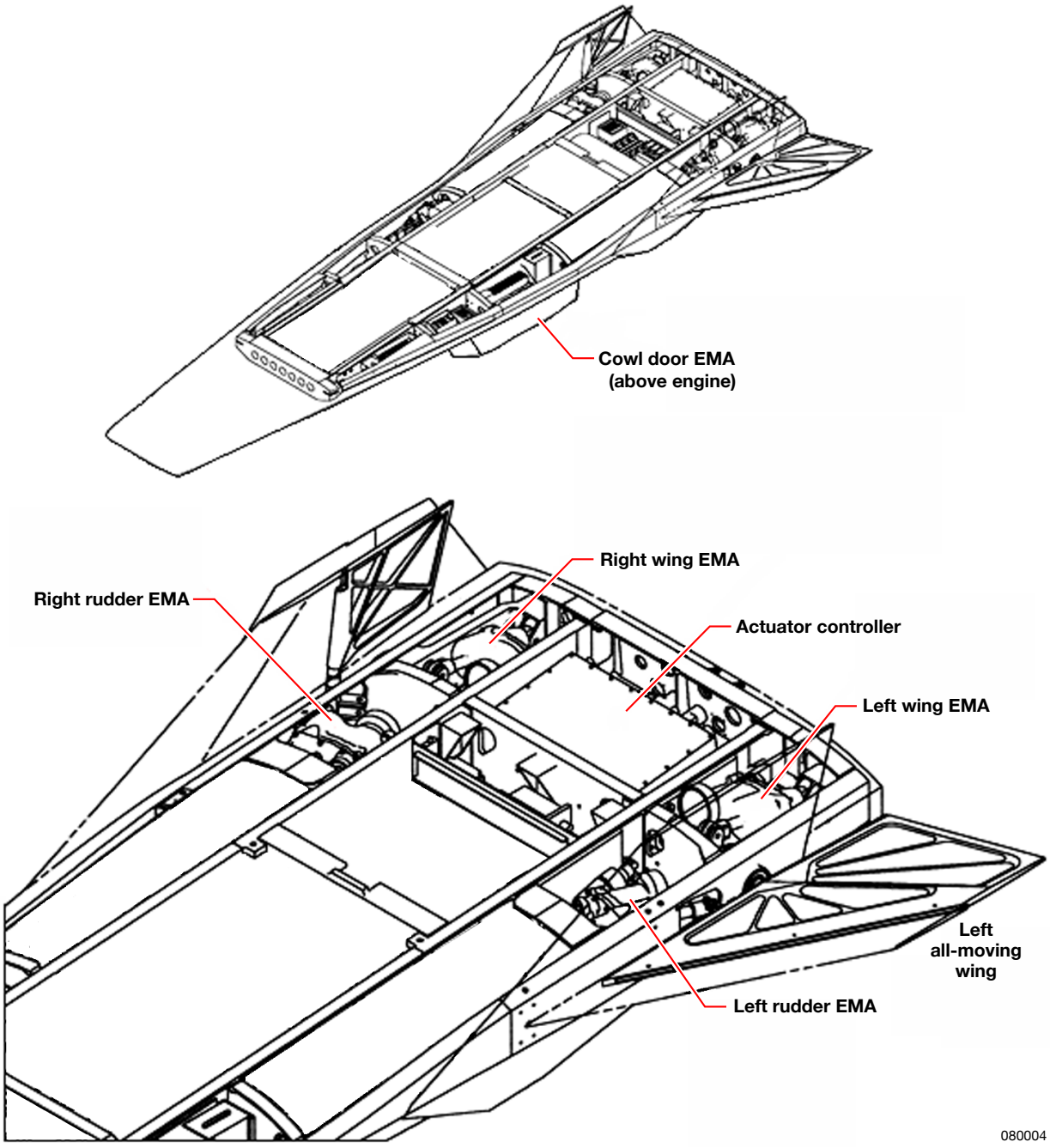

Figure 6. Actuator and controller locations on the Hyper-X Research Vehicle.

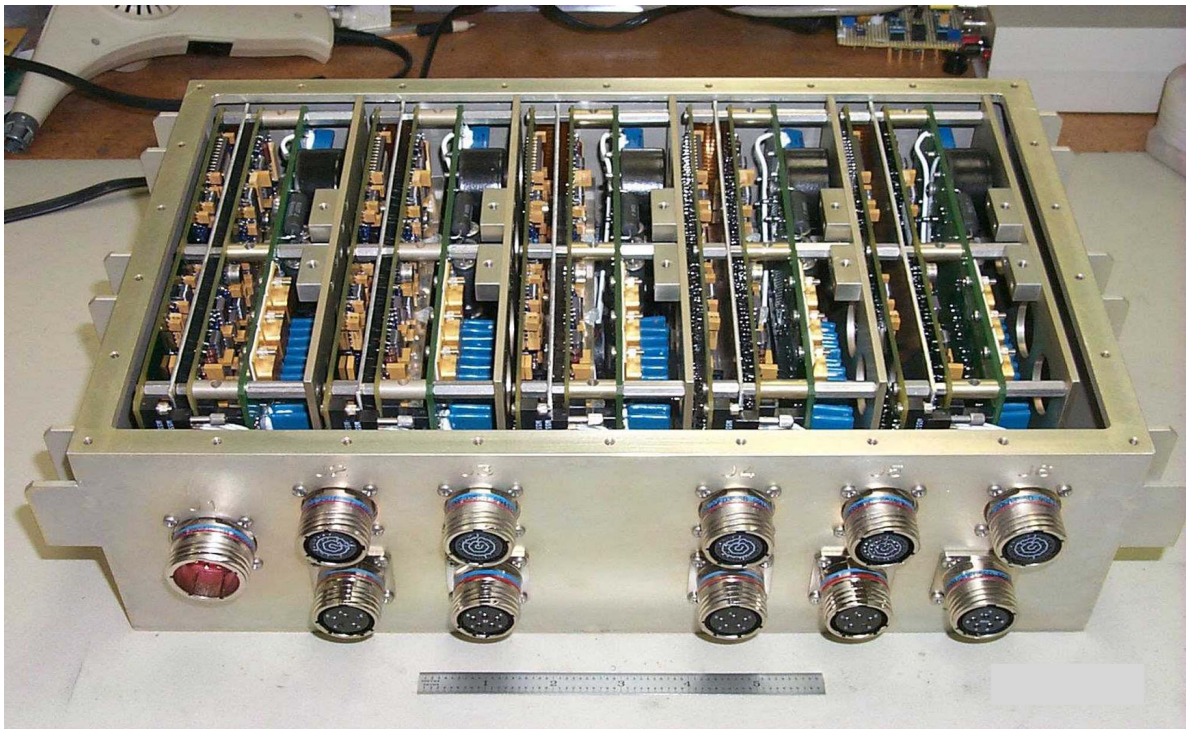

Photo courtesy of Charlie Nichols

Figure 7. Electromechanical actuator controller.

The HXRV flight control computer, known as the flight management unit (FMU), sends the actuator commands to the EMAC, which passes the signal to the EMA. As the actuator moves, an internal linear variable differential transformer (LVDT) measures the amount of distance the ball screw has traveled. A servo crank arm connected to the end of the ball screw converts linear motion into rotational motion (fig. 8). This motion causes the control surface spindle to start rotating. The LVDT position feedback signal is sent to the EMAC, where loop closure is performed. The error signal between command and position is used to drive the surface or cowl door to the desired position. Current and position feedback signals are reported to the FMU by the EMAC. All actuator command and feedback signals are scaled to the range of ±10 Vdc. Each actuator has a brake located in series with the motor and is normally engaged when the system is powered off. Table 1 shows the actuator specifications.

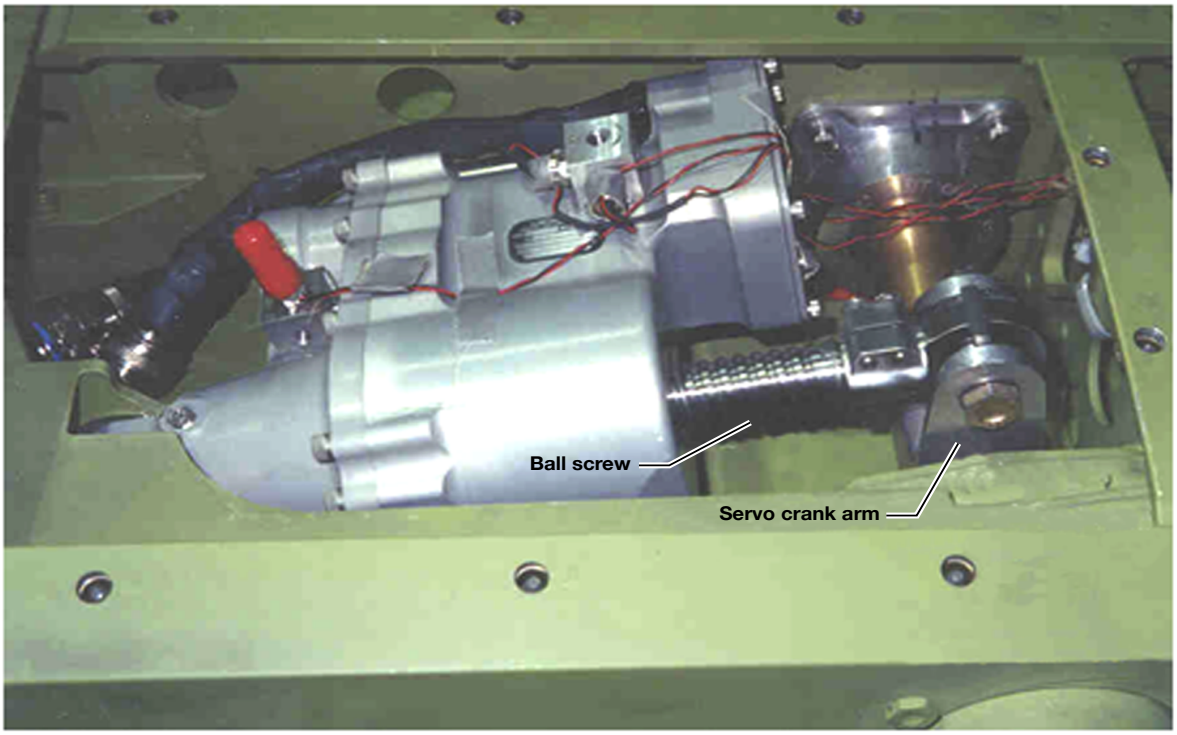

Figure 8. Left wing electromechanical actuator with servo crank arm.

A onetime qualification test was conducted to prove that the actuator design could meet the environmental requirements of the X-43A mission. After production began, each actuator underwent an acceptance test to verify that the as-built unit met project performance requirements. Tables A1 and A2 of Appendix A list specific requirements for the qualification and acceptance tests.

Table 1. Hyper-X Research Vehicle electromechanical actuator specifications.

Specification	Measurement
Load capability	2,500 lbf stall
Slew rate, unloaded	3.5 in/s or 115.8 deg/s
Bandwidth, unloaded	7.5 Hz minimum
Stroke	2.6 in.
Power requirements	28 Vdc control (minimum 20 Vdc) 150 Vdc motors (minimum 125 Vdc)
Backlash	0.005 in.
Stiffness	400,000 lb/in.
Motor type	Three-phase brushless direct current
Brake rating	> 4,000 lbf
Operating temperature	–40 to 160 °F
Weight	~ 8.5 lb

2.0 ELECTROMECHANICAL ACTUATOR TESTING

The following sections describe the characterization and performance tests that were conducted on the X-43A EMAs. All tests were unloaded except for the free play, compliance, and hysteretic damping tests. Most of the tests were conducted on the first HXRV before the mishap occurred. In preparation for the second and third flights, the compliance and hysteretic damping tests were conducted not only for the HXLV, but also for the HXRV. Table A3 lists the accuracy of all test sensors.

2.1 Threshold Tests

Static and dynamic threshold tests were conducted to characterize the minimum input command voltages required for the installed actuation system. The results from these tests defined the lower command limit for which the actuator performance was considered acceptable.

2.1.1 Static Threshold Test

The static threshold test was used to determine the minimum command voltage required to move a control surface from the static position. These values helped determine the lower limits of the actuator command so that meaningful PID flight maneuvers could be developed. Low-amplitude, 0.1-Hz triangular waves were commanded to the X-43A actuators. An external LVDT was used to detect surface movement, as shown in figure 9. As the amplitude of the command signal was slowly increased from 0 Vdc, surface movement was monitored until the output of the external LVDT matched the waveform of the command in a qualitative manner. The recorded amplitude was defined as the minimum static command voltage. The EMA command and sensor data were recorded on an oscilloscope (O-scope). Note that the external LVDT must have adequate resolution to perform these threshold tests.

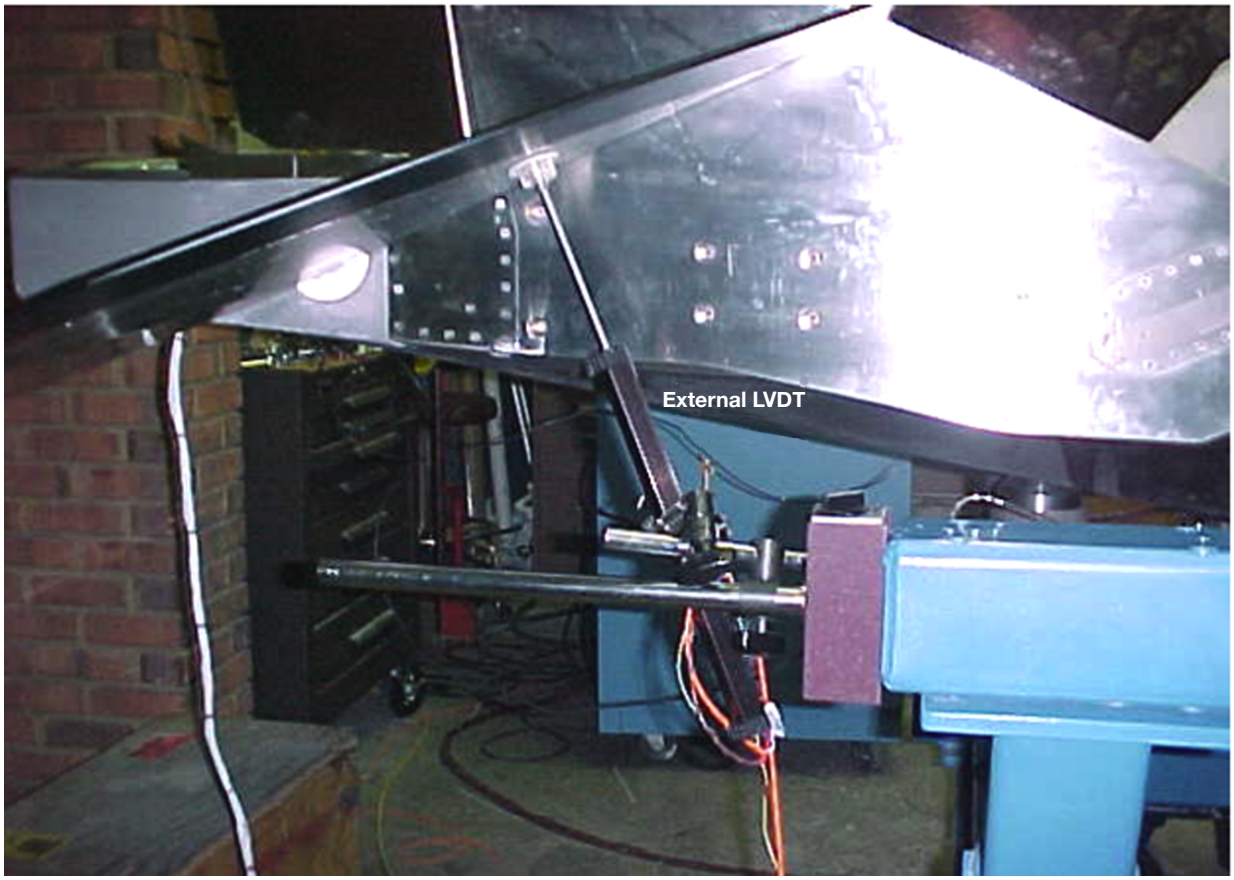

Figure 9. Linear variable differential transformer setup for threshold testing on the Hyper-X Research Vehicle wings.

This test was conducted once for each control surface of HXRV 1. The remaining vehicles were not tested, because no changes were made to EMA electronics gain. Furthermore, the friction level in the actuation system was assumed to remain relatively the same for the other vehicles, as the internal material used for each EMA was identical. (Large differences in friction levels can be detected by comparing frequency response tests of the actuator before and after material substitution.)

2.1.2 Dynamic Threshold Test

This test was used to determine the minimum command voltage required to cause the surface response to match the commanded signal at a fixed frequency. This test is analogous to the static threshold test and helped determine the lower limit of the dynamic actuator commands so that meaningful PID maneuvers could be developed. Dynamic threshold measures the ability of a system to respond to rapidly changing commands. Actuators that have low force gains and high inertias may not be able to respond adequately to the dynamic commands and may exhibit poorer performance than those that have higher gains and lower inertias.

Low-amplitude, 5-Hz sinusoidal waves were sent to the actuators, using a command voltage of 0.1 volts peak to peak V_{p-p}, 1-percent full scale (FS). The output of the external LVDT was monitored while the command voltage was slowly increased. When the waveform of the surface matched the commanded signal, that amplitude was recorded as the minimum dynamic value. The EMA command, position feedback, current, and external LVDT data were recorded on an O-scope. Figure 10 shows a plot of the right rudder dynamic threshold. This test was conducted once for each control surface of HXRV 1. The actuator design and material did not change, so the other two vehicles were not tested.

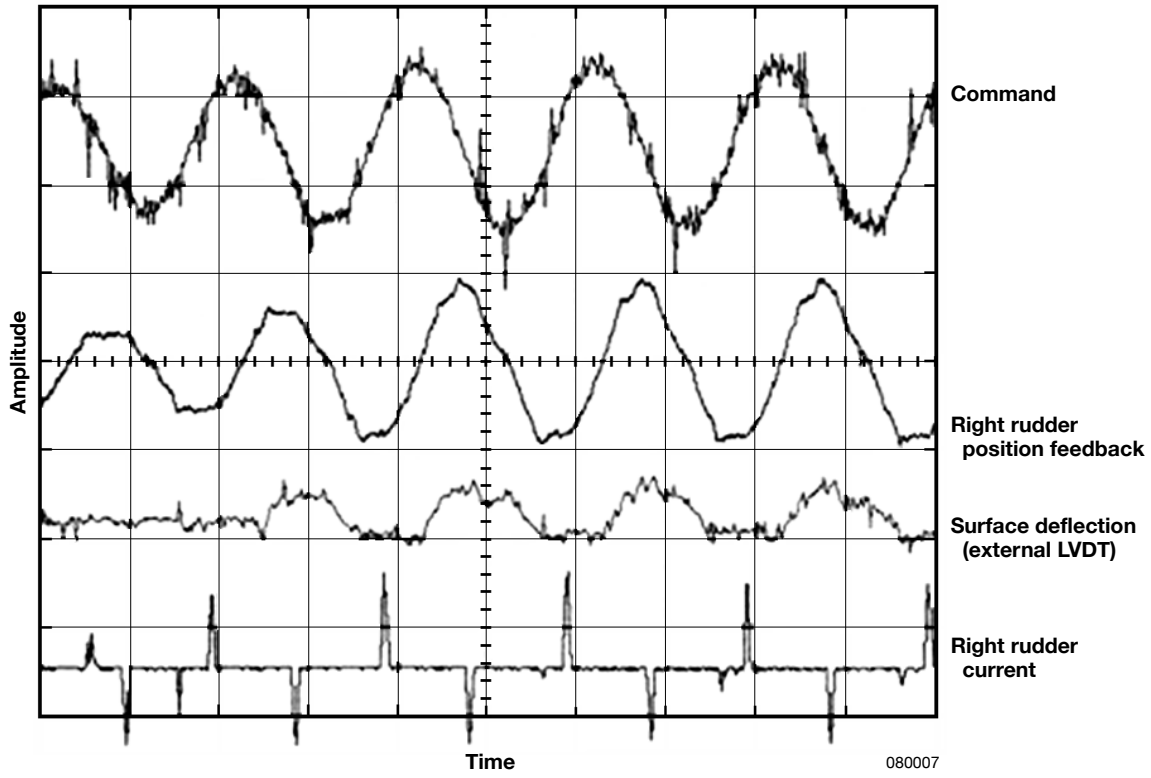

Figure 10. Right rudder dynamic threshold test.

2.2 Multichannel Crosstalk Tests

The multichannel crosstalk tests were designed to determine whether any of the EMAC channels could generate cross channel noise in static and dynamic operating conditions. The command signal of one actuator could cause an output motion in another actuator if significant crosstalk exists. In a worst-case scenario, cross-coupling could create aircraft control instability. The purpose was to ensure that the actuator channels, which were located in close proximity to each other, were properly isolated.

2.2.1 Static Crosstalk Test

This test determined whether noise existed on a steady-state channel while other channels were being dynamically excited. A number of pretests were conducted on each surface to verify that no prior anomalies existed within the system and that the input voltages and frequencies to be used did not excite the structural resonance of the vehicle. After the pretest, the goal was to determine the largest amplitude and highest frequency square waves that would cause the actuator to almost reach the saturation point (when the output no longer follows the input). Staying below saturation ensures that the pulse width modulation (PWM) is operating to limit the current. The amplitude of the current required for operation increases as the frequency is squared to accelerate the inertia of the motors. Staying just below saturation at the highest frequency creates the most severe condition for crosstalk testing. The amplitude and frequency was used to excite three channels, while the observed channel was commanded with a constant value (0 Vdc, ~20° wings, 19.5° rudders).

A total of four tests were conducted (table 2). The EMA position and current feedback of the observed channel were recorded on an O-scope, along with the square wave input and the current of a dynamic channel. Initially the tests were kept to 10-s durations to prevent the sensitive EMAC electronics from overheating. As confidence was gained, the test time was increased. Figure 11 shows a typical plot of this test. The test did not indicate any signs of cross-coupling noise for the right rudder. The right wing static crosstalk test (figs. 12, 13) showed approximately 0.02 Vdc (~0.086°) of noise in the right wing feedback channel. The noise was below the threshold command level of the right wing actuator; therefore, it was not significant enough to initiate any changes to the system. All other channels were nominal. This test was conducted once for each control surface of HXRV 1.

Table 2. Static crosstalk test matrix.

Test	Right wing	Left wing	Right rudder	Left rudder
1	Observed (static)	Dynamic response	Dynamic response	Dynamic response
2	Dynamic response	Observed (static)	Dynamic response	Dynamic response
3	Dynamic response	Dynamic response	Observed (static)	Dynamic response
4	Dynamic response	Dynamic response	Dynamic response	Observed (static)

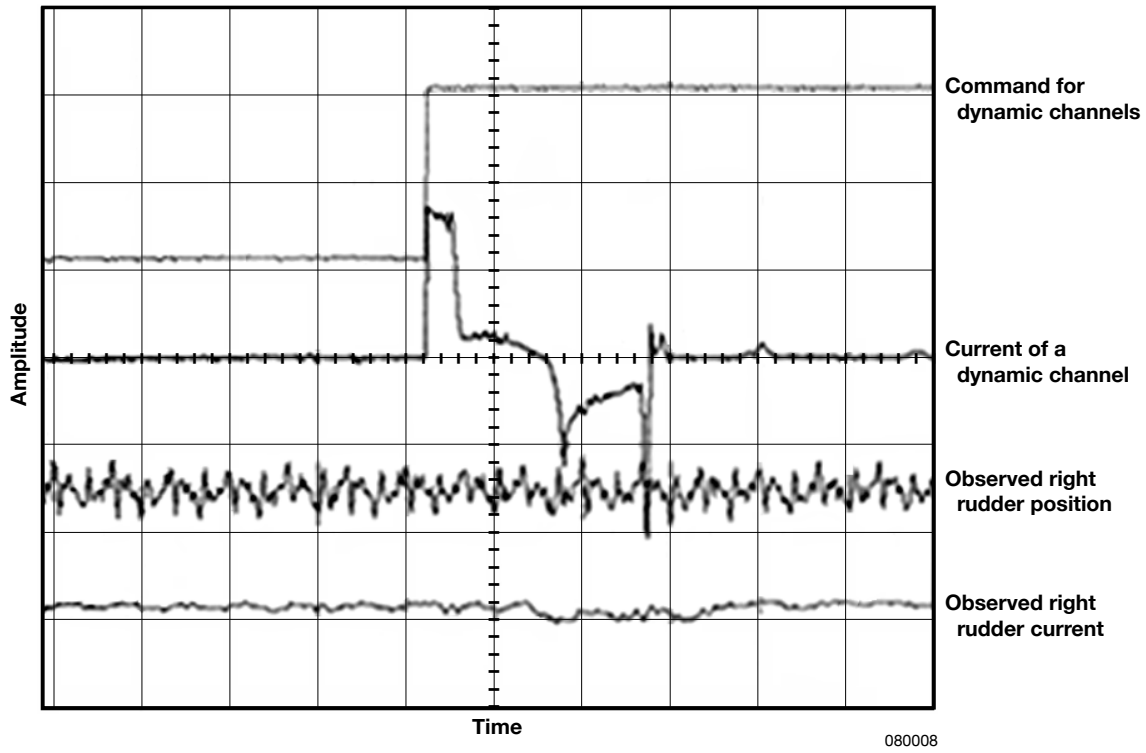

Figure 11. Right rudder static crosstalk test.

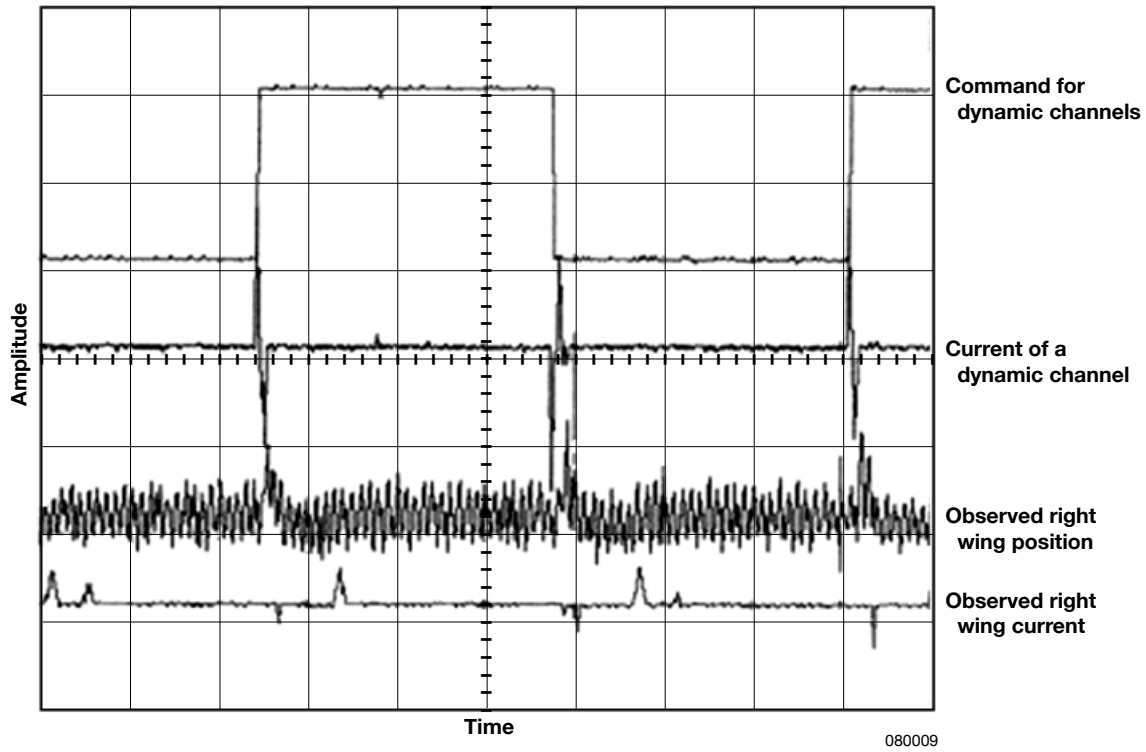

Figure 12. Right wing static crosstalk test.

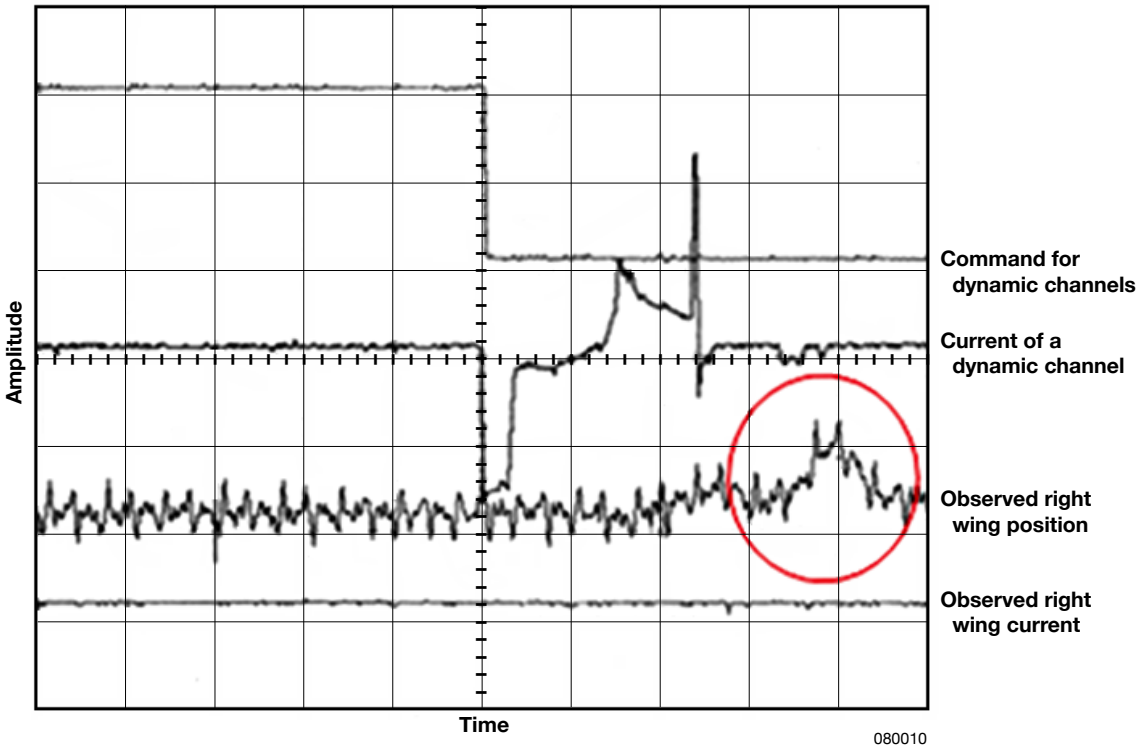

Figure 13. Right wing static crosstalk test (magnified), showing noise on position feedback.

2.2.2 Dynamic Crosstalk Test

This test determined whether noise existed within the actuation system while all channels were active. Typically, a dynamic channel has greater sensitivity than a static channel, because dynamic friction has a lower value than static friction. Static friction can mask cross-coupling between channels when they are not moving. By exciting all channels, any masked crosstalk could be detected. The observed channel was commanded with a slow triangular signal at 0.5 Hz, ± 1 $V_{p\text{-}p}$ (10-percent FS), and the remaining channels were excited with square waves discussed in section 2.2.1. Table 3 lists the four test cases. The EMA position and current feedback of the observed channel were recorded on an O-scope, along with square wave input and the current of a dynamic channel. The tests were kept to 10-s durations to prevent the hardware from overheating. Any noise in the system would present itself riding on top of the slow triangular ramp of the feedback signal. Acceptable noise levels would have to be below the threshold command levels. No observable noise was detected. This test was conducted once for each control surface of HXRV 1.

Table 3. Dynamic crosstalk test matrix.

Test	Right wing	Left wing	Right rudder	Left rudder
1	Observed (ramp)	Square wave	Square wave	Square wave
2	Square wave	Observed (ramp)	Square wave	Square wave
3	Square wave	Square wave	Observed (ramp)	Square wave
4	Square wave	Square wave	Square wave	Observed (ramp)

2.3 Command-to-Surface Timing Test

The objective of this test was to measure the timing loop of the actuator. The loop was measured in two parts: the time it took the FMU actuator command to cause the first surface motion, and the time from the surface motion to receipt of the steady-state EMA position feedback by the FMU. The data were used to measure delay for simulation implementation and verification of adequate surface response performance. A servoaccelerometer-inclinometer was mounted to the surface under test to detect motion. The command signal was a 1-Hz square wave, set at 10 percent of the total surface travel range. The command, feedback, and sensor output were recorded on an O-scope.

Only one wing was tested, because it was assumed that the wings have similar characteristics. Timing information for the rudders was not critical to the mission, thus the rudders were not measured. The average time delay from the right wing actuator command to the first motion of the surface was measured at 4 ms. Another 2 ms elapsed before the actuator's LVDT position feedback was received by the FMU. The total actuator loop time from command to feedback path was 6 ms. This test was conducted once on HXRV 2, as part of the return-to-flight activities to enhance the understanding of HXRV actuator time delays and their contribution to the overall control loop timing. The servoaccelerometer-inclinometer filters and time delays were taken into account for the analysis.

2.4 Free Play Test

The objective of this test was to measure the free-floating angle, or "slop" of each unloaded actuator surface. This nonlinear element is common in actuators that employ gear systems, and it is caused by incomplete surface contact between pairs of gear teeth as they rotate relative to each other. This element is also known as the dead zone, and it is used to improve the fidelity of actuator models.

The technique for measuring free play is relatively simple. For the HXRV, a dial indicator was mounted at a known distance aft of the surface spindle (or hinge line). A calibrated fish scale mounted forward of the hinge line was used to measure the amount of load applied to the surface. A 10-lb load was applied downward by hand on the control surface, and the indicator was zeroed out. This 10-lb load was then immediately shifted in the opposite direction, and the indicator reading was taken. Initially, the free play test was performed on all HXRV 1 surfaces using this

method. Results were 0.179° for the right wing and 0.171° for the left wing. For HXRV 2 and 3, the free play measurements were obtained from the hysteretic damping tests, which were added after the mishap investigation (see section 2.9). Data from those tests indicated that the right and left wing free play values were approximately 0.200°.

2.5 Voltage Regeneration Test

The objective of the voltage regeneration test was to measure the regenerative voltage contributed by the rotor inertia of the EMA. The main purpose was to determine whether the regenerative voltage (also known as back EMF voltage) was significant enough to degrade or damage the EMAC electronics over time. With an aiding load or rapid deceleration, the motor becomes an electrical generator, applying current to the 150-Vdc bus. This current increases the voltage on the bus and could possibly raise it to a level above the voltage rating of the components connected to it. Some vehicles are designed with a resistive load circuit on the power bus to counteract the regenerative voltage. Because a resistive load circuit was not considered in the design of the X-43A vehicle, this test was required. It was conducted shortly after the actuation system was installed in the first vehicle to determine whether a redesign was necessary.

A 5-percent FS square wave sweep from 0.1 to 5.0 Hz was used to command the actuator. An O-scope was connected to the 150-Vdc bus to monitor for any signs of excess voltage. The H-bridge of the motor controller is connected to this bus, so this area is where the regenerative voltage would occur. The O-scope was monitored for high voltage spikes above the manufacturer's allowable limit, which was 185 Vdc. The result was within specification and the hardware did not change; as such, this test was performed only once for the duration of the project.

2.6 Surface Calibration Tests

The primary objective of this test was to obtain the relationship between the command (degrees to volts) and feedback (volts to degrees) calibration curves of the actuation system. This test was conducted for two reasons. The first reason was to provide the calibration equations to the FMU so that it could command the control surfaces properly. The second reason was to use the data to determine whether the calibration itself caused any command errors. More than one calibration test was conducted for vehicles 1 and 2. As confidence in the data was gained, the number of calibration tests were reduced and only one calibration was performed on HXRV 3.

The wings of HXRV 1 were initially calibrated using an inclinometer, and the rudders were calibrated using custom-made protractors. When the requirement for more accurate calibrations arose after the mishap, a laser tracker was used as the primary source for determining surface position, and inclinometers were used as backup. The command was supplied by a Dial-a-Source® (Prime Technology, LLC, North Branford, Connecticut) precision power supply that provided precise command voltages to the EMA, and 6.5-digit voltmeters were used to accurately display the command and feedback voltages. Typically, surface calibrations were performed annually or whenever an actuator was reinstalled in the vehicle after servicing. Because free play was modeled separately, loads were not applied to the surfaces to take out the free play during the calibration.

In addition to the control surfaces, the cowl door actuator, which was used to open and close the engine cowl, was calibrated for each vehicle. No additional tests were required, as the operation was straightforward and could be easily modeled in the simulation. The calibration data were used to verify that the open and closed cowl positions met the design criteria.

2.7 Step, Frequency, Schroeder, and Ramp Tests

These tests helped determine the slew rate, frequency response, and slow response characteristics of the installed actuation system. Results from all of these tests were used to enhance the fidelity of the actuator models. The X-43A simulation bench provided the step, frequency, Schroeder, and ramp command signals to the EMAs. Step inputs of 0.5°, 1.0°, and 20.0° were used to determine small and large amplitude slew rates. Sinusoidal sweeps from 0.2 to 18.0 Hz at ±0.4° or ±1.0° were used to determine frequency response, in addition to custom Schroeder sweeps (ref. 3), which were designed for the in-flight PID maneuvers. These dynamic tests were limited to 60 s each to prevent the electronics from overheating and provide adequate time to test the desired waveform.

The slow response ramp tests used triangular waves from 0° to 2° to 0° at 0.01 deg/s, and 0.005 deg/s. The extremely slow rates helped determine how well the actuator tracked the command and identified any evidence of excessive "stiction" (static friction) that could lower the effective bandwidth of the EMAs. The EMA command, position, and current feedback signals were recorded. All surface EMAs for each vehicle underwent these characterization tests. No anomalies were observed.

2.8 Compliance Test

The objective of the compliance test was to characterize the steady-state elastic deformation of the actuators and their mechanical linkages under load. During flight, aerodynamic forces on the control surfaces can either aid the deflection or counter it. In either case, the surfaces are not at the true commanded angles, because the loaded EMA gear trains and linkages undergo elastic deformation. Compliance is the inverse of system stiffness and consists of two parts: (1) compliance within the servo loop, which consists of the actuator, gear train, shaft, and internal LVDT, and (2) compliance outside the servo loop, which consists of the mechanical servo crank arm and linkages that are not measured by the EMA feedback system. Total compliance is defined as the sum of both parts. When the EMA is active and closing the loop on the command in the presence of load, the actuator's steady-state stiffness increases significantly. The result is a smaller term for compliance within the servo loop, with most of the compliance occurring outside the loop at the linkages.

The purpose of performing this test was to increase the fidelity of the actuator models and determine whether there were significant amounts of compliance, which could reduce the gain and phase performance of the actuators. These reductions could lead to loss of control loop stability margins. This test should be conducted with the real flight hardware, because compliance could vary from actuator to actuator, especially if design changes occur in material or linkage geometry.

A major contributor to the loss of the first Hyper-X stack was the lack of fidelity in the HXLV FAS second-order model and seventh-order model (ref. 4, unpublished). The second-order linear actuator model used for HXLV preflight linear stability and controls analysis was independent of load and did not include compliance. Also, the model did not include a position feedback filter that reflected the hardware electronics characteristics. These omissions contributed to the incorrect determination of the true vehicle gain margin.

The seventh-order FAS model did have compliance but did not have the correct values, as accurate test data of the HXLV flight actuators were not available at that time. Although this seventh-order model existed, it was not used for vehicle stability analysis. Only the second-order model was implemented. The mishap investigation team reported, "The use of a single FAS transfer function over the entire mission is inadequate for linear analysis" (ref. 4, unpublished).

Following the mishap, the HXLV return-to-flight activities involved a thorough suite of compliance tests that utilized an actuator, spindle, and fin surface assembled in the flight configuration. Compliance within the actuator feedback sensor loop and total compliance from the actuator to the fin were measured. As much as 88 percent of the total compliance was found to occur outside the servo loop (ref. 5, unpublished), which meant that the angle commanded by the HXLV control system could have been significantly different from the actual fin deflection, depending on the magnitude and direction of the load during flight. Because most of the compliance was outside the servo loop and could not be deduced from the HXLV onboard telemetry data, the project felt that accurate modeling of this element was crucial for control systems analysis of the remaining two vehicles. Corrected FAS models showed a 3.5-dB gain difference from the original second-order model during the time when the Hyper-X stack began to lose its stability (ref. 4, unpublished).

In conjunction with the HXLV return-to-flight activities, the project tested HXRV 2 and 3 for EMA compliance to determine whether elastic deformation had occurred within the actuation system that was not accounted for. Another reason for this test was to increase the fidelity of the HXRV EMA models, as this element was not incorporated in the HXRV 1 simulation. Ideally, compliance should be tested with the flight actuation system powered on and brakes disengaged. The actuation or control system will try to close the loop on the error imparted by the loading mechanism. This configuration provides more accurate results, because during flight the actuation system will try to counter the effect of aerodynamic forces on the actuator position.

The Hyper-X program did not invest in a representative vehicle (iron bird) dedicated exclusively for ground testing and troubleshooting. As such, there was concern that the flight hardware could be damaged when loads were applied to the control surfaces while the actuation system was active. The danger exists in a potential force fight between the control systems of the vehicle and the hydraulic loading equipment. To avoid this problem, the compliance test was divided into two sections. The first test involved the use of static weights attached to the lower wing surfaces while the actuation system was active and the actuator brakes were disengaged. The second test involved the use of hydraulic load jacks that applied load on the surfaces while the actuation system was powered on but locked into position by the actuator brakes. The maximum test torque applied was ±1780 in-lb on the wings and ±470 in-lb on the rudders. These values

represent approximately 30 percent of the maximum expected in-flight hinge moment. Typically, compliance curves are nonlinear up to 10 percent of the maximum load, and beyond that the curve begins to become more linear. The 30-percent maximum load values were chosen to provide adequate test coverage.

2.8.1 Static Weight Compliance Test

Swivel load pads were mounted onto the leading and trailing edges of the wings at known distances from the center of the spindle. Care was taken to mount them only along the web structure so that the skin of the surface would not warp or buckle. A weight assembly was attached to the right wing leading-edge swivel pad and was kept orthogonal to the surface, similar to the setup shown in figure 14. The vehicle was powered on and the wing was commanded to 0°. An inclinometer and a laser tracker were used to measure the total compliance at the surface. The design of the test apparatus required that the leading and trailing edges be loaded separately. Therefore, the highest torque (890 in-lb) for each edge was one-half the maximum test torque. Initially, 10-lb weights were incrementally stacked for the leading edge, and at each data point, the compliance angle, actuator command, and feedback values were recorded. After 890 in-lb was reached, the process was reversed and the weights were removed in 10-lb decrements. The weight assembly was then moved to the trailing-edge load point, and the entire test was repeated.

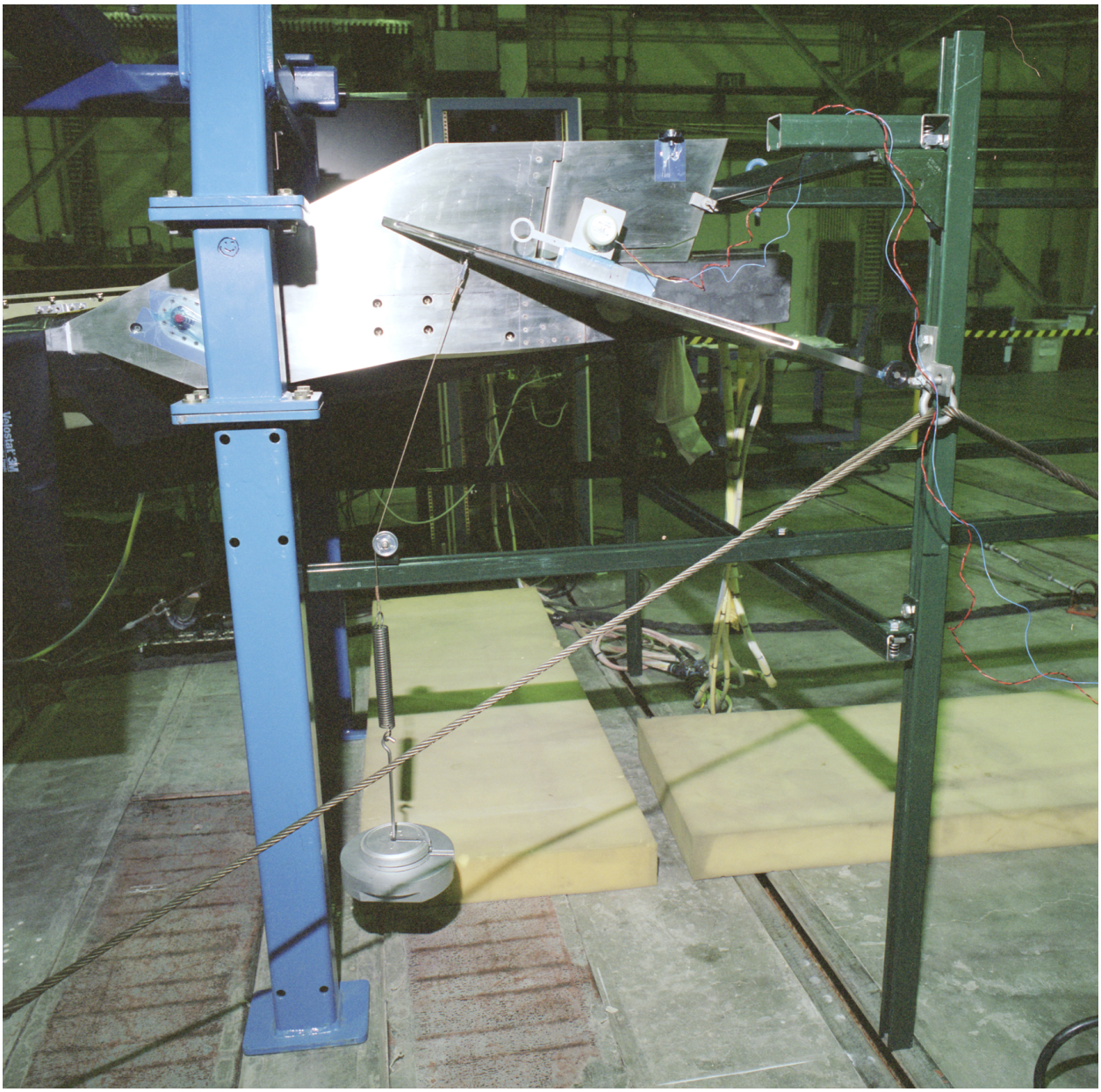

EC01-0341-05

Figure 14. Static weight compliance test configuration.

Only the right wing was tested. Results indicated that the EMA feedback did not change significantly during the load process to cause the actuator control system to close the loop on the error. Most of the observed compliance was on the order of 0.01° but was not compensated by the actuation system, because it occurred outside the servo loop. The leading edge was not loaded simultaneously with the trailing edge to provide the maximum test torque; therefore, the contribution of the inner loop compliance did not emerge.

2.8.2 Hydraulic Load Compliance Test

Two hydraulic load jacks were attached to the leading and trailing swivel load pads on the right wing. Both jacks were set up to provide a torque-summed load. A laser tracker sensor mirror mounted on the tip of the surface measured total compliance. As a backup, two inclinometers and a digital dial indicator were mounted at the root of the wing near the spindle to provide additional surface deflection information. Figure 15 shows this setup. The vehicle nose and aft most bulkhead were also instrumented with laser tracker sensors to provide vehicle position data. These additional sensors were necessary, as the loading mechanisms caused the entire vehicle to move relative to its support cradle, which introduced small errors in the compliance measurements. The angles were later corrected for this movement.

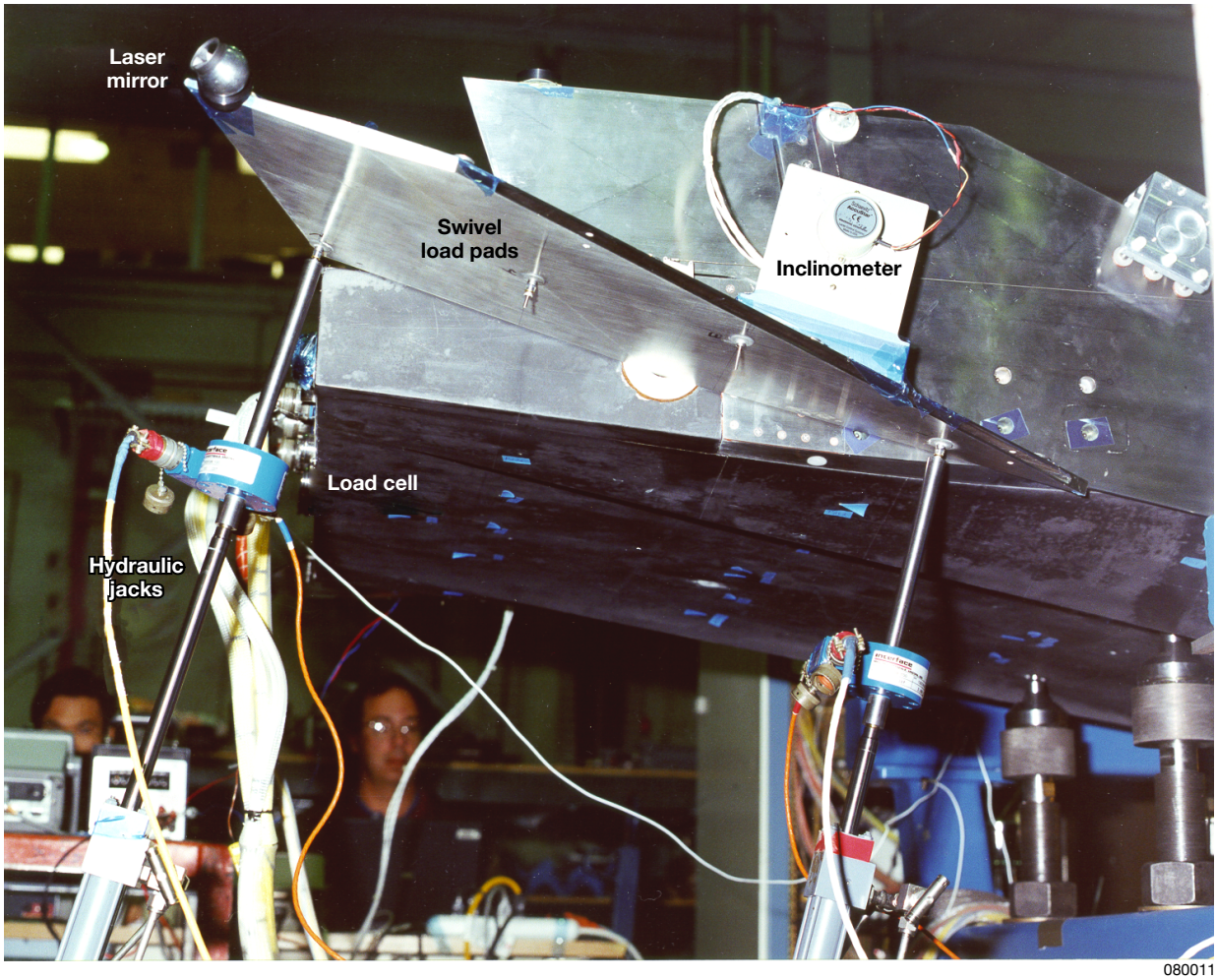

Figure 15. Hydraulic load compliance test configuration for the right wing of Hyper-X Research Vehicle 2.

Because compliance varies as the actuator and linkage geometry changes, the wing was tested at two positions, 0° and 15° leading edge down. An angle of 15° was chosen, because it

corresponded to one side of the HXRV wing deflection limit in which the aerodynamic load would aid the deflection, the worst-case scenario from a compliance standpoint.

The wing was tested at a deflection of 0°, from 0 to +1780 in-lb, then down to –1780 in-lb, and returning to 0 in-lb, pausing at 222.5 in-lb intervals (10 lbf equivalent for each jack). All actuator signals were recorded on a data acquisition unit (DAU), in addition to the compliance angles obtained from the laser tracker and inclinometers. Onboard strain gage data from the vehicle telemetry stream were also archived. After completion of this test, the right wing was deflected to 15° and the same load profile was applied. The entire process was then repeated for the left wing at both angles. Figure 16 shows the right wing total compliance and compliance within the LVDT servo loop. In flight, the FMU computer would be able to detect only the LVDT servo loop compliance, but in reality the vehicle would experience the total compliance at a given load. Figure 16 also illustrates that a stand-alone, uninstalled actuator tested for compliance would provide only the LVDT compliance curve, which can lead the user to model the actuators incorrectly.

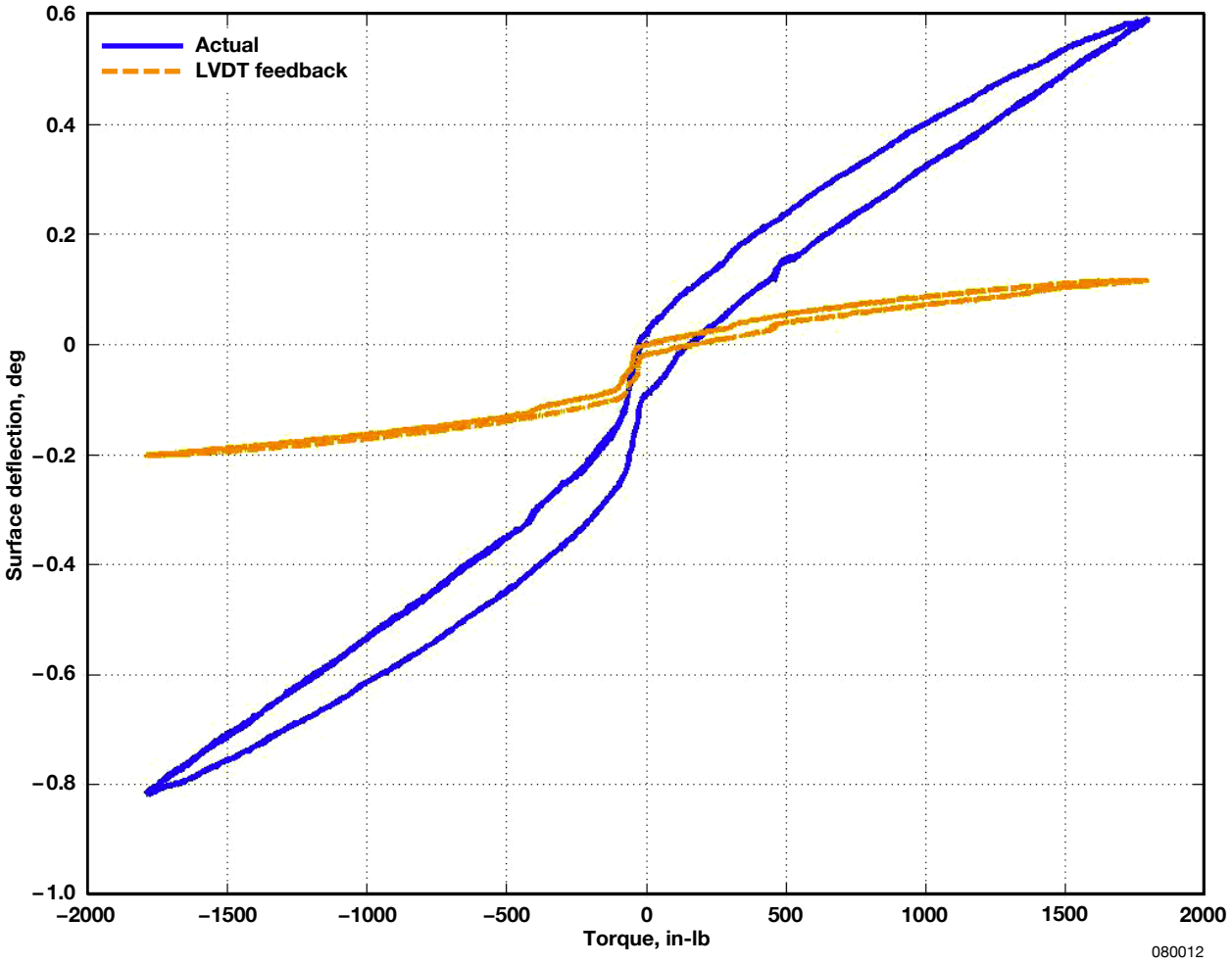

Figure 16. Compliance inside servo loop (linear variable differential transformer) and total compliance (actual) for the right wing of Hyper-X Research Vehicle 2.

As discussed previously, a total of four different sensors were used to measure surface deflection: two types of inclinometers, a digital dial gage, and a laser tracker. The inclinometers were placed in the same location, near the root of the wing, and provided similar results for wing compliance. The dial gage also proved to be beneficial and served as a backup to the inclinometers. It was also placed near the inclinometers. The laser tracker sensor mirrors, however, had been mounted on the tip of the surfaces, which produced a more conservative data set that yielded a maximum difference of 0.03° from the inclinometers. This discrepancy was identified during the testing. Efforts were made to measure potential surface warp with the laser, but the results were not conclusive.

One possible explanation attributes the method of wing loading as the primary cause of the discrepancy. The point loading provided by the opposing jacks near the root of the wings imparts not only torque but also a force that induces an upward shift of the spindle, resulting in a slight twist along the span of the surface. This twist most likely explains the differences between the sensors. For the HXLV, an alternative method was used for the compliance test. A rectangular enclosure was fabricated to surround the entire fin. It served to protect the surface under test and acted as an interface plane to the jacks instrumented with load cells. The enclosure contained rigid foam that encapsulated the surface, which provided an even load distribution.

For the HXRV rudder, a U-bracket machined out of stainless steel and fitted with a protective rubber liner was used as the structural interface between the load jack and the surface. The U-bracket protected the rudder and sufficiently transferred the load from the jack. A laser tracker and digital dial indicator were used to measure compliance. The right rudder was set at a deflection of 0° and tested at 0, 470, -470, and 0 in-lb, in discrete steps. The rudder was then set at an outboard position of 20° and the tests were repeated again. The left rudder was tested in the same manner. Body rotation caused by the loading mechanism was removed during the posttest data processing phase.

From the HXRV 2 compliance data, more than 81 percent of the total wing compliance was outside the servo loop (worst case). More than 69 percent of rudder compliance was outside the servo loop. For vehicle 3, only the wings were tested because of time constraints, and results showed that 77 percent of the total wing compliance was outside the servo loop.

2.9 Hysteretic Damping

The objective of this test was to characterize the amount of hysteretic damping in the actuators and associated linkage structures. Hysteretic damping dissipates energy by a combination of plastic straining and internal friction. It could increase the area within a hysteresis loop, such as the total compliance curve shown in figure 16. From a modeling perspective, this test determined whether hysteretic damping at various load amplitudes could affect the magnitude and phase response of the actuation system. If hysteretic damping losses were significant enough to affect the performance of the actuators, then this element would be included in the EMA models.

The test was conducted after compliance measurements were taken, because it used the same hardware setup. For the wings, the hydraulic load control system was programmed to output

sinusoidal loads at ±100 in-lb total from two jacks, one under the root leading edge of the wing, and the other at the trailing edge. They worked in opposite directions so that when one was in full compression, the other was in full tension. The wings were set to 0°. Three sinusoidal load cycles were conducted at 0.025 Hz and then at 0.25 Hz. The process was repeated at ±500 and ±1780 in-lb for trend analysis. The test setup was removed and the wings were set at 15° leading edge down. All load profiles were repeated again.

The inclinometers and digital dial gage data, in addition to the standard actuator signals, were recorded on the DAU. Laser tracker data were not used, because they could not be time-synched with the load system. The rudders were tested in the same manner, but at ±100, 200, and ±400 in-lb at null and 20° outboard deflections. Figures 17 and 18 show the results from these tests (see TS90 curves; simulated curves are discussed in section 3.2.2). The area within the curve was caused by hysteretic damping. Near zero force, the curve slope increased, because the loading system was passing through the actuator's free play region. This high rate of travel for the load jacks would sometimes cause the hydraulic emergency shutoff system to stop the test prematurely. The emergency shutoff was set to activate whenever the load cells would indicate a drastic drop in load, as this condition was usually associated with the load jacks slipping from the test article. Gain adjustments were made to the hydraulic load equipment to decrease the sensitivity of the shutoff system. A retest was usually required when this condition occurred.

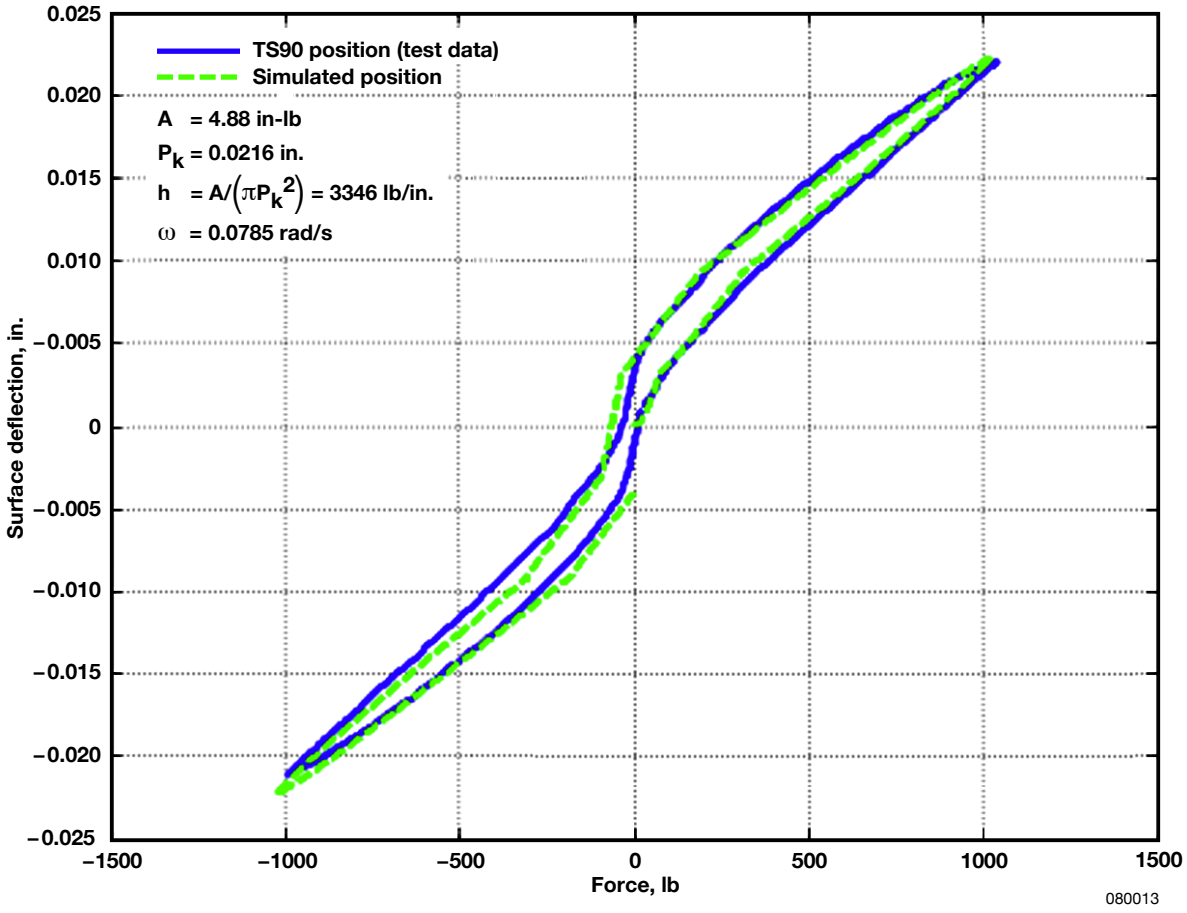

Figure 17. Right wing hysteresis loop; 0.0785 rad/s.

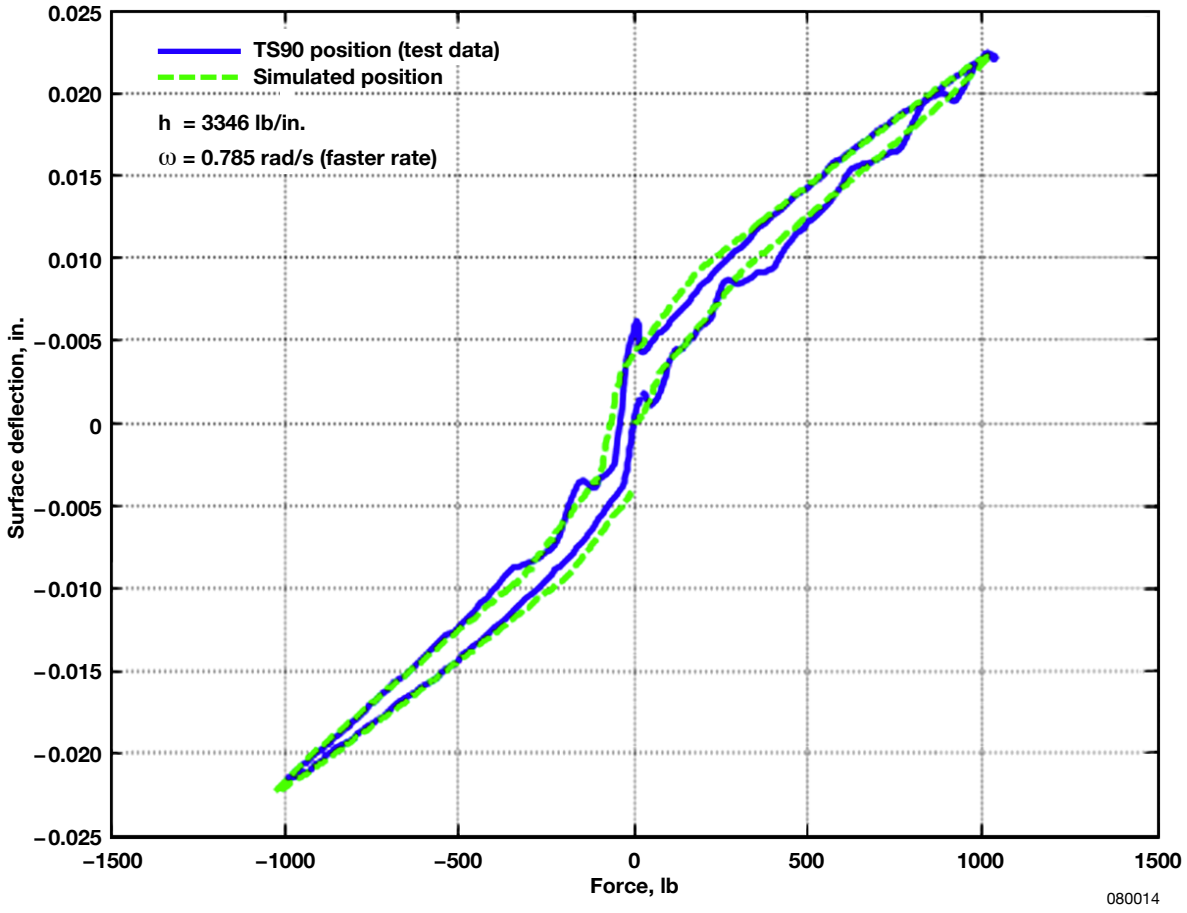

Figure 18. Right wing hysteresis loop; 0.785 rad/s.

For the higher frequency test, the quality of the TS90 inclinometer data was not as good as that of the low-frequency tests, so the backup dial gage was used to verify the integrity of the TS90 data. The sensor was reaching its frequency response limit for that particular test case.

2.10 Aircraft-in-the-Loop Tests

Aircraft-in-the-loop (AIL) tests were used to evaluate the performance of the actuation system in a closed-loop test environment. These tests validated the hardware and software of the flight control system and ensured that the flight test objectives could be achieved. The project conducted nominal and off-nominal test cases (ref. 6) and compared them with the all-software simulation results, which were considered the "truth" data set.

The test required the use of a simulation bench, which was configured between the FMU and the rest of the HXRV systems. It consisted of a simulation interface device, a simulation computer, an inertial navigation simulator, and a decommutation computer (fig. 19). The interface device served as the input and output junction for all of the hardware. The simulation computer contained the vehicle system models and databases (aerodynamics, propulsion, engine, actuators, wind),

and the inertial navigation simulator provided the FMU with incremental velocities and angles to simulate the in-flight dynamics (see section 4.1 for details). Aircraft telemetry data from the FMU were monitored using a decommutation computer.

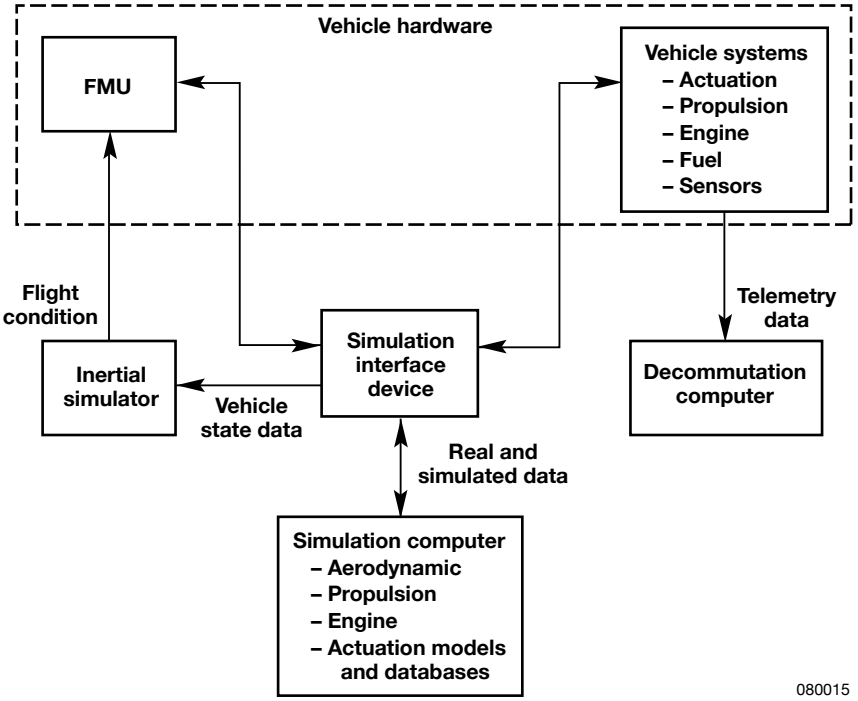

Figure 19. Aircraft-in-the-loop test configuration.

The AIL test was designed to simulate the flight phases of the HXRV after separation from the HXLV. When an AIL test is initiated, navigation data that simulate in-flight conditions are sent from the inertial navigation simulator to the FMU. Based on this information, the FMU responds and sends the appropriate system commands to the hardware system or simulation model, depending on the selected configuration of the interface device. Signals that are passed to the real hardware will cause it to execute the command and report back to the FMU. This configuration is defined as closed-loop testing. For open-loop testing, command signals are sent to the simulated systems and processed using the representative models and databases.

During the course of the simulated mission, the software within the FMU transitions into different preprogrammed modes of operation. After the simulated separation from the HXLV occurs, the HXRV enters the experiment mode in which the scramjet engine experiment algorithms are executed. Once this event is complete, the FMU transitions into the descent mode and PID maneuvers are conducted. These maneuvers are designed to provide information on the aerodynamic and control characteristics of the vehicle (ref. 7). They are made up of step inputs, frequency response, and guidance and control Schroeder sweeps (fig. 20).

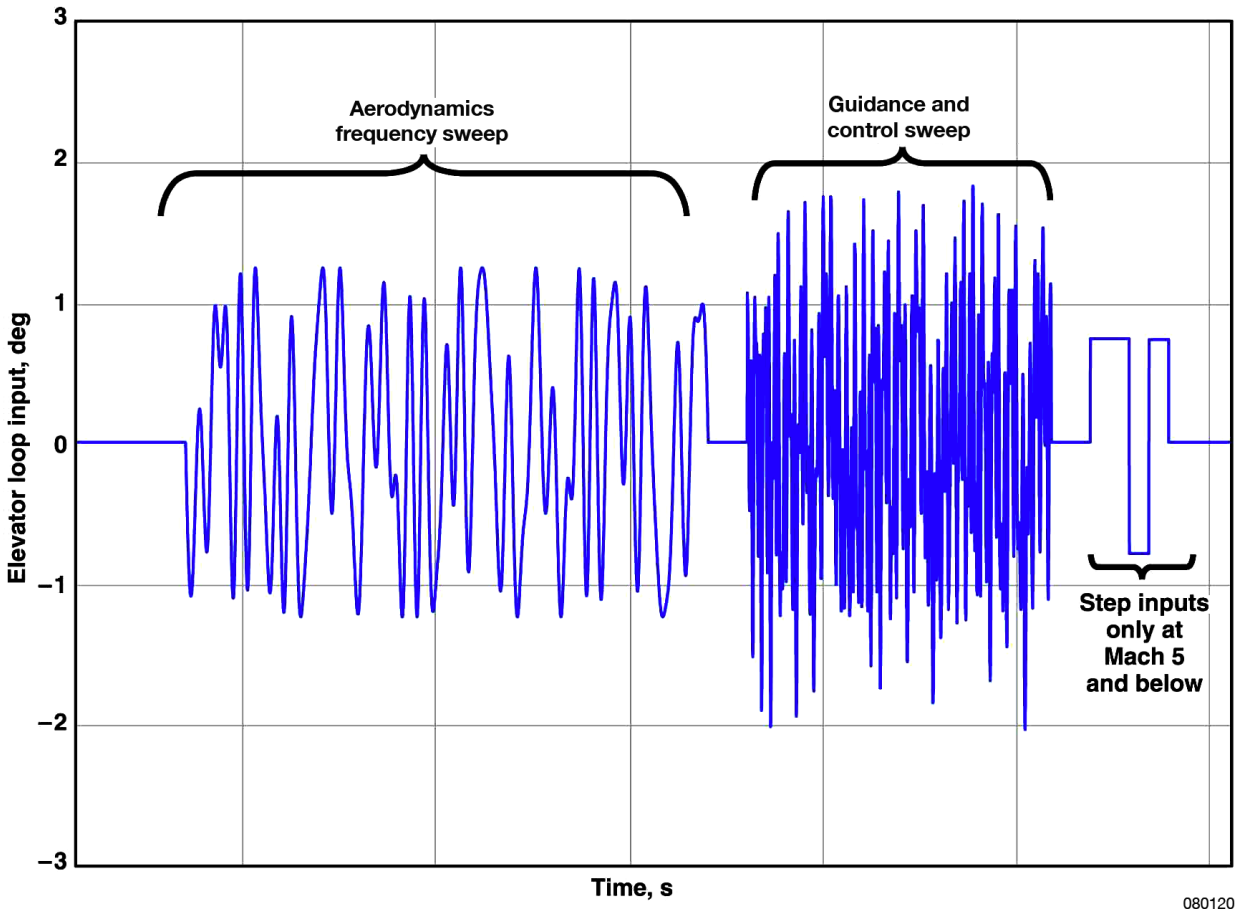

Figure 20. Typical parameter identification maneuvers used for flight 3.

To ensure mission success, it was critical that the actuation system met the performance requirements for the experiment and descent modes. The AIL test provided a means of validating the EMA performance during the mission. For the closed-loop AIL tests, the actuation system was active from separation to the final vehicle maneuver. The EMA LVDT feedback signals were fed into the simulation to provide the vehicle response. Actuator command and feedback tracking, signal noise, and current draw were carefully examined against the all-software simulation data.

Closed-loop AIL test results from all three vehicles showed a stable 3-Hz dither on the actuator position feedback, roll rate, pitch rate, roll angle, and angle-of-attack data (ref. 8, internal report). The amplitude of the actuator dither was approximately 0.1° peak to peak during periods of trimmed flight. Open-loop AIL test data did not show any signs of dither. For these tests, the control surfaces were commanded open-loop, and a low-order actuator model that was running in the simulation was used to model the EMA response.

Closed-loop simulation results demonstrated that even with the observed dither, the HXRV was able to meet mission objectives. Nevertheless, the project decided to investigate the dither after the flight 1 mishap. The test setup and actuation system were carefully examined. High-fidelity models were used as an aid for the troubleshooting effort. The findings indicated that dither

was caused by time delays and noise in the test environment that coupled with the EMA PWM dead band used in the actuator controller (ref. 8, internal report). Details of the investigation are presented in section 4.3.

2.11 Lessons Learned from Electromechanical Actuator Testing

Most of the tests described could have been conducted on an iron bird test bench to minimize any possibility of damaging the flight hardware. As discussed previously, the project did not account for a representative iron bird in its budget. Therefore, extreme care and attention was given to the test-planning phase to minimize excessive wear and tear on the actuators. The use of an iron bird would have simplified the compliance test, as it would have required only the hydraulic load test. This setup would be a more realistic configuration and the static weight test could have been eliminated, because the flight hardware would not be at risk. In addition to the actuator characterization tests, an iron bird could have been used for high-pressure propulsion system tests or hardware troubleshooting to reduce wear and tear on parts that have extremely low life cycles.

For the compliance and hysteretic damping tests, redundant sensors were used to measure surface deflection angles. This redundancy provided insurance against sensor failures and the additional data set provided a "sanity" check against the primary data. Redundant sensors should be placed in the same location if possible. Otherwise, the data between the different sets may be difficult to correlate if the test hardware causes a slight change to the geometric configuration from one measurement location to another, as was the case for the wing compliance testing.

During high frequency hydraulic compliance testing, the hydraulic safety shutoff system would sometimes activate when the load jacks passed through the free play region of the actuators. The safety shutoff system was used to prevent hardware damage in case the load jacks slipped off the attachment points. At the free play region, the load cells detected a rapid decrease in load, which triggered the shutoff system and disrupted the test. The gains for the load cell and shutoff system were adjusted to minimize the problem.

For the hysteretic damping test, it was known before the test that the inclinometers would provide good data quality for the slow sinusoidal input waves but only adequate results for the fast input waves. The added redundancy of the digital dial gage provided extra confidence in the inclinometer data for the high frequency case, even though the inclinometer data sometimes appeared "ratty" (fig. 18).

Closed-loop tests such as the AIL test can be very complicated to set up and execute. When anomalies occur, not only should the hardware or simulation be examined, but also the interaction between the two. In the case of the dither that was present in the AIL tests, a thorough understanding of all test equipment and its impact on the data was necessary to uncover the root causes.

3.0 HYPER-X RESEARCH VEHICLE ELECTROMECHANICAL ACTUATOR MODELING TECHNIQUES

A total of nine distinct actuator models were used throughout the history of the Hyper-X program to model the HXRV actuators. Table 4 lists these models and the associated tests that produced the data necessary for constructing them. All of the models in the table can be classified as second-order, high-fidelity, or linear types. This section discusses the construction methods or enhancements for each type. Section 4.0 follows the discussion with details of how each of the actuator models was implemented into the X-43A simulation.

Table 4. The X-43A electromechanical actuator models and applicable tests.

Model number	Model name	Acronym	Type	Usage	Applicable tests
1	Low-order actuator continuous model	LOAC	Second-order model	Model validation	Step, frequency response, free play
2	Low-order actuator discrete FORTRAN model	LOADF	Second-order model	Nonlinear simulation	Step, frequency response, free play, AIL
3	Low-order actuator discrete auto-code model	LOADA	Second-order model	Nonlinear simulation	Static threshold, frequency, ramp, Schroeder, compliance, hysteretic damping, AIL
4	High-order actuator continuous model version 1.0	HOAC1	High-fidelity model	Model validation, troubleshooting	Not applicable; manufacturer provided
5	High-order actuator discrete model version 2.0	HOAD2	High-fidelity model	Nonlinear simulation	Step, frequency, ramp, Schroeder, compliance, hysteretic damping, AIL
6	High-order actuator discrete model version 3.0	HOAD3	High-fidelity model	Nonlinear simulation	Step, frequency, ramp, Schroeder, compliance, hysteretic damping, timing, AIL
7	Simplified low-order actuator continuous model	SLOAC	Linear model	Linear analysis	Step, frequency response, free play
8	High-order actuator linear model	HOALM	Linear model	Linear analysis	Step, frequency response, free play
9	Low-order equivalent system actuator model	LOES	Linear model	Linear analysis, Monte Carlo	Step, frequency, ramp, Schroeder, compliance, hysteretic damping, timing, AIL

3.1 Construction of Second-Order Actuator Models

Second-order actuator models specified by natural frequency and damping ratio were used primarily for gain design and linear analysis. Variations on this basic model included nonlinear elements such as rate and position limiting and additional details such as free play, compliance, and command error. These variants were used in nonlinear simulations, particularly in support of statistical analysis such as Monte Carlo batch mission simulations.

3.1.1 Basic Second-Order Model

The basic second-order model is defined by the natural frequency and damping ratio (fig. 21). Early in the program, typical values were assumed for these variables that were consistent with the class of actuators anticipated ($\omega_n = 5.0$ Hz, $\zeta = 0.7$). Once the EMA test data were available, second-order model parameters were reconciled with the actual flight hardware. The primary technique used for this task was parameter optimization using both step and frequency response results from the flight 1 acceptance test program (ATP), and later from the HXRV characterization tests (section 2.7). The ATP data were obtained from the manufacturer in the stand-alone configuration, whereas the HXRV data were obtained with the actuators installed on the vehicle. The unloaded ATP data accounted for surface inertia through the use of an inertial load simulator.

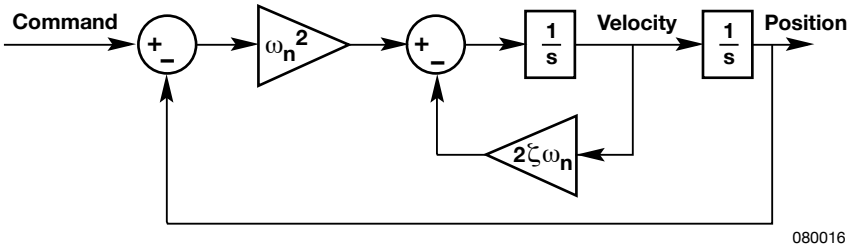

Figure 21. Basic second-order actuator model.

To perform the parameter optimization, a least squares minimization approach was used to determine estimated values of the frequency and damping ratio. This technique reduced, in a least-squares sense, the error between the model and test response. Several estimates were produced in this manner, one for each step and frequency response test performed for the wings and rudders. In addition to natural frequency and damping, time delay in the actuation system was also incorporated using data from the command-to-surface timing test. It was often necessary to use time delay to add more phase loss to the actuator model.

Figure 22 provides an example comparison between test data, optimization results, and hand calculations. Hand calculations were produced based on the rise time and settling time of the step response. Figure 23 shows the spread of estimates seen for the flight 1 actuators. To be on the conservative side, uncertainty in the estimates was defined to be uniformly distributed, covering minimum and maximum values across both wing and rudder tests.

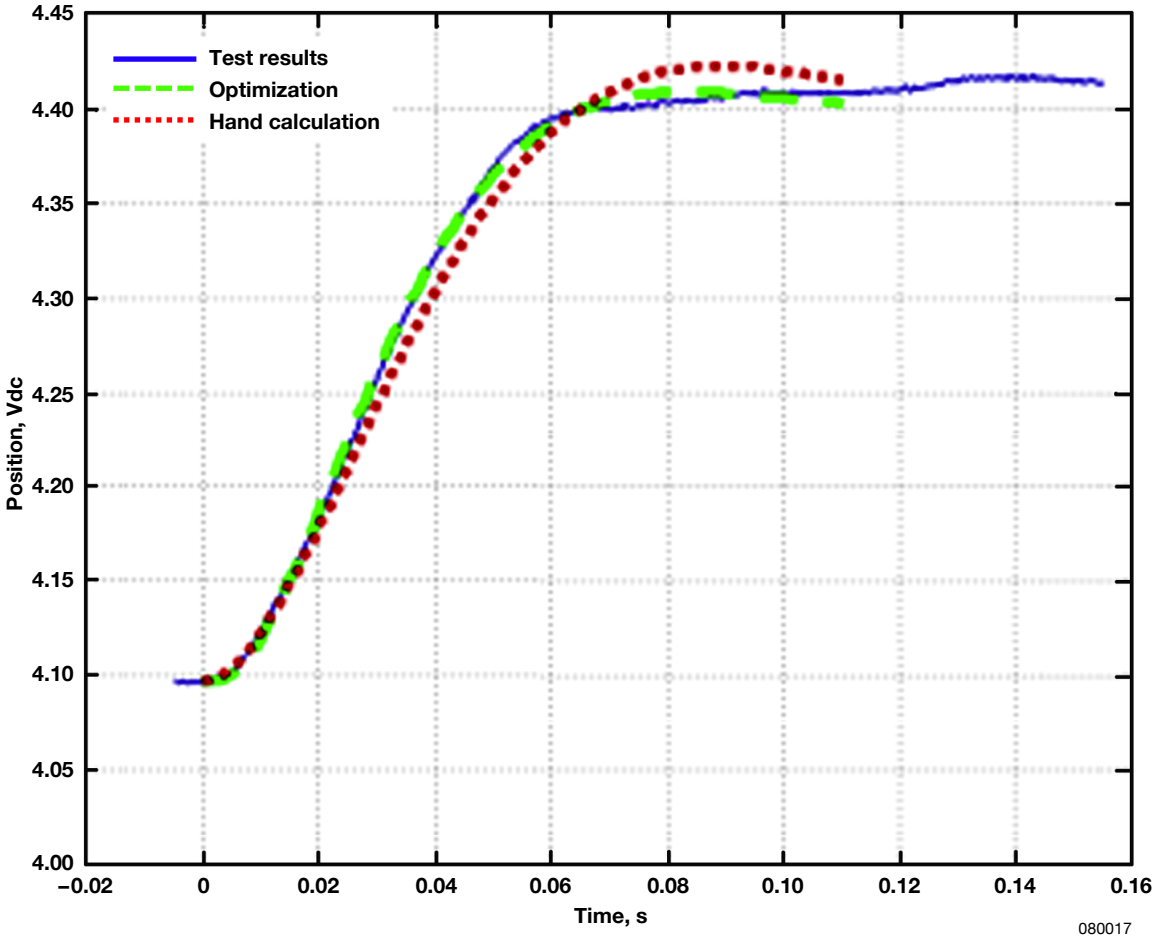

(a) 1-deg step.

Figure 22. Model data compared to Hyper-X Research Vehicle test data (left wing).

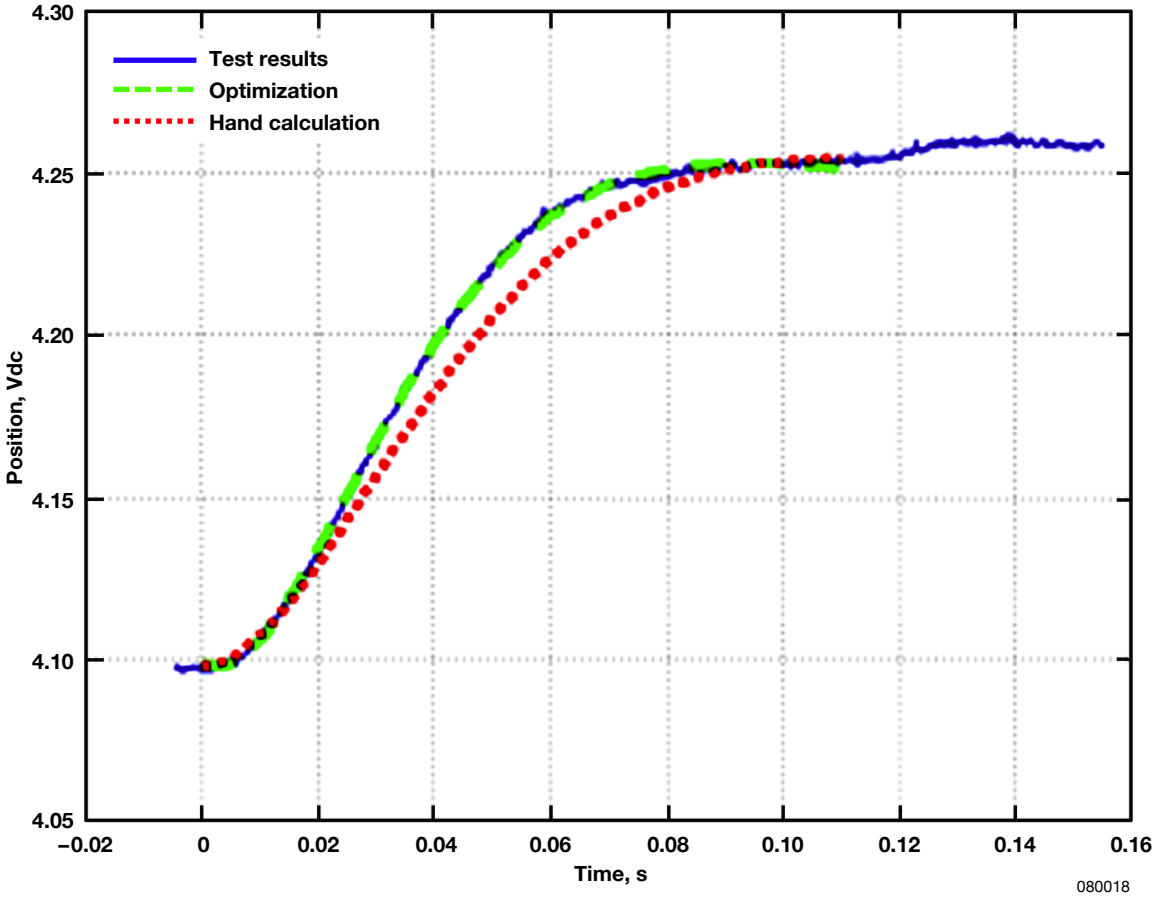

(b) ½-deg step.
Figure 22. Concluded.

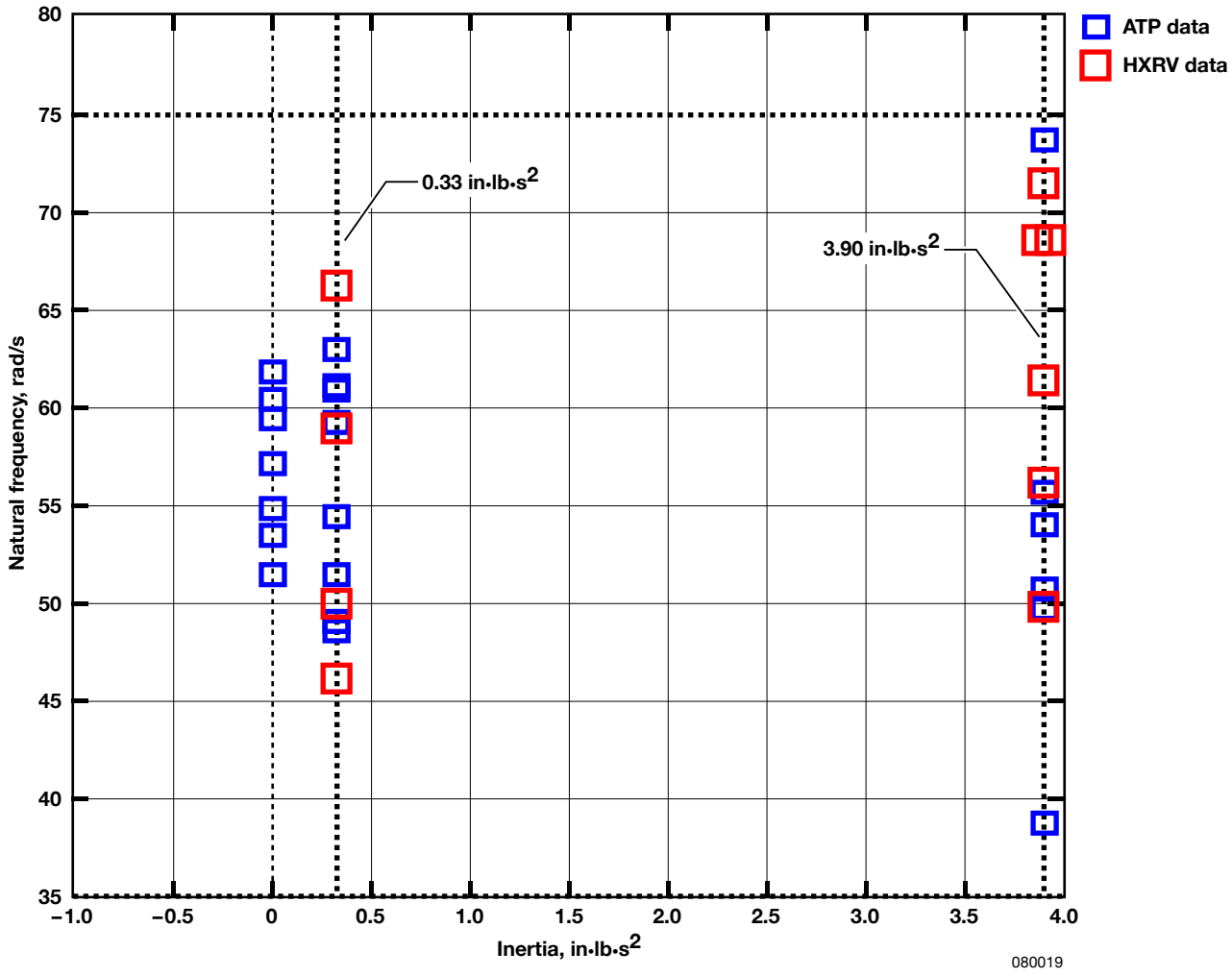

(a) Natural frequency.

Figure 23. Second-order actuator parameters.

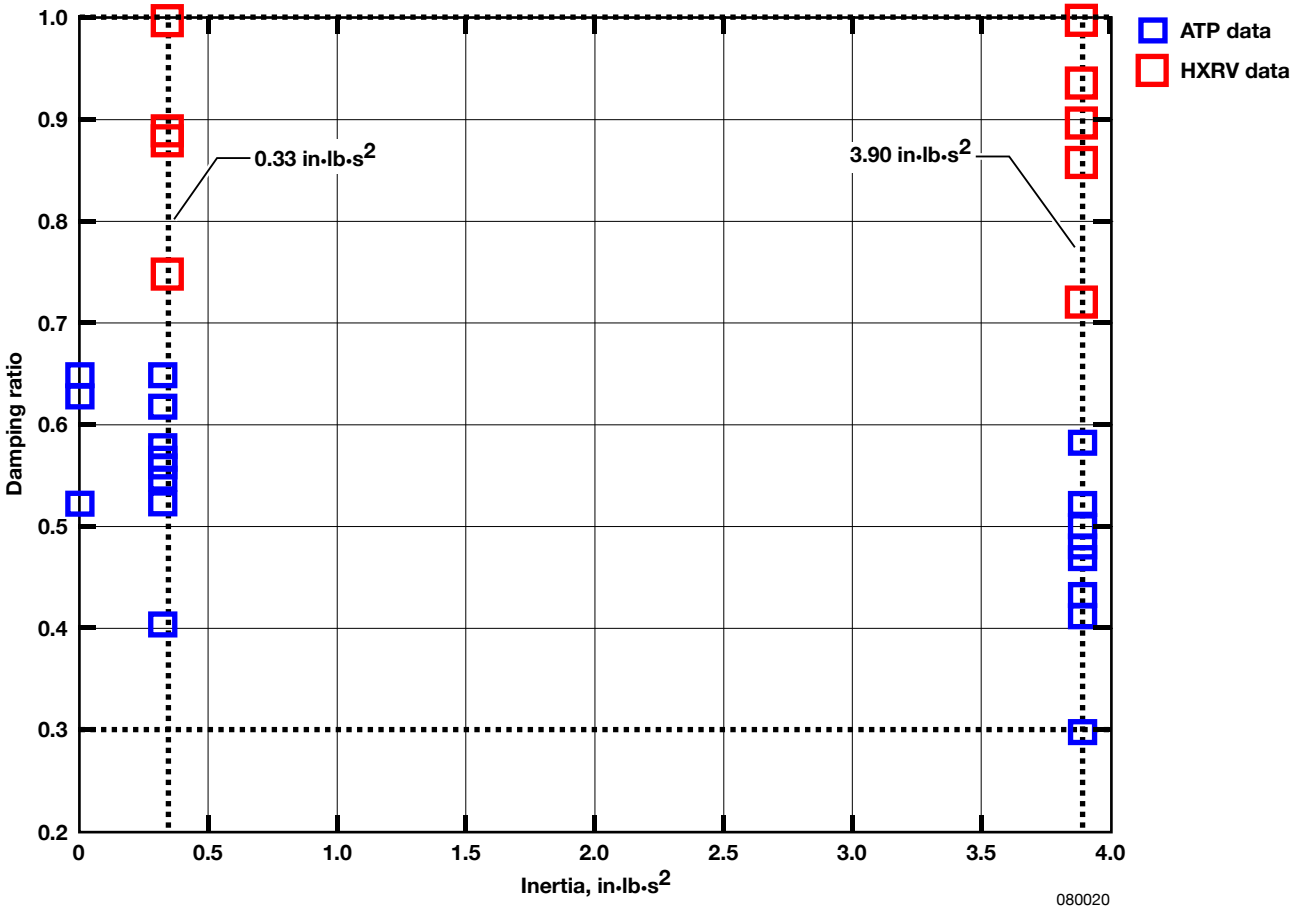

(b) Damping ratio.
Figure 23. Concluded.

The natural frequency and damping ranges indicated in figure 23 were based on vehicle 1 data. Tests included step commands, slow sweeps, and Schroeder sweeps. Results from the Schroeder sweeps were converted to a frequency response using a discrete fast Fourier transform. In turn, new values of natural frequency and damping were estimated. The wing data set is associated with an inertia of 3.9 in•lb•s^2, and the rudder data set is associated with an inertia load of 0.33 in•lb•s^2. The horizontal dashed lines on the top and bottom represent the recommended model bounds for all data sets. As more test data were obtained from vehicles 2 and 3, the natural frequency and damping ratio range was reduced. Figure 24 compares second-order model bounds with frequency response test data for the rudders for vehicle 3. The second-order model (solid line) provided a reasonable bound to the test data.

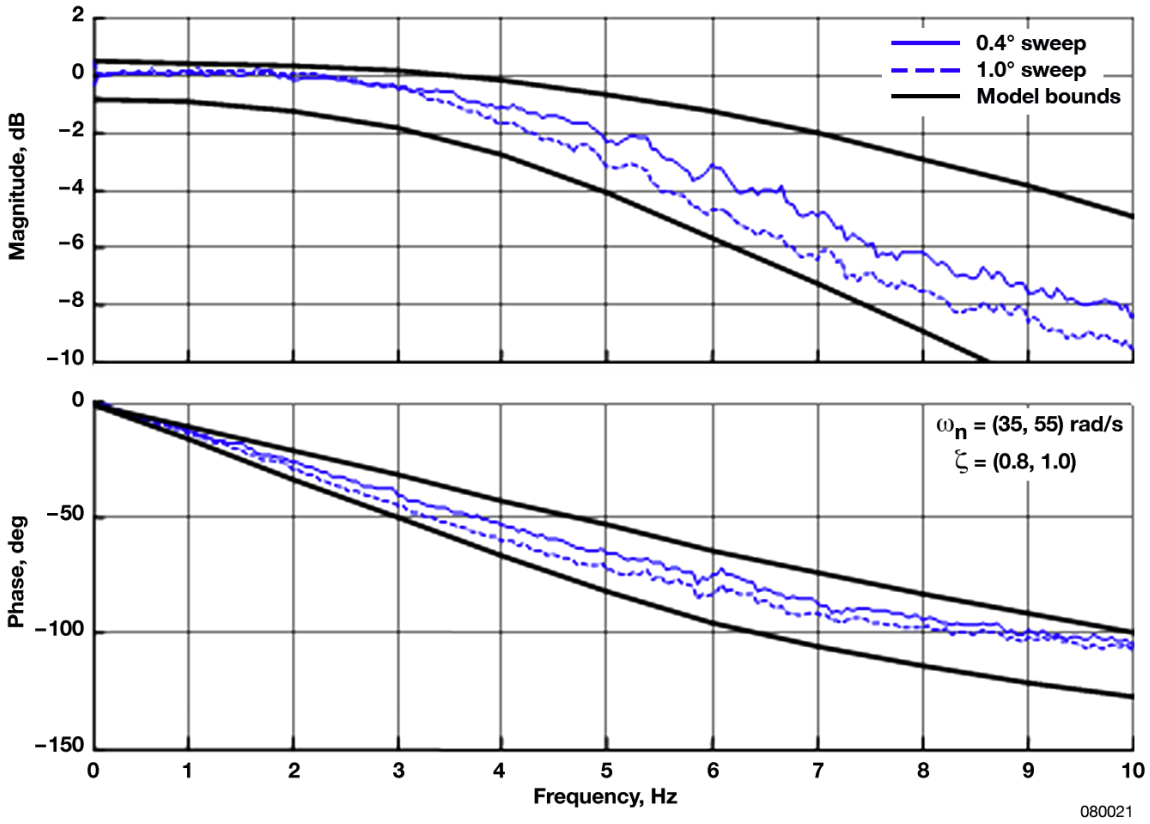

Figure 24. Test-derived rudder frequency response compared with second-order model bounds.

In general, the actuator performance derived from the characterization tests was found to be more consistent across ship-sets, whereas the ATP data did not show this trend. After further discussion with the actuator manufacturer, it was determined that the test setup for the ATP did not accurately reflect the installed configuration. This finding provided an additional rationale for updating the second-order model parameter bounds based on the characterization test results from flights 2 and 3. Figure 25 compares the left wing frequency response of an uninstalled ATP actuator with that of the vehicle 2 installed configuration. The ATP setup included surface inertia forces, and both cases were unloaded.

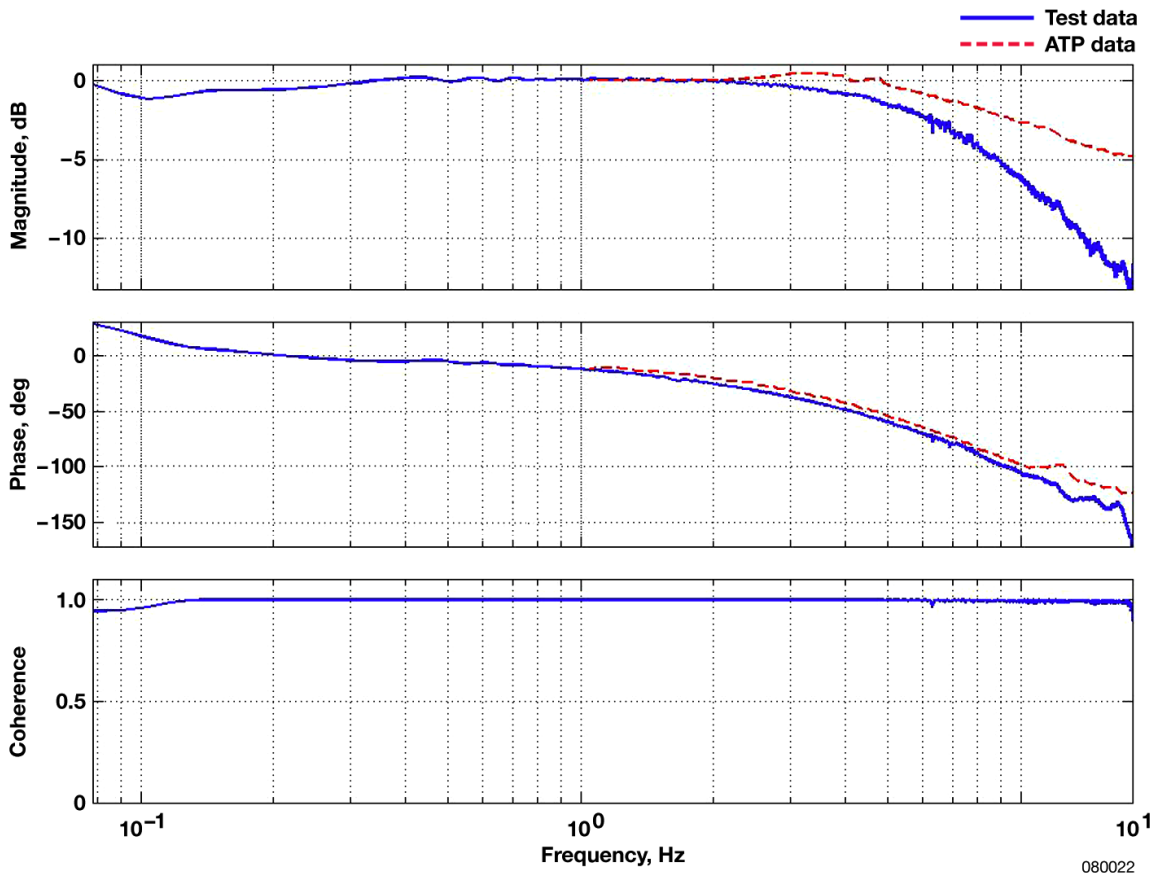

Figure 25. Left wing frequency response of uninstalled actuator (acceptance test program) compared with the left wing frequency response of the vehicle installed actuator.

3.1.2 Nonlinear Elements of Second-Order Models

The basic second-order actuator model captured the performance of the EMA in a general sense. Model elements were added to this basic model, however, to cover other details that have potential stability or performance implications. Figure 26 illustrates these additional elements, which include rate and position limiting, command error, quantization, free play, and compliance.

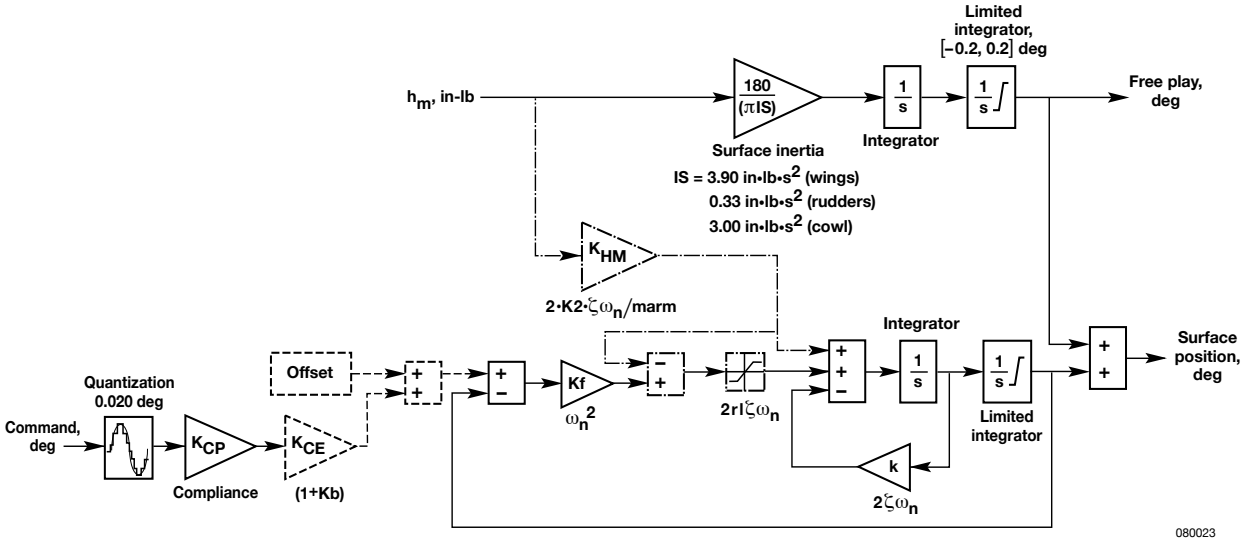

Figure 26. Modified second-order electromechanical actuator model with nonlinear elements.

3.1.2.1 Rate and Position Limiting

To provide accurate simulation of EMA performance, particularly in the presence of large commands, rate and position limiting had to be modeled. A variation of the basic second-order model had been produced for this purpose by Fred Lallman of NASA Langley Research Center. The implementation had two principal features. First it allowed the rate limit to be a function of load (that is, hinge moment). Referring to the dashed-dot elements of figure 26, the parameter *rl* represents the unloaded rate limit. The gain, *K2*, represents the slope of the rate curve with respect to load. This slope was estimated based on ATP data and has units of deg/(s•lb). This gain necessitated the division by the actuator spindle moment arm (marm), which converted the hinge moment to the appropriate linear force.

The other principal feature of this second-order model enforced the rate limit by limiting the velocity command, as opposed to the acceleration. With the load included, the velocity command has a value of $2rl\zeta\omega_n + 2K2\ \ h_m\zeta\omega_n / \text{marm}$ or $2\zeta\omega_n(rl + K2\ \ h_m / \text{marm})$, in which h_m is the hinge moment. Thus in a steady state, the velocity is limited to $(rl + K2\ \ h_m / \text{marm})$.

3.1.2.2 Command Error

An additional detail of the modified second-order model was the command error, which was intended to cover steady-state errors in the actuator position. Indicated by the dashed blocks in figure 26, the command error was modeled as a linear function of command, which was defined by a slope $(1 + Kb)$ and a bias (offset). Steady-state errors may arise because of inaccuracies in the actuator controller. The majority of errors seen in the Hyper-X system, however, were caused by uncertainty in the calibration curves that translate the autopilot control command (in degrees) to the actuator command (in volts) and in turn, the actuator position feedback (in volts) to the surface position (in degrees).

On flight 1, the model parameters, *Kb* and offset, were based on error estimates illustrated in figure 27. From the surface calibration test, a set of command and feedback data was gathered. The command data were used to obtain a third-order command calibration curve (degrees to volts). The actuator feedback position data were used to obtain a third-order feedback calibration curve (volts to degrees). A set of nominal command angles was defined as the input for the command curve, which resulted in a set of EMA command voltages. These voltages were then used as the input for the feedback curve. The resulting feedback angles were subtracted from the nominal command angles. A linear equation was fitted to this set of error data. The *Kb* parameter was derived from the slope of this equation, and the offset was derived from the bias. For each surface calibration test conducted on the vehicle, a distinct linear equation was generated.

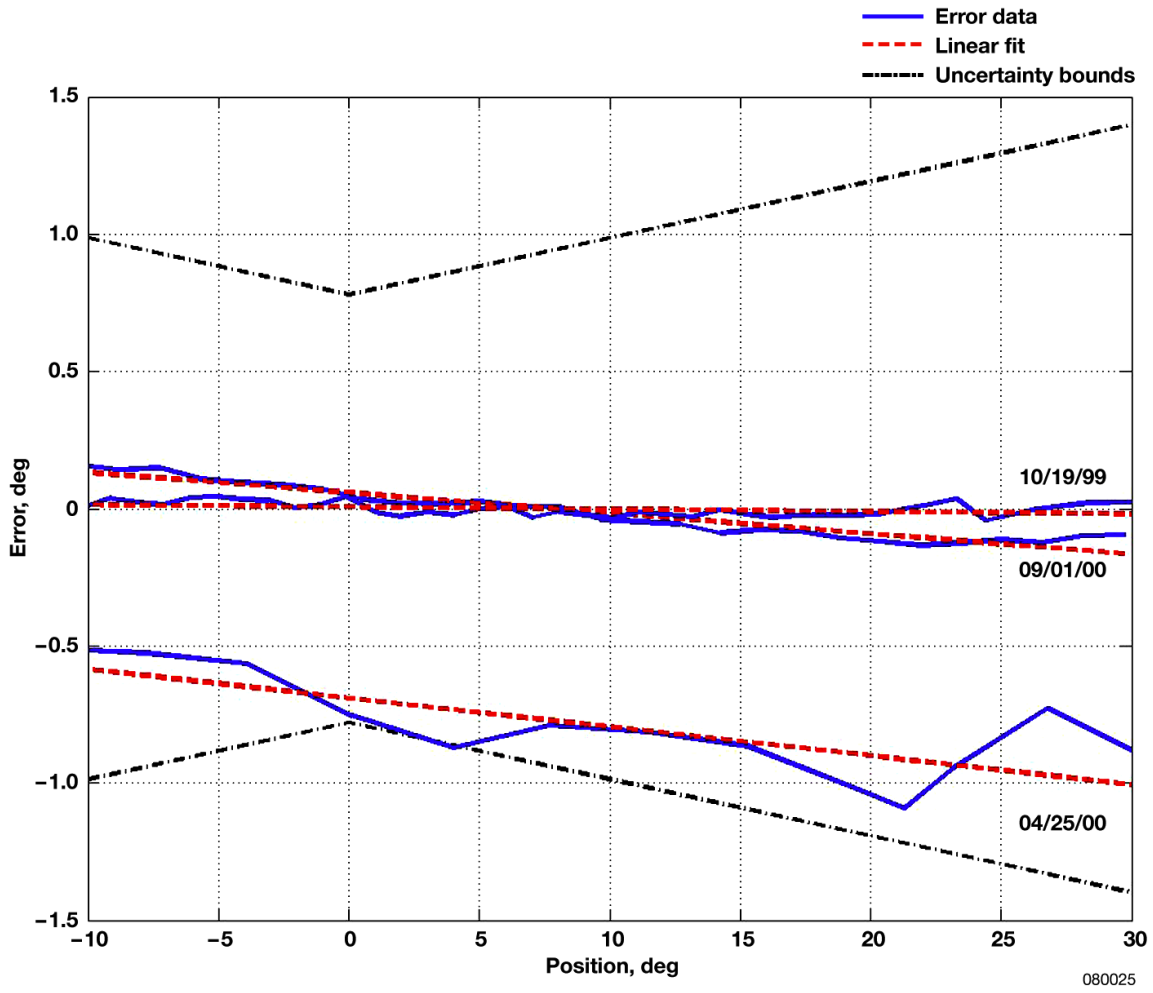

Figure 27. Hyper-X Research Vehicle 1 command error limits derived from three sets of calibrations.

For Monte Carlo analysis, the *Kb* and offset boundaries were determined in a systematic manner. Out of all the linear error curves for the four control surfaces, the magnitude of the highest slope and offset was selected. Four linear equations were then generated using the selected slope

and offset: minimum slope and minimum offset, minimum slope and maximum offset, maximum slope and minimum offset, maximum slope and maximum offset. Next, a set of nominal surface deflection angles was used as input to these four equations to find the corresponding error values. This calculation produced four sets of error data that corresponded to each nominal angle. The highest and lowest error values were then chosen as the upper and lower boundary points. These limits were applied to all control surface actuator models. As the calibration tests were refined by using more accurate instruments such as a laser tracker, the bounds for *Kb* and offset were smaller for the third vehicle, as shown in figure 28. When command error is modeled, several calibration tests should be performed for each vehicle so that the uncertainty derived is attributed to polynomial fit errors, and not to test measurement errors.

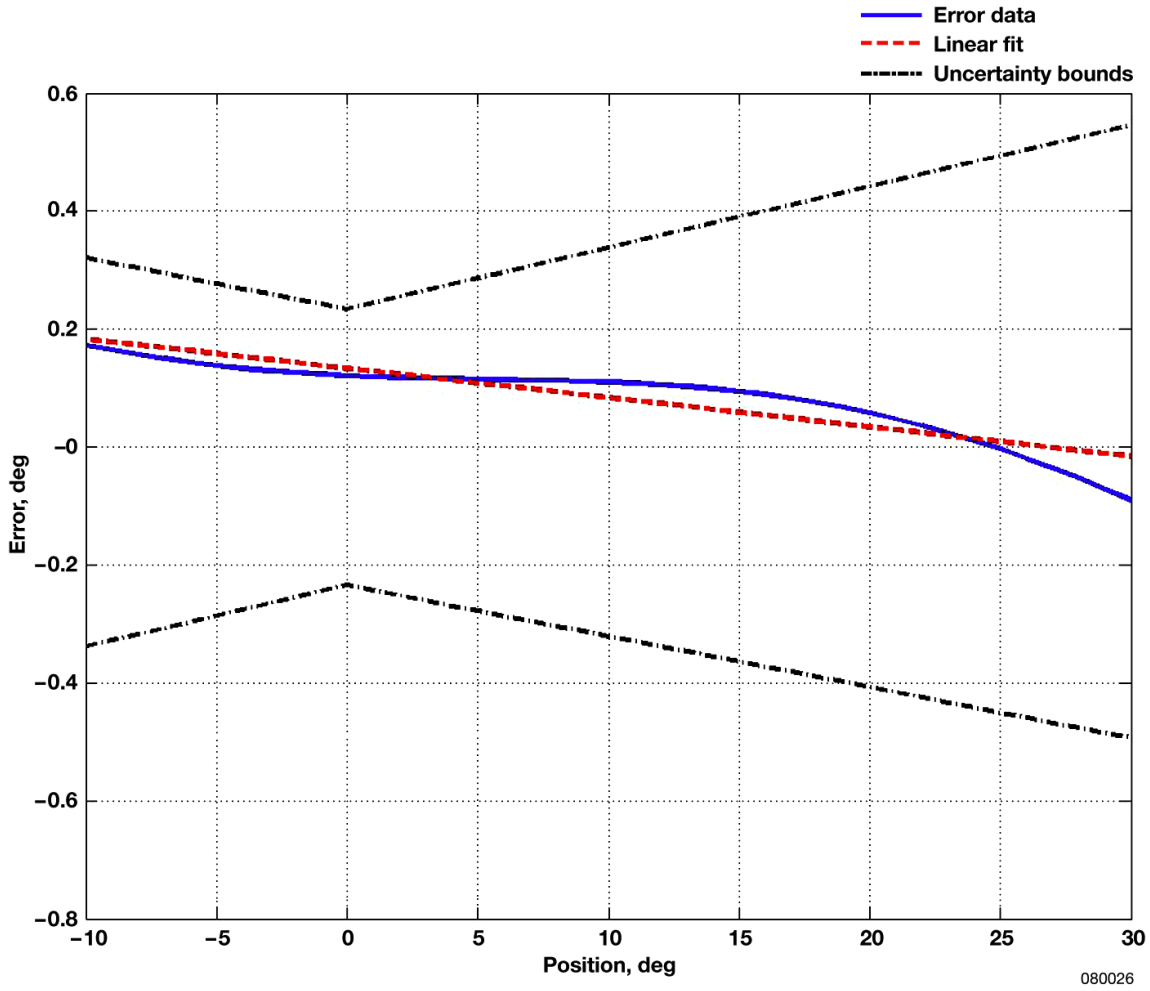

Figure 28. Flight 3 command error limits derived.

In addition to calibration errors, the actuator command is also subject to quantization, which is driven by the resolution of the digital to analog (D/A) converter used in FMU electronics. For the D/A cards used on the HXRV, in consideration of each control surface's range of motion,

quantization was modeled to be on the order of 0.020°, which was verified using the slow ramp tests and the static threshold tests.

3.1.2.3 Free Play

In practice, an installed actuator is subject to free play, which is unrestricted motion caused by slop in the gears and linkages found within the actuator and in the coupling to the control surface. This characteristic predominantly comes into effect at load reversal (that is, when the hinge moment changes sign). In the high-fidelity model, free play amounts to a nonlinearity in the actuator as coupling stiffness (or compliance). For the second-order model, pure free play was modeled using an additional second-order system, which amounts to a double integration of the hinge moment divided by the control surface inertia (fig. 29). Based on the free play and compliance test data, the free play angle in the Hyper-X actuation system was on the order of 0.200°. This value was used as the upper and lower boundaries for the limited integrator. Moments of inertia, calculated from computer-aided design (CAD) models of the control surfaces, represent the inertia about the rotational axis of each surface.

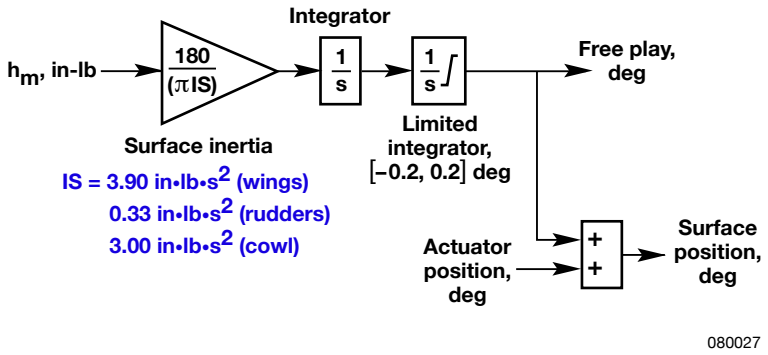

Figure 29. Free play subsystem.

3.1.2.4 Compliance Correction

The final element of the modified second-order model is the compliance correction, which is a simplified representation of the total actuator compliance. Any compliance in the system has the potential of changing the gain of the system. If not included in the model, compliance may result in inaccuracies in stability margin predictions. As discussed previously, inadequate estimation of compliance outside the HXLV actuator feedback loop contributed to the Hyper-X flight 1 mishap.

From a modeling standpoint, the compliance correction was modeled as an additional gain, K_{CP}, on the actuator command (fig. 26). This gain was adjusted to match test results and was varied as a function of load. Compliance uncertainty bounds were determined based on a Monte Carlo frequency response analysis using the linear actuator models (see section 3.4).

3.2 Construction of High-Fidelity Actuator Models

The actuator manufacturer should be involved in the construction of high-fidelity models. The importance of this approach should not be underestimated. Data for the electronics or mechanical elements of the actuator may not be available to the user because of the proprietary nature of this technology. The omission of such elements may result in significant loss of accuracy. If access to the manufacturer is not possible, then the development of these models will need to be based on a large set of test data with a high percentage of parametric uncertainty (10 to 30 percent) applied to the models.

For the Hyper-X program, the original high-fidelity continuous model was provided by Moog, Inc. It contained compliance, load, Coulomb friction, force, controller electronics, and motor subsystems. The model was designated as the high-order actuator continuous model version 1.0 (HOAC1). Figure 30 shows a top-level diagram of this model. Although the model was quite detailed and matched well for small amplitude commands, it did not compare well with the installed actuator test data (fig. 31). Several improvements were made as part of the return-to-flight activities. The compliance element was modified to reflect the compliance test data, and a hysteretic damping element was investigated to determine whether it was required for the high-fidelity model.

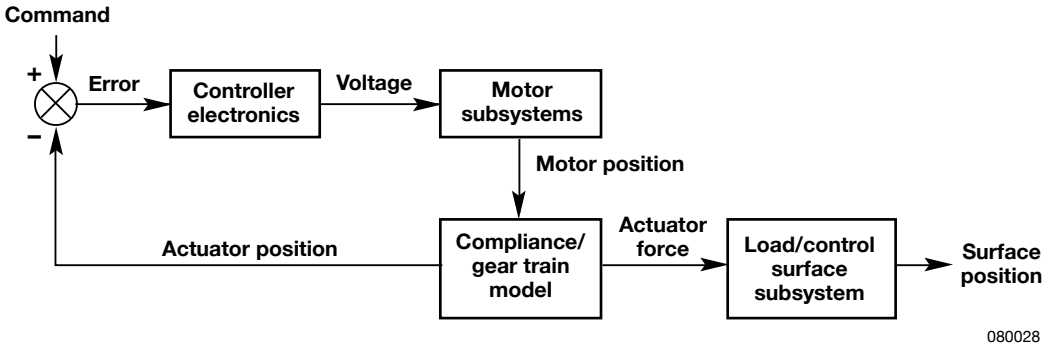

Figure 30. Top level version of the high-order actuator continuous (HOAC1) model.

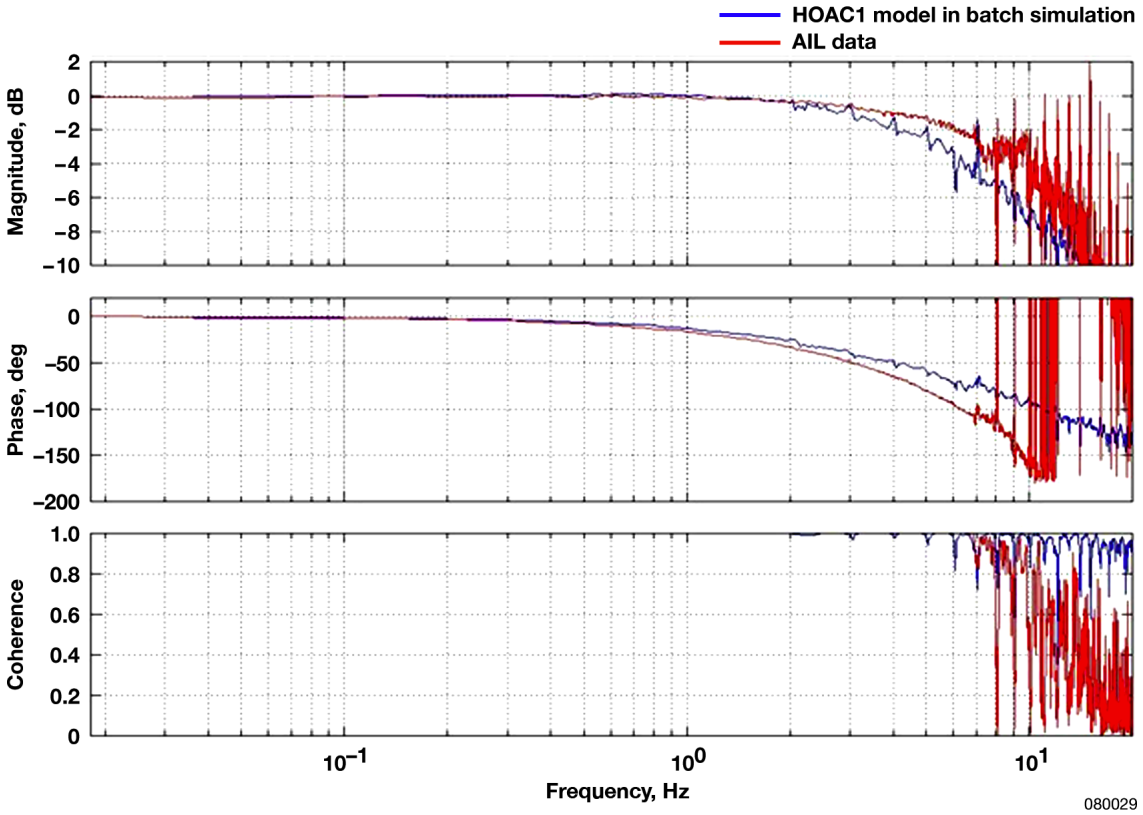

Figure 31. Frequency response of manufacturer's high-order actuator continuous (HOAC1) model compared with frequency response of installed flight actuator.

3.2.1 Modeling Compliance

Compliance in a high-fidelity actuator model is captured in the gear train model, which couples the load from the control surface to the actuator motor. Figure 32 illustrates a typical gear train model. The inputs and outputs for this figure are associated with figure 30.

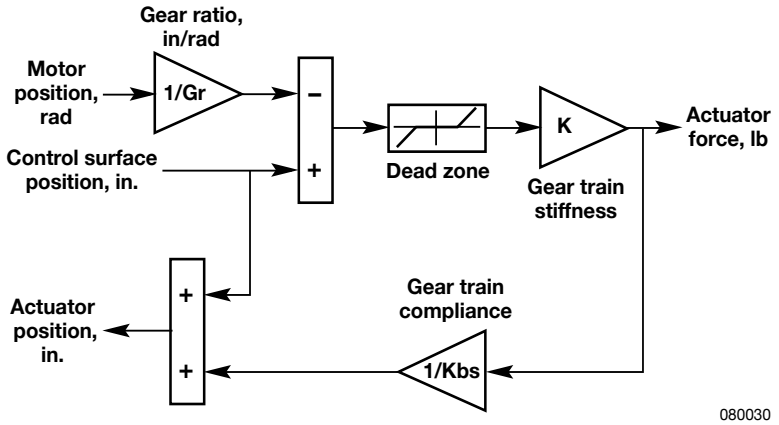

Figure 32. Typical actuator gear train model.

In the typical model, the difference between motor and control surface position, which is essentially deformation in the gear train, is passed through a dead zone (that is, free play) before being multiplied by the gear train stiffness. The result is that the effective force is transmitted from the actuator to the control surface. This same force is then used to compute the component of the gear train deformation that is caused by structural backup stiffness. This component is added to the control surface position to modify the gain of the actuation system. The range of the dead zone should reflect the free play in the system.

The project team recognized the importance of accurately modeling compliance. Therefore, the model illustrated in figure 32 was improved for flights 2 and 3. The following changes were made:

1. The stiffness of the gear train and linkages was modeled using the total compliance data (actual total compliance curve, figure 16). This type of implementation allows the variation in force with deflection to be accurately captured.
2. The actuator compliance within the servo loop was modeled using the LVDT compliance data (LVDT feedback curve, figure 16). This method also allows variation in compliance with load to be accurately captured.
3. The pure free play subsystem was removed, as it was already captured within the gear train stiffness and actuator compliance models. Figure 33 illustrates these modifications.

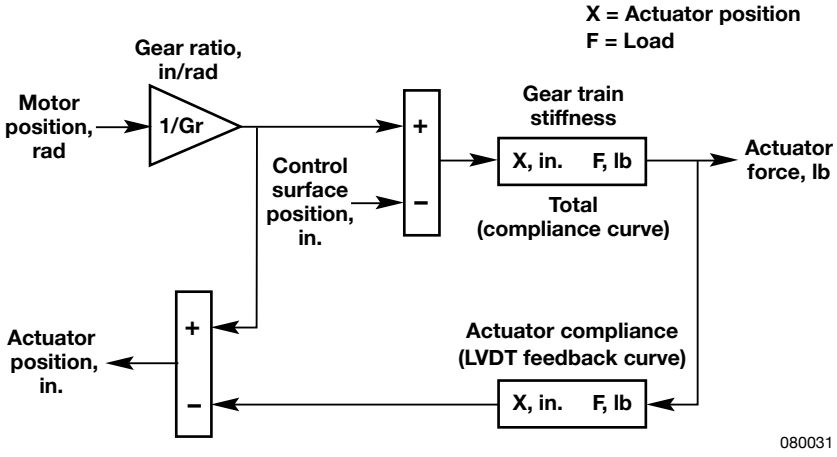

Figure 33. Enhanced gear train model.

The data supporting these model enhancements, specifically the gear train stiffness and actuator compliance, were provided through actuator compliance testing. The load curves compared with the deflection curves from these tests demonstrate the characteristic hysteresis loop seen in figure 34 (solid line), which was measured at the root of the control surface.

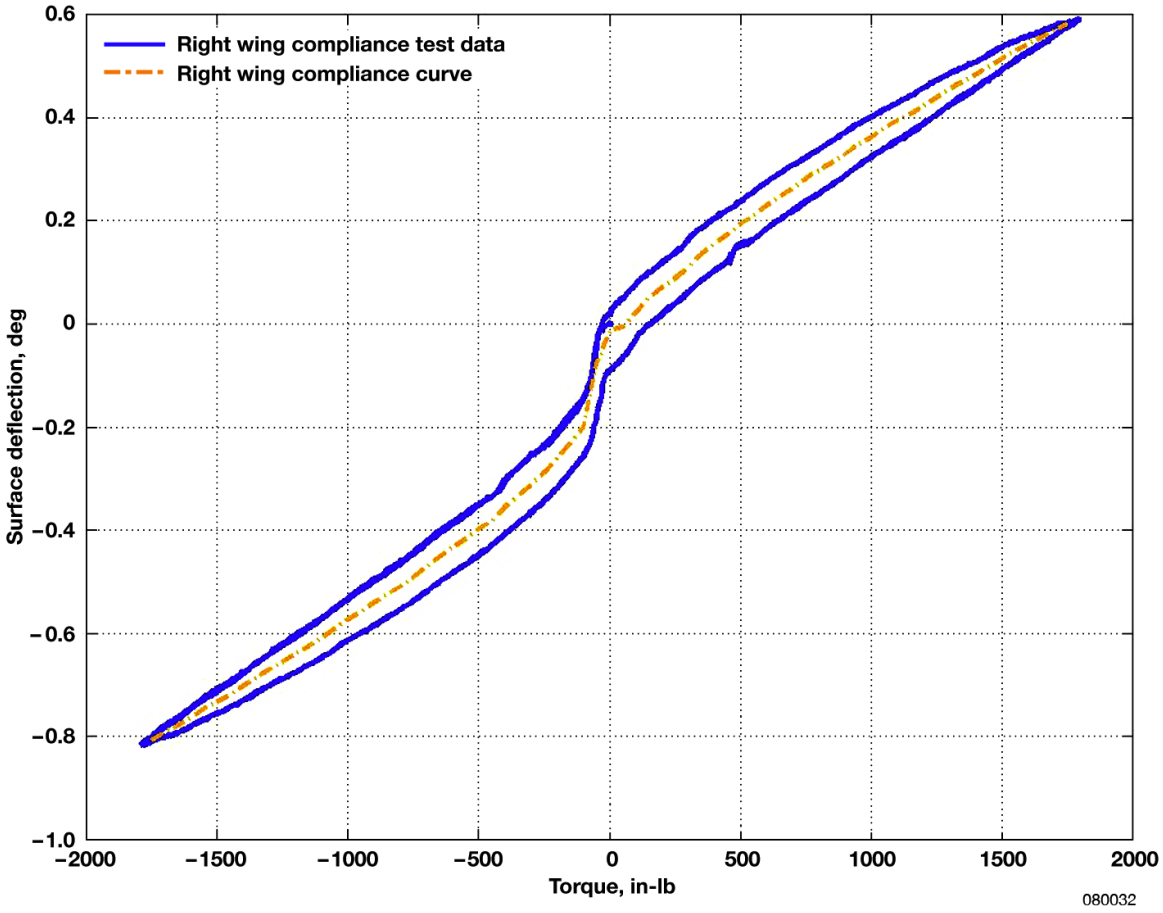

Figure 34. Deflection as a function of torque from vehicle 2 right wing compliance test.

The loop illustrated in figure 34 shows the total gear train characteristics of the Hyper-X actuators. It accounts for the compliance inside and outside the servo loop. In general, the bisection of the hysteresis loop represents the compliance of the system, indicated by the dashed line in figure 34. The area or thickness of the loop is the level of hysteretic damping. Note that the compliance curve is nonlinear, and strictly speaking, there is no pure free play.

To determine the gear train stiffness function (fig. 33), scripts were written to smooth the data and calculate the bisecting curve. Two methods of representing this curve in the actuator model were considered. The first method captured the curve in tabular form. The second method modeled the curve as the combination of three linear segments: the first segment to capture the relatively high slope characteristic of the free play region, the second segment for compliance at moderate load, and the final segment for compliance at high load. In the end, the second method was chosen, because it was easier to parameterize for use in Monte Carlo simulation analysis. Figure 35 illustrates the mean, upper, and lower bounds of the three-segment model compared with the compliance curves derived from HXRV 2 compliance testing for the total gear train stiffness. Torque was converted to force by using the geometry of the servo crank arm. The actuator compliance function (fig. 33) was developed in a similar manner using the LVDT servo loop compliance curve (fig. 16).

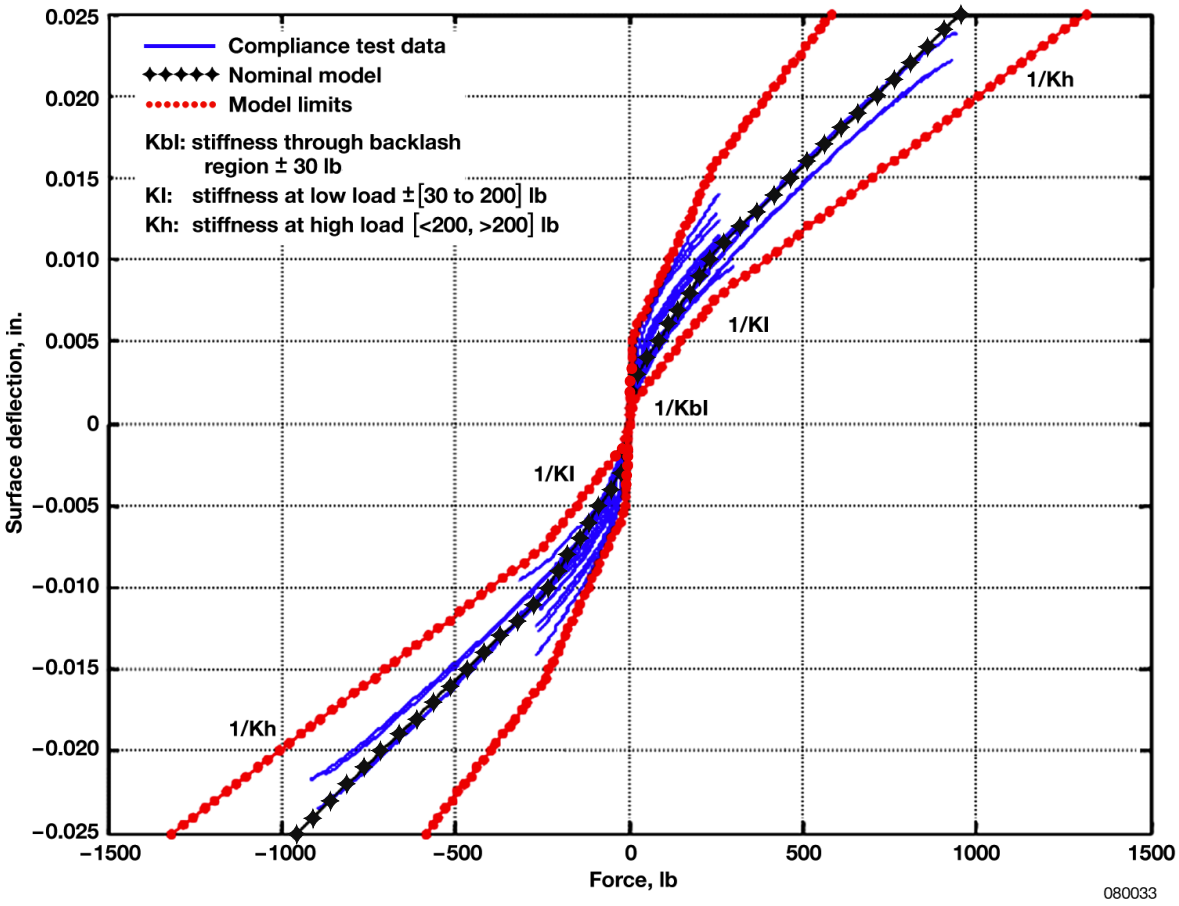

Figure 35. Total gear train compliance model derived from compliance test data curves.

3.2.2 Modeling Hysteresis

As discussed previously, dynamic hysteresis in the actuator is caused by hysteretic or structural damping. Dynamic hysteresis can be simulated by adding the appropriate level of damping to the gear train model. Figure 36 illustrates this model addition. The inputs and outputs of this figure are associated with figure 30.

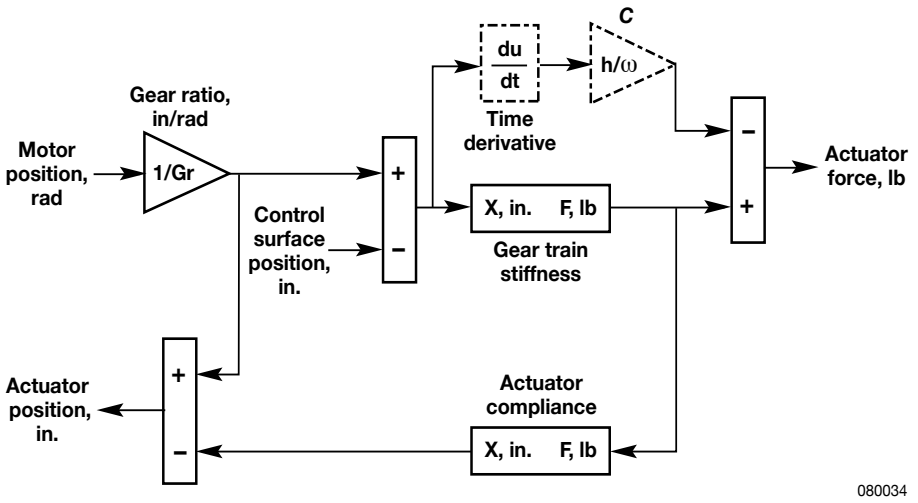

Figure 36. Gear train model with hysteretic damping.

Theory holds that hysteretic damping can be approximated as viscous damping with a damping coefficient of h/ω, in which h is the hysteretic damping constant and ω is the frequency of the load (ref. 9). As such, damping is inversely proportional to frequency and the hysteresis loop is invariant with frequency. To capture the impact of hysteretic damping on actuator performance, h must be estimated. With h in hand, a frequency response analysis of the actuator model can be performed. In turn, the results can be compared to the response estimated with $h = 0$.

Hysteresis tests performed on vehicle 2 were designed with sinusoidal load inputs at two specific frequencies: low, 0.0785 rad/s, and high, 0.785 rad/s. For sinusoidal loads, the hysteretic damping constant can be estimated in a straightforward manner as $A / \pi P_k^{\,2}$, in which A is the area inside the hysteresis loop and P_k is the peak amplitude of the deflection (ref. 9).

This calculation was performed, for example, for the right wing on the low-frequency and high-amplitude hysteresis test case known as rw13. Figure 17 illustrates the hysteresis loop resulting from this test. The area inside the loop was estimated at 4.88 in-lb. The amplitude of deflection was approximately 0.02155 in., resulting in

$$h = A / \pi P_k^{\,2} = (4.88) / 3.14159 \bullet (0.02155^2) = 3344.84 \text{ lb / in.}$$

To verify this estimate of the hysteresis damping constant, a modified version of the actuator model was developed for temporary use. The changes impacted the coupling subsystem, as illustrated in figure 36. Basically, the coupling force was augmented to include the hysteretic damping term. The stiffness of the coupling is nonlinear, so the damping term was scaled by a stiffness ratio: current stiffness divided by the average stiffness for the range of motion anticipated. Further, to simulate the actual hysteresis test setup, the motor subsystem and actuator control logic were removed. The resulting model consisted of only the coupling and load subsystems.

Test rw13 was replicated in the simulation by applying the test load profile to the modified actuator model. As illustrated in figure 17, the simulated and test position were in excellent agreement. Next, the high frequency test case was simulated by updating only the load frequency (that is, the same *h* was used). Although the TS90 sensor used for gathering the data was reaching its frequency response limit, the actual hysteresis loop was tracked fairly well by the simulated model, as shown in figure 18.

3.3 Impact on Frequency Response

With the hysteresis model verified, the impact of hysteresis on actuator frequency response could be investigated. Severe cases of hysteresis could have an impact on magnitude and phase in the bandwidth of the control system, leading to inaccurate stability margin estimates. Sinusoidal commands of specific frequencies were used with the enhanced actuator model to estimate the frequency response. For each case, the frequency in the hysteresis damping term was updated for consistency with the command frequency. Magnitude and phase was then estimated by comparing command and position response. Overall, the impact of hysteresis on frequency response was found to be negligible, as demonstrated in figure 37. For this reason, hysteresis was not included in the final Hyper-X high-fidelity actuator models.

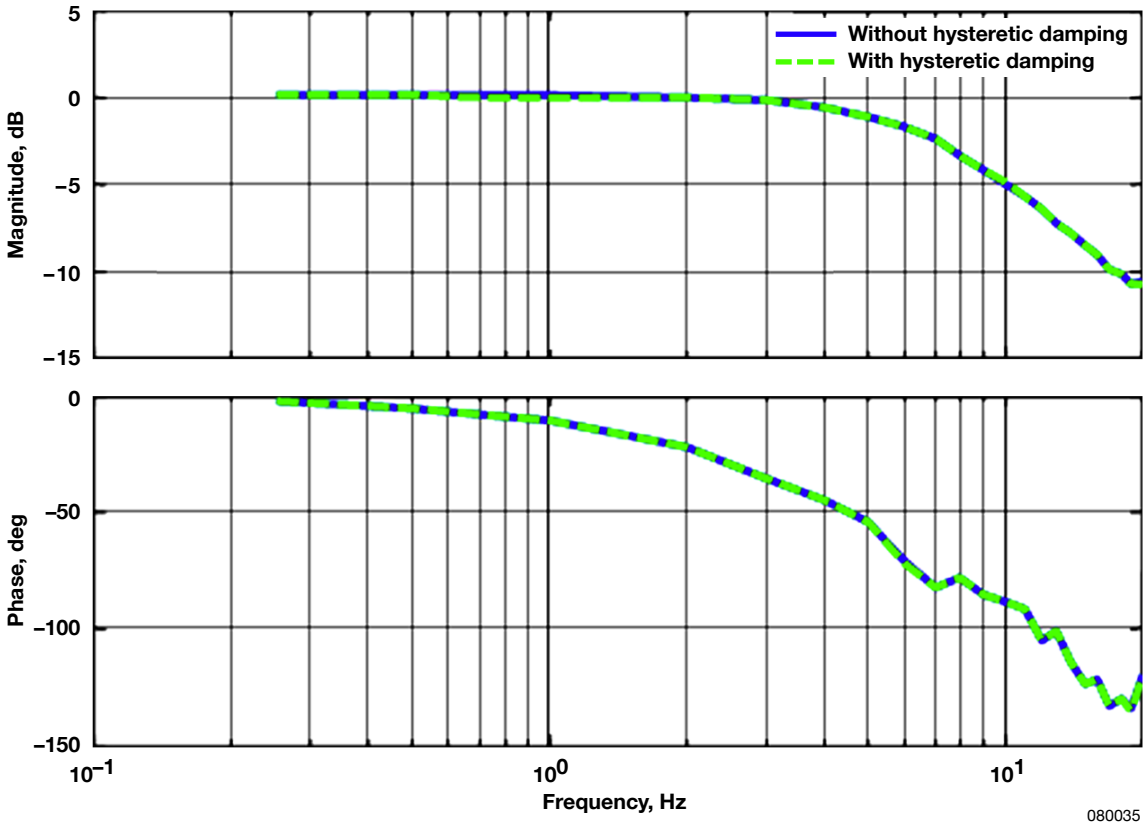

Figure 37. Right wing frequency response curves with and without hysteretic damping.

3.4 Construction of Linear Models

For the first flight, a simplified second-order transfer function derived from a second-order actuator model was used for linear analysis. After the mishap, this linear model was determined to be inaccurate. For the second and third flights, a different technique was used to construct the linear models. They were derived from the nonlinear high-fidelity model through the use of the low-order equivalent system (LOES) approach.

For this method, the frequency response of the high-fidelity actuator model was determined by applying a time history input of a single frequency and calculating the gain attenuation and phase shift of the output response. A range of single frequency signals were input to the high-fidelity discrete model to build up the gain and phase response in the MATLAB® Simulink® (both registered trademarks of The MathWorks™, Inc., Natick, Massachusetts) environment. The MATLAB® function "invfreqs" was then used to determine a second-order transfer function from the frequency response of the high-fidelity model. Although this process required many iterations and was time-consuming, the linear model that was constructed was highly accurate.

4.0 MODEL IMPLEMENTATION AND INTEGRATION INTO THE SIMULATION

This section describes the different methods used to implement the actuator models into software for use in simulation. Comparisons between simulation and flight data are also provided. Problems and lessons learned from the modeling and simulation integration efforts are presented at the end of the section.

4.1 Hyper-X Simulation Description

The Hyper-X project developed two HXRV simulations: a high-fidelity 6-DOF nonlinear simulation model of the X-43A vehicle, and a simplified linear model used for control law design and analysis. The actuator models developed for the Hyper-X project were used in these tools to assess their impact on vehicle performance.

The 6-DOF simulation was based on the standard Dryden Flight Research Center (DFRC, Edwards, California) simulation architecture (ref. 10) and contained detailed system models of the flight control laws, vehicle aerodynamics, actuators, and sensor and time delay implementation. Uncertainty models were provided for each of these items. The nonlinear simulation consists primarily of a FORTRAN code with a graphical user interface written in C. This simulation can incorporate C auto-code generated by the Real Time Workshop® (The MathWorks™, Inc.) from Simulink® models. The nonlinear simulation was used primarily to assess the time history performance of the vehicle for nominal and Monte Carlo missions. When connected to the aircraft, it was used as a test tool to validate the vehicle hardware and software systems.

The linear HXRV model consists of linearized 6-DOF system models. The linear model and analysis tools were built up in the MATLAB® and Simulink® environments. Each of the linear models has an associated uncertainty model, which allowed for a linear Monte Carlo analysis.

The linear analysis tools were used primarily for control law design and linear stability margin estimation for nominal and Monte Carlo cases. Both the linear models and 6-DOF simulation were exhaustively compared and validated in terms of the vehicle time history and frequency responses.

4.2 Types of Hyper-X Research Vehicle Actuator Models Used For Mission Analysis

As stated in section 3.0, nine actuator models were used throughout the history of the Hyper-X program to represent the HXRV actuators. Two of the models were constructed in the continuous time domain and used for verification and validation activities. Four of the models were constructed in the discrete time domain and incorporated into the DFRC nonlinear simulation. The remaining three actuator models were linear and used in the linear analysis tools. Table 5 describes each actuator model and its usage. For discussion purposes, the high-order models referred to in this section are the high-fidelity models.

Table 5. Types of actuator models used for Hyper-X simulation analyses.

Model name	Acronym	Description	Implementation	Usage	Flight
Low-order actuator continuous model	LOAC	Simplified second-order model of actuator	Continuous	Model validation	1
Low-order actuator discrete FORTRAN model	LOADF	Discrete FORTRAN implementation of LOAC	200-Hz discrete	Nonlinear simulation	1
Low-order actuator discrete auto-code model	LOADA	Discrete Simulink® model of LOADA used for auto-coding	800-Hz discrete	Nonlinear simulation	2,3
High-order actuator continuous model version 1.0	HOAC1	High-fidelity model provided by vendor	Continuous	Model validation, troubleshooting	2,3
High-order actuator discrete model version 2.0	HOAD2	Discrete implementation of HOAC1	10,000-Hz discrete	Nonlinear simulation	2,3
High-order actuator discrete model version 3.0	HOAD3	Updated version of HOAD2 that had been adjusted to match test data	10,000-Hz discrete	Nonlinear simulation	2,3
Simplified low-order actuator continuous model	SLOAC	Simplified version of the LOAC model	Continuous	Linear analysis	2,3
High-order actuator linear model	HOALM	Linearized version of HOAD3	10,000-Hz discrete	Linear analysis	2,3
Low-order equivalent system actuator model	LOES	Low-order equivalent system representation of the HOAD3 model frequency response	Continuous	Linear analysis Monte Carlo	2,3

4.2.1 Continuous Time Domain Models

Two actuator models were developed for the HXRV in the continuous time domain. These continuous models were used for verification and validation work with the test data and formed the basis for the discrete models that were implemented in the nonlinear simulation. Both continuous models were constructed in Simulink® and were referred to as the low-order actuator continuous (LOAC) model and the high-order actuator continuous (HOAC1) model.

The LOAC model, as described in sections 3.1.1 and 3.1.2, consisted of a simplified second-order representation of a generic actuator, which was modified to simulate the performance

characteristics of the HXRV actuators. The actuator frequency and time history responses from the test data were used to validate the LOAC model after it was constructed. It was developed early on in the history of the Hyper-X program and remained the "truth" actuator model until the HOAC1 was obtained from the manufacturer and validated after the mishap.

As described in section 3.2, HOAC1 is a Simulink® model of the actuator system, which represented the individual actuator components in detail. The model, provided by Moog, Inc., did an excellent job of matching the response to small inputs. It did only an adequate job, however, of matching the time history and frequency response of the installed characterization test data. The project decided to create discrete implementations of the HOAC1 model and update it to better match the installed actuator performance.

4.2.2 Discrete Time Domain Models

A total of four separate discrete models were created for integration in the DFRC 6-DOF nonlinear simulation. Two of the implementations were based on the LOAC model, and the remaining two were based on the HOAC1 model. All were used for nonlinear analysis of the HXRV system performance.

4.2.3 Second-Order Discrete Time Domain Models

The first discrete implementation of the LOAC model was hand-coded in FORTRAN and referred to as the low-order actuator discrete FORTRAN (LOADF) model. The LOADF model was implemented in the simulation at a rate of 200 Hz. The second model was an 800-Hz discrete Simulink® implementation of the LOAC model referred to as the low-order actuator discrete auto-code (LOADA) model. The Real Time Workshop® was used to generate C code from the Simulink® implementation before simulation integration.

4.2.4 Second-Order Model Integration into Nonlinear Simulation

The LOADF model was developed from the LOAC model before the first flight. It was used in all nonlinear analyses leading up to the first flight attempt. After the first flight mishap, there was a desire to reexamine all of the HXRV models. The mishap investigation board had concluded that inadequate system modeling of the HXLV had contributed to the mishap. The HXRV was not a factor in the mishap, but the project expressed a desire to reevaluate all HXRV models to ensure that the same problems that occurred with the HXLV modeling were not present within the HXRV.

After the mishap investigation, the LOADF actuator model was compared in detail with the LOAC and was found to be deficient. Figure 38 shows that the LOADF implementation did not match the LOAC in time response, and figure 39 shows the frequency domain mismatches. It effectively added lead to the vehicle response by responding to a step command more quickly than the validated LOAC model. The problems with the LOADF model were traced to the use of a backwards Euler method for the integrators, improper handling of the position feedbacks, and use

of a 200-Hz implementation rate, which was not sufficient to model the actuator dynamics. The LOADF model implementation was inadequately validated against test data before the first flight, which resulted in a significant overprediction of the HXRV performance and open-loop stability margins by as much as 7 dB and 20° of phase.

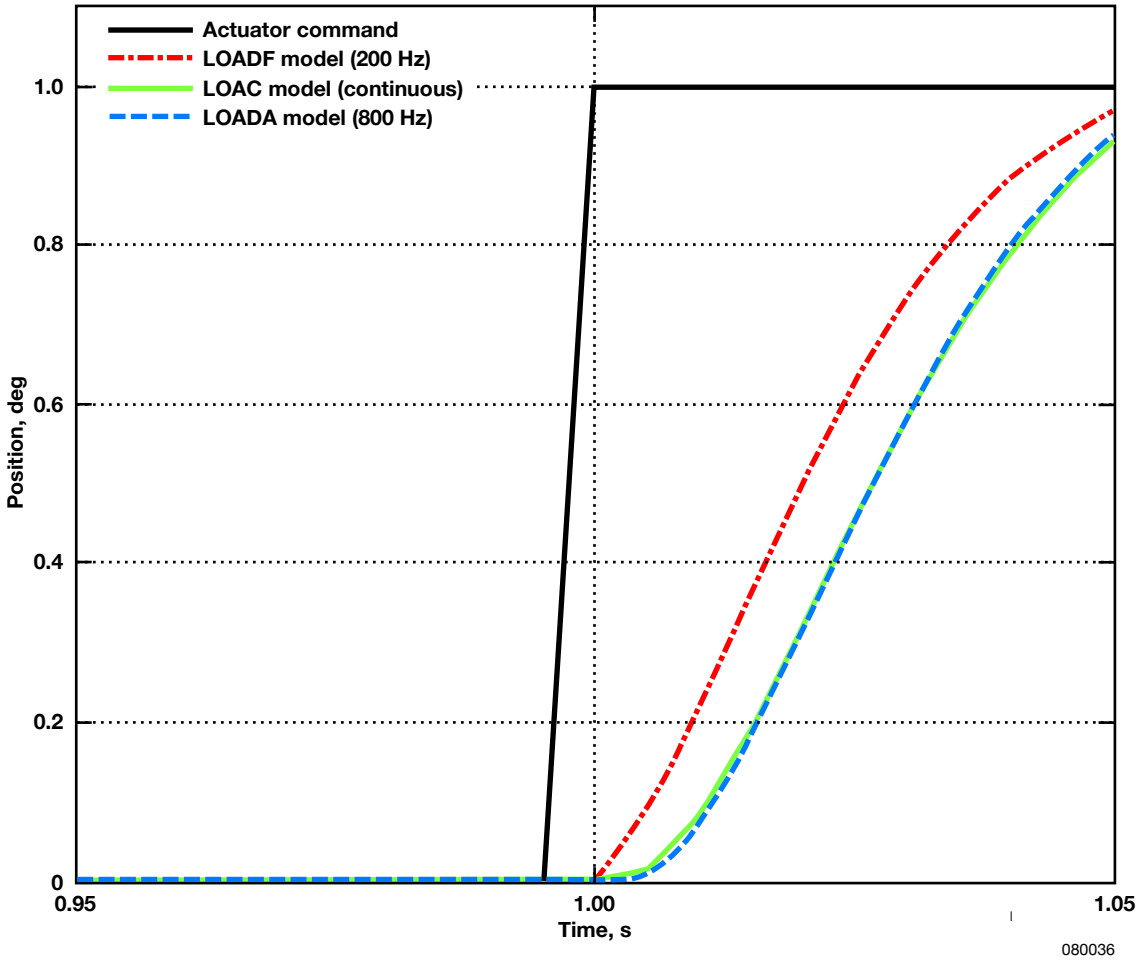

Figure 38. Step response curves for low-order actuator discrete FORTRAN, low-order actuator discrete auto-code, and low-order actuator continuous models.

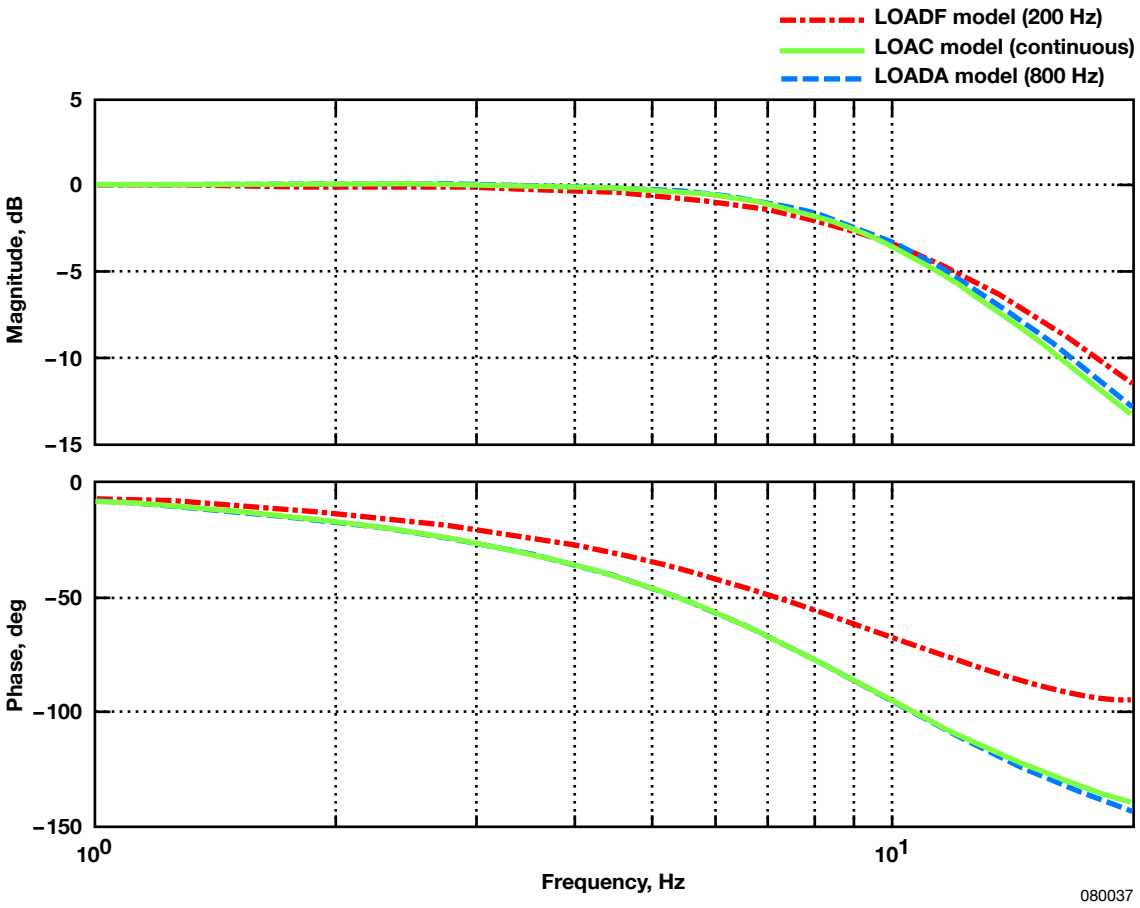

Figure 39. Frequency response curves for low-order actuator discrete FORTRAN, low-order actuator discrete auto-code, and low-order actuator continuous models.

The X-43A guidance, navigation, and controls team decided to create a discrete Simulink® model from the LOAC model for use in the nonlinear simulation. The discrete implementation became the LOADA model. In addition to improved fidelity, this decision had several advantages. The MATLAB® Simulink® environment simplified the direct comparison between the LOADA and LOAC models. Model changes were easier to implement in the Simulink® environment than in the FORTRAN hand code. The Real Time Workshop® made it possible to quickly incorporate any LOADA model updates into the simulation by automatically generating C code, which could be easily incorporated into the nonlinear simulation.

Various implementation rates were studied for the LOADA model. Increasing the rate at which the LOADA model operated increased the fidelity of the comparison with the continuous model. The simulation runs at an update rate of 200 Hz, and running the model at a faster rate can greatly slow down the simulation execution. Model implementation rates greater than 200 Hz would require that the model be called multiple times for each simulation frame. For example, a 1000-Hz implementation rate for the LOADA model would require that it be called five times for each 200-Hz simulation frame.

Table 6 shows the error between the LOAC and various rate implementations of the LOADA model. An implementation rate of 800 Hz was chosen for the LOADA model, as it was close in performance to the LOAC model, and there appeared to be minimal advantages to increasing the rate. Table 7 shows that a nominal nonlinear simulation run took only 10 s longer when the 800-Hz LOADA model was used compared with the 200-Hz LOADF implementation. Figures 38 and 39 compare the performance of the LOADA model with that of the LOAC model in the time and frequency domains. The performance of the high rate LOADA model closely mirrored that of the LOAC model.

The low-order actuator models did an adequate job of replicating the large-scale actuator time history and frequency response, once they had been tuned to the installed actuator frequency and damping ratio characteristics. In addition, the damping and natural frequency uncertainties initially used for the low-order actuator model more than covered the boundaries of the expected in-flight actuator performance. These uncertainties were valuable for Monte Carlo analysis in terms of assessing the sensitivity of the vehicle performance to actuator characteristics.

Table 6. Implementation rate and error of LOADA and LOADF relative to LOADC.

Model	Implementation rate	Average error	Standard deviation	Maximum
LOADF	200 Hz	0.0284	0.0802	1.1627
LOADA	200 Hz	0.0098	0.0276	0.2797
LOADA	400 Hz	0.0049	0.0137	0.139
LOADA	800 Hz	0.0024	0.0068	0.0693
LOADA	1,000 Hz	0.0019	0.0055	0.0554
LOADA	2,000 Hz	0.001	0.0027	0.0276

Table 7. Nominal Hyper-X Research Vehicle simulation run time of discrete actuator model implementations.

Model	Execution rate, Hz	Time, s
LOADF	200	248
LOADA	800	258
HOAD2	10,000	502

4.2.5 High-Fidelity Discrete Time Domain Models

Another model used in the nonlinear simulation was a 10,000-Hz discrete implementation of the HOAC1 model called the high-order actuator discrete 2.0 (HOAD2) model. It was also generated in C code using the MATLAB® Real Time Workshop®. The HOAD2 contained additional elements that replicated the flight and test environments, such as time delay, quantization, and noise, which were not in HOAC1. As more EMA characterization test data became available,

HOAD2 was updated and evolved into HOAD3, which was used for all simulation work before the second and third flights.

4.2.6 High-Fidelity Model Integration into the Nonlinear Simulation

The HOAC1 model had several features that greatly increased the fidelity of the comparison with the installed actuator characteristics. In stand-alone analysis, the HOAC1 model had shown the ability to accurately replicate the actuator response for very small amplitude changes at low frequencies (0.005 deg/s). Small nonlinearities in the actuator performance were believed to have caused the actuator dither, so it was desirable to implement the HOAC1 model in the closed-loop nonlinear simulation in an attempt to understand this phenomenon.

After the mishap, the model was converted into the HOAD2 model and incorporated into the simulation. Implementation rates between 10,000 and 100,000 Hz were examined and compared with the HOAC1 model response. Figure 40 compares the HOAC1 and HOAD2 models at various implementation rates. These higher rates resulted in a significant time penalty in the nonlinear simulation. The decision was made to use 10,000 Hz as the implementation rate for HOAD2, as it approximated the small amplitude input response and did not prohibitively extend the time for a nonlinear simulation run. The goal was to keep the total batch simulation implementation running faster than the real-time simulation so that the higher rate model could be implemented in the real-time AIL test environment. Also, the simulation run time was considered a more important factor than the slight loss of accuracy in amplitude.

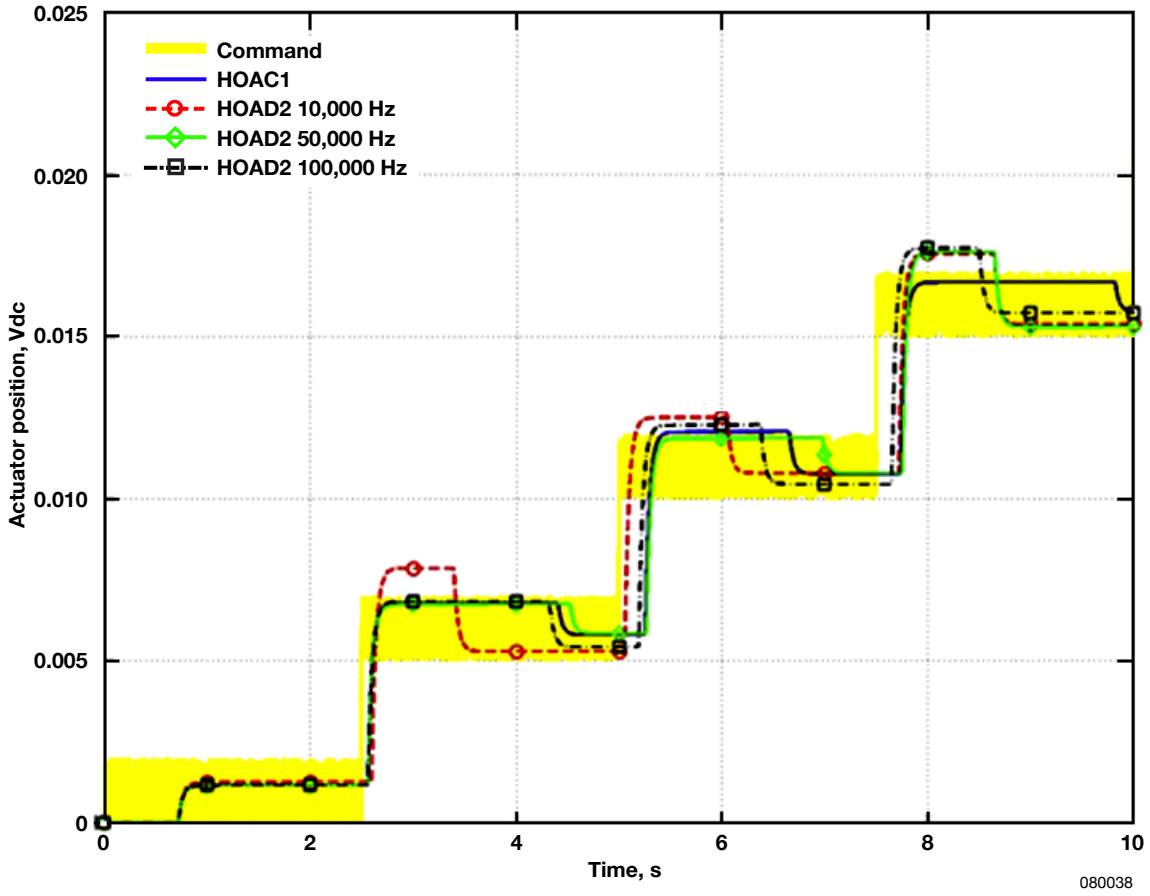

Figure 40. High-order actuator continuous (HOAC1) model response compared with high-order actuator discrete (HOAD2) model response curves at various implementation rates.

Table 7 compares the nominal simulation run time with the LOADF, LOADA, and HOAD2 actuator models. Because the HOAD2 significantly increased the run time for a nominal simulation, the LOADA model was used during the flight 2 and 3 simulation work, when quick results were needed, and during the initial control law update work for the Mach 10 mission. All detailed and final analysis was conducted with the HOAD3 for both flights. The HOAD3 was the refined version that was modified to better match the test results.

4.2.7 Linear Analysis Models

A simplified low-order actuator continuous (SLOAC) model was developed from the LOAC model. The model performance was reduced to a second-order transfer function and incorporated in the linear analysis tool set along with uncertainties. Because of its simplicity, the SLOAC model did not measurably impact the linear analysis run time. The model was used for nominal and Monte Carlo linear analysis for flight 1. After the mishap, the nominal SLOAC frequency response was found to be inaccurate and did not model the nominal actuator response.

A linearized version of the HOAD3 model, called the high-order actuator linear model (HOALM), was also examined for use. When the HOAD3 was linearized, care was taken to ensure the removal of nonlinear elements that could be problematic to the MATLAB® linearizer, such as dead zones, stiction logic, current and voltage limits, and plus-minus switching logic. The frequency response for the linearized model underpredicted the gain of the wing actuators for low load conditions. The comparison improved at higher loads. Nonlinearities likely played a more significant role at low load. In addition, the HOALM for the wing and rudder underpredicted the phase loss. As a result, it was not used for any linear analysis. Instead, a LOES actuator model based on the HOAD3 was developed and used for nominal mission analysis for flights 2 and 3 (see section 3.4).

4.2.8 Linear Model Integration into the Linear Simulation

The LOES model that was constructed was high in fidelity relative to the SLOAC and LOAC models. It was incorporated into the linear analysis tool set and used for linear analysis at specific points along the nominal trajectory of the nonlinear simulation. The LOES actuator model was used for all nominal linear preflight analyses for vehicles 2 and 3. The time-consuming calculations were performed outside of the linear analysis tool, and the LOES transfer function implementation was very simple. As a result, the LOES model did not measurably impact the linear analysis run time.

4.3 Additional Model Elements for Simulation Analysis

One of the major accomplishments of the actuator modeling effort was the ability to model HXRV actuator dither in the nonlinear simulation. As described in section 2.10, dither is a low-amplitude limit cycle oscillation in the control surface position seen only in the AIL test environment. Dither was poorly understood before the first flight, as the low-order actuator models available at the time did not adequately model the nonlinearities in the actuators. After the mishap, an effort was initiated to understand the cause of the actuator dither and evaluate its risk to the HXRV mission. The availability of the HOAC1 model made this task possible.

The nonlinearities in the test environment were believed to be the cause of the actuator dither for the closed-loop AIL tests, based on the absence of dither in the open-loop AIL test environment. Dither was present only when the actuator feedback position was fed into the AIL simulation to drive the vehicle aerodynamics. When the real surfaces were commanded open loop and an actuator model output was fed into the test simulation, the actuators did not dither, as shown in figure 41. In addition, a closed-loop test was conducted in which the wing surfaces were loaded with bungee cords to simulate the aerodynamic loads expected during the engine experiment phase. This AIL bungee test was designed to apply approximately 50 to 100 in-lb of torque to the control surfaces. They still dithered in the test setup with this load applied. The results further proved that the cause was most likely an artifact of the test environment and not the vehicle hardware. It was therefore important that the test elements were identified and modeled in the simulation.

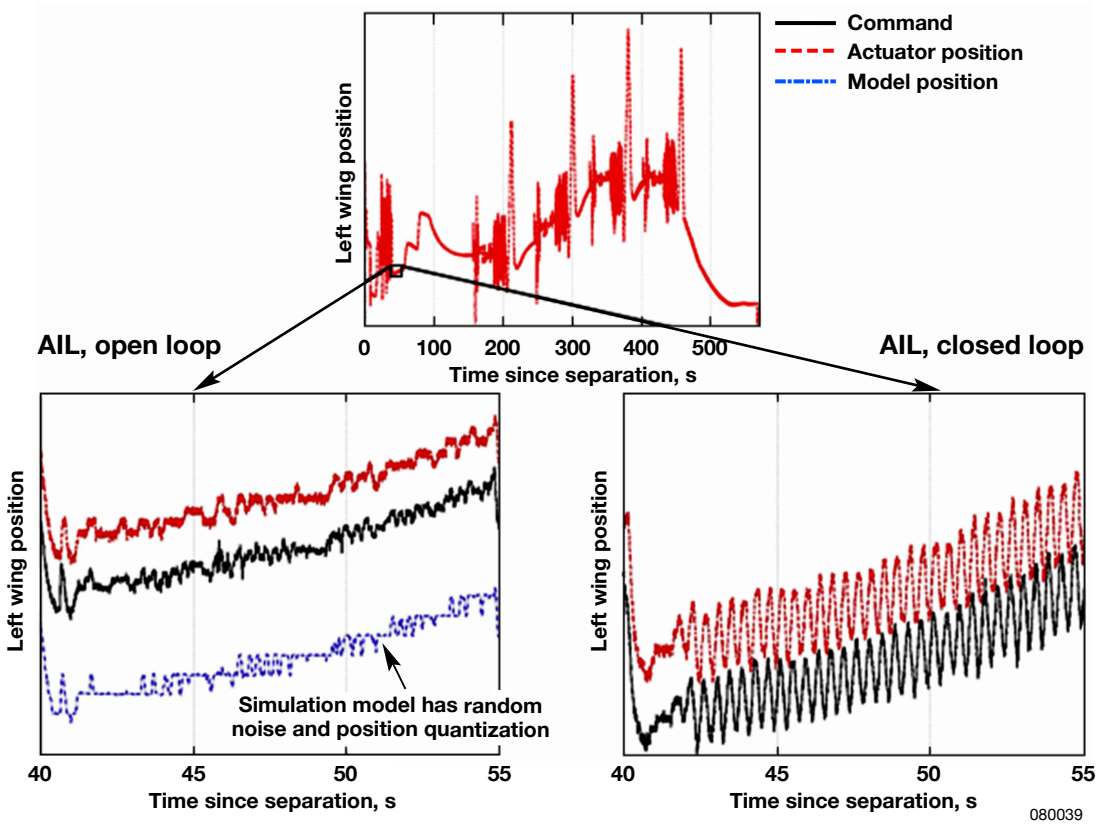

Figure 41. Left wing position during an open-loop aircraft-in-the-loop (AIL) test compared with left wing position during a closed-loop AIL test.

A comprehensive study of the HXRV flight control computer and AIL test setup was initiated to fully characterize the AIL and flight environments. The time delays in the vehicle and test setup were carefully measured. Figure 42 details the timing of the various components in the AIL closed-loop setup. The total loop delays from FMU command input to first motion of the actuators was approximately 11 ms (worst case) for the HXRV in the flight configuration. The test equipment required for the AIL closed-loop tests nearly tripled this delay to 30 ms. Some of these delays were attributed to the transport lag between the simulation computer and the inertial simulator. In addition, the FMU applied a 50-Hz first-order lag filter to the actuator command and position feedback signals, which increased the system lag.

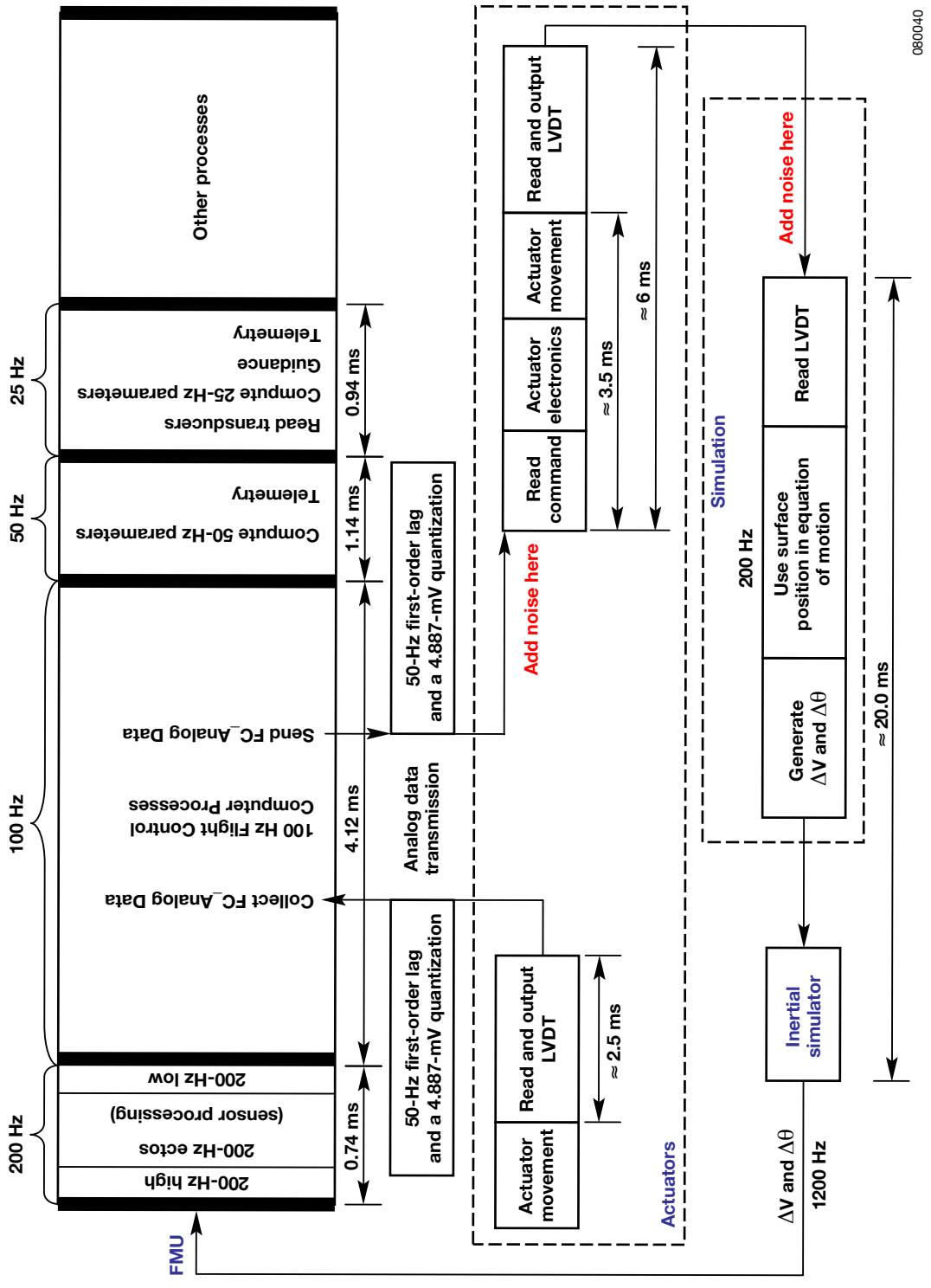

Figure 42. Timing of aircraft-in-the-loop test setup.

The electrical noise in the test setup was caused by the extra length associated with the test wire bundles and the analog and digital input-output electronics of the simulation interface device. The flight computer electronics also applied a 5-mV quantization to the command and position feedback. The actuator command and position feedback noise levels were also measured. The time delays, lag filters, quantization, and noise levels were modeled in the nonlinear simulation to replicate the flight and closed-loop AIL test environments as accurately as possible.

The detailed modeling of the closed-loop AIL test environment and the implementation of the HOAD2 actuator model in the nonlinear simulation provided a better insight into the dither problem. Figure 43 compares the left wing control surface position from a closed-loop AIL test with that of the all-software nonlinear simulation configured to represent the AIL environment. The simulation replicated the control surface dither fairly well. The combination of the nonlinearities in the test environment was found to interact with the dead band in the PWM electronics of the actuator controller. The original high-fidelity model provided by the manufacturer included the PWM dead band element, which helped identify one of the underlying causes of dither.

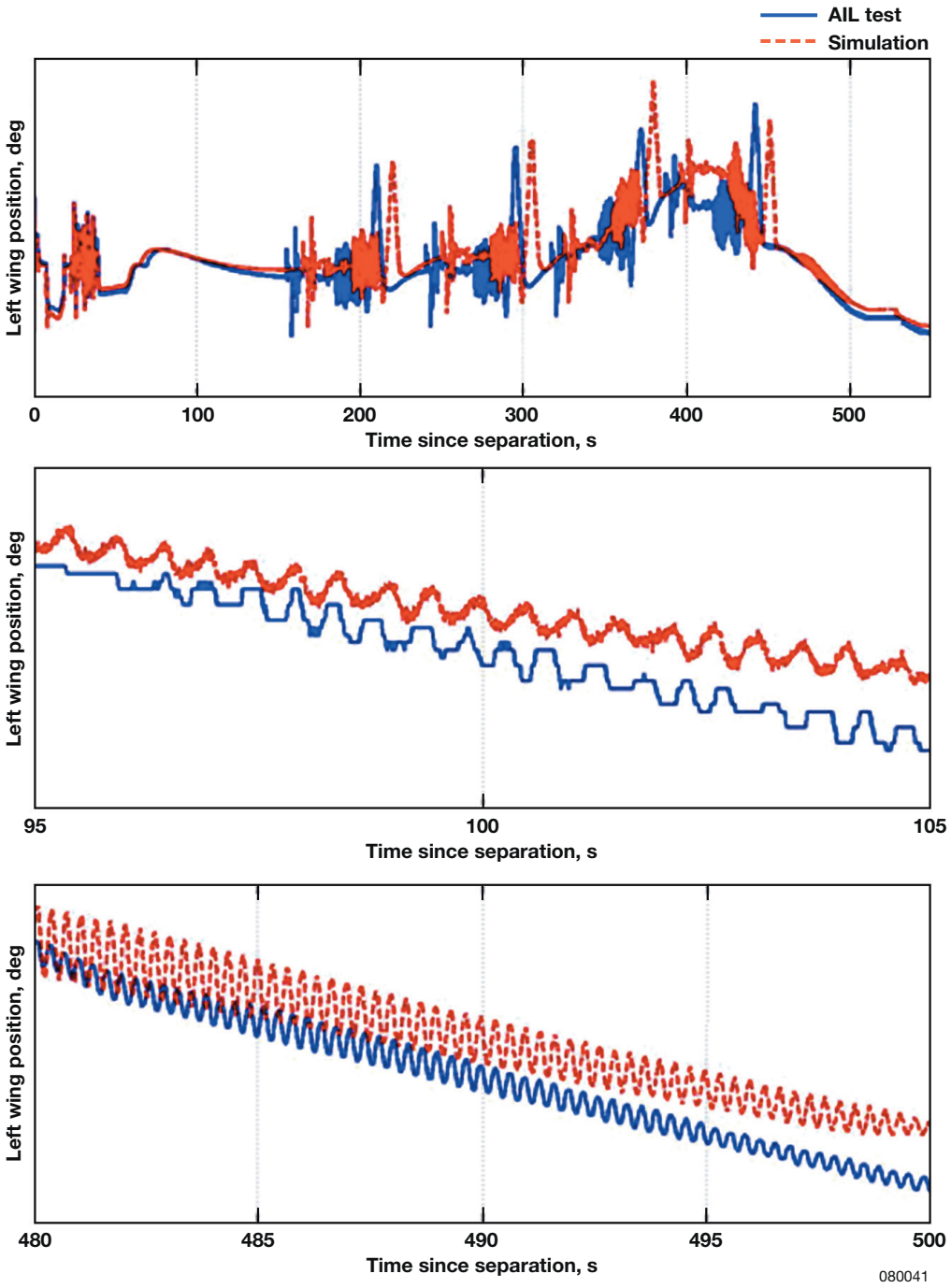

Figure 43. Left wing position from closed-loop aircraft-in-the-loop test compared with simulation prediction.

During the closed-loop AIL test, the control surface was unloaded, so the actuator did not draw enough current to move outside of the dead band. The nonlinearities in the test environment caused the actuator position to fluctuate between the upper and lower current draw limits of the dead band. It is believed that the AIL bungee test, performed before these in-depth analyses, did not provide enough load to make the actuator move outside the dead band. Detailed calculations

indicated that the required loading was significantly more because of the nonlinear effects of the test environment.

A study was conducted to explore whether dither would occur during the HXRV free flight. The delays and nonlinearities unique to the test environment were turned off in the all-software simulation, leaving it in a mode to replicate the flight system performance. The aerodynamic hinge moment model in the simulation was used to calculate the surface loading throughout the nominal mission. No actuator dither was observed in the nominal simulation set to replicate the expected flight system performance. The results indicated that the primary cause of actuator dither was a combination of extra time delay, lag filter, quantization, and noise levels in the closed-loop AIL test setup.

4.4 Comparisons With Flight Data

The in-flight performance of each control surface actuator was examined and compared with the HOAD3 model. All actuator position feedback data came from the actuator LVDTs. The comparisons were made using the model outputs with preflight hinge moment models. The in-flight control surface frequency responses were determined by separately examining the frequency sweeps included in the PID maneuvers.

4.4.1 Flight 2 Comparison

Figure 44 shows the performance of the left wing during the Mach 7 PID maneuver for flight 2 and the HOAD3 model. The model matches the flight performance very well. Figure 45 compares the left wing frequency response during the Mach 5 PID maneuver with the model. The data sets match fairly well.

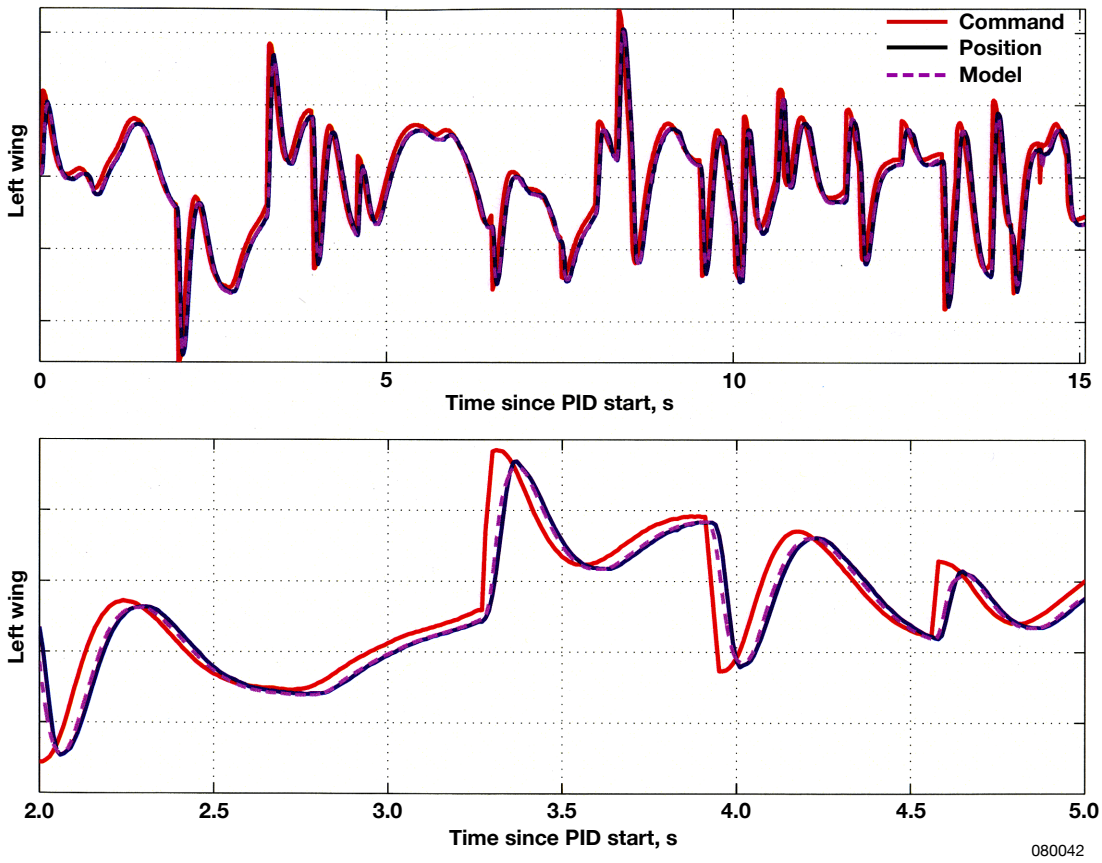

Figure 44. Left wing performance for the flight 2, Mach 7 parameter identification maneuver compared with model.

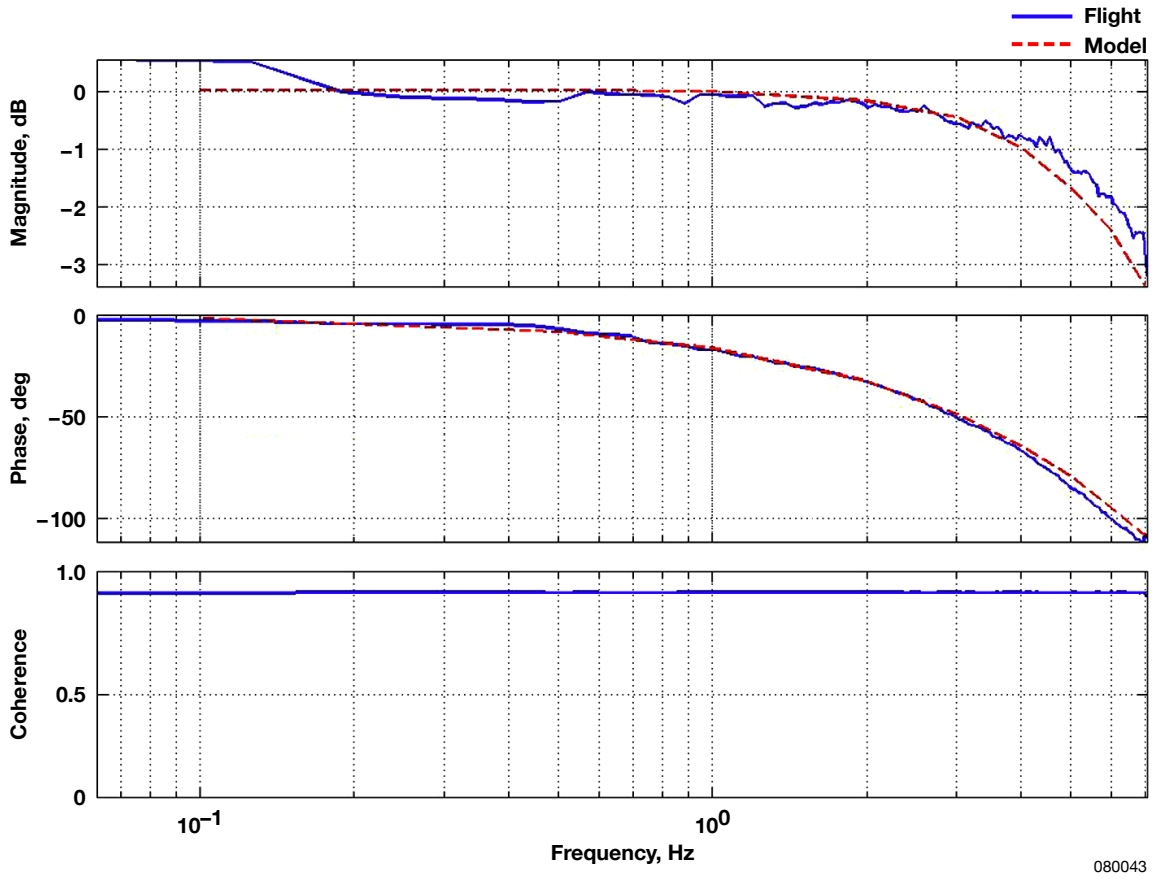

Figure 45. Left wing in-flight frequency response compared with high-order actuator discrete (HOAD3) model predictions; flight 2, Mach 5 parameter identification maneuver.

A detailed examination of the flight 2 data showed a discrepancy between the high-fidelity model and the in-flight time history response. The discrepancy was traced to an incorrect application of the aerodynamic hinge moment sign to three of the four control surface actuator models in the nonlinear simulation. The hinge moment model sign convention had been verified with a stand-alone version of the HOAC1 model, which used the test command inputs in volts. Positive command voltages were assumed to produce deflection angles that resulted in positive hinge moments for all surfaces. In the simulation, however, inputs were passed to the actuator models in units of degrees. For three out of four surfaces, there was an inverse relationship in the conversion from degrees to volts. As a result, the aerodynamic loading was incorrectly applied to both the left and right wings, and to the left rudder actuator models. This error had no impact on the actuator model frequency response, but it did impact the time history response by changing the direction of the control surface compliance.

4.4.2 Flight 3 Comparison

Figure 46 shows the left wing time history performance during the Mach 8 PID maneuver for flight 3. The left wing LVDT feedback position is compared with model feedback position using the same EMA command from flight. The system operated as expected.

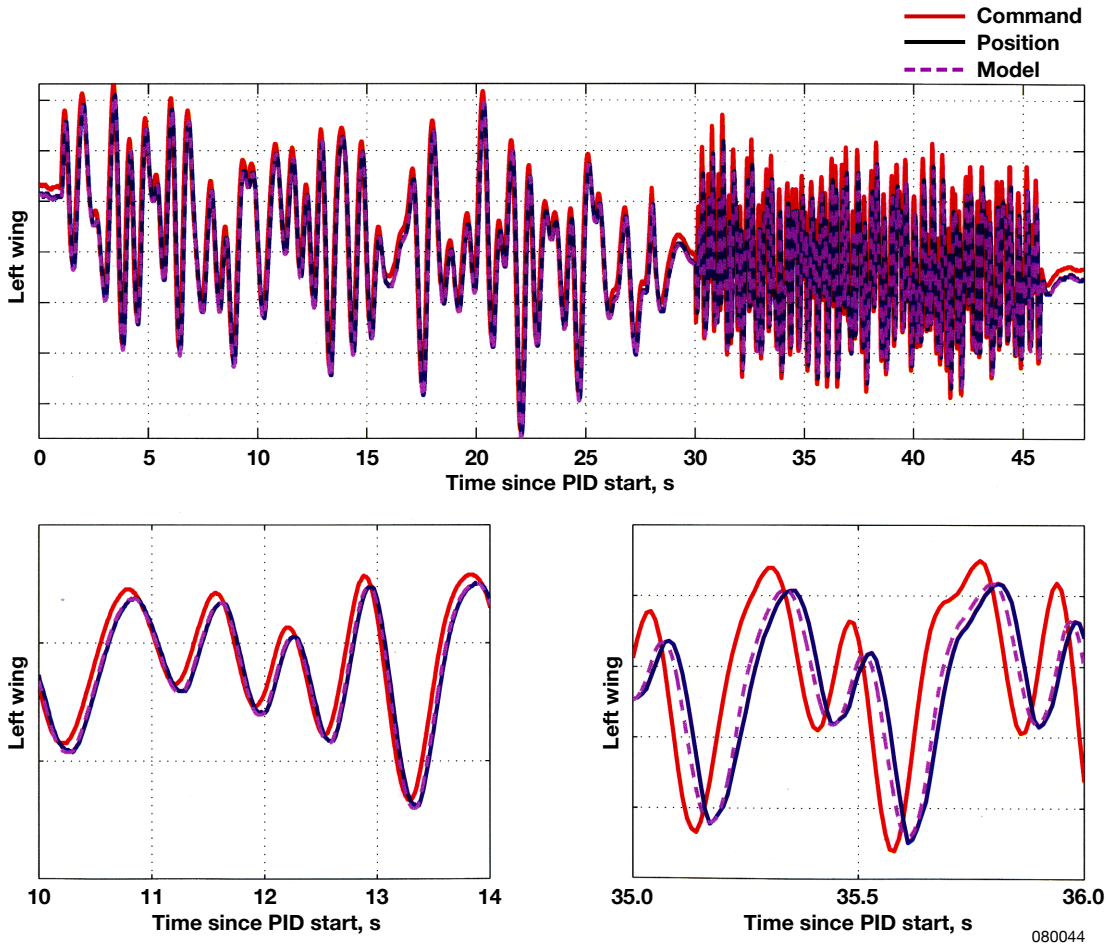

Figure 46. Left wing performance for the flight 3, Mach 8 parameter identification maneuver compared with model.

Figure 47, which also shows the left wing performance during the Mach 8 PID maneuver for flight 3, provides a comparison of the in-flight frequency response with model predictions. A slight downward bias of the flight data can be seen when compared with the model response. The actuator performance was influenced by aerodynamic loads on the surface, and this bias was likely caused by differences in the true aerodynamic loading and the preflight predictions that were fed into the actuator model.

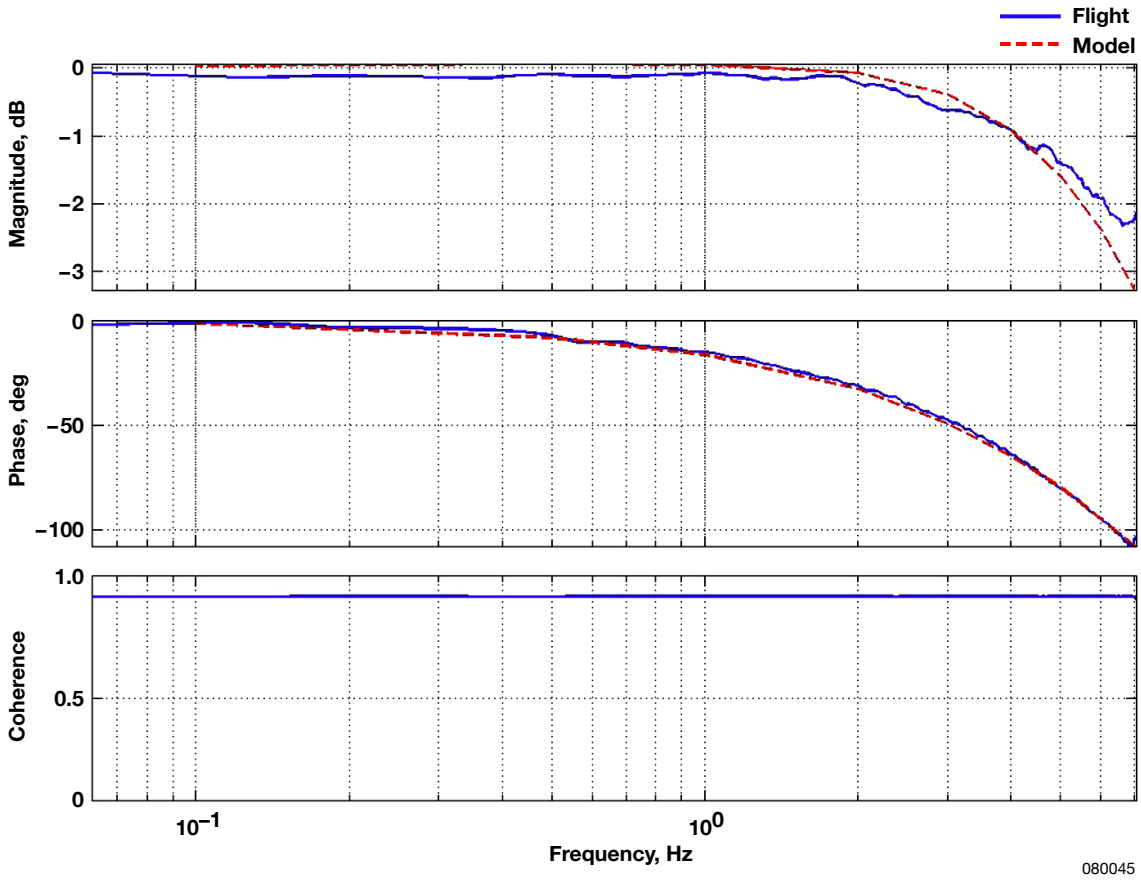

Figure 47. Left wing in-flight frequency response compared with high-order actuator discrete (HOAD3) model predictions; flight 3, Mach 8 parameter identification manuever.

Figure 48 shows the left wing responses as determined from each of the flight 3 PID maneuver sets during the descent. The frequency responses are very similar for each Mach number, and some of the differences might be explained by the different aerodynamic loading of the surface at each flight condition.

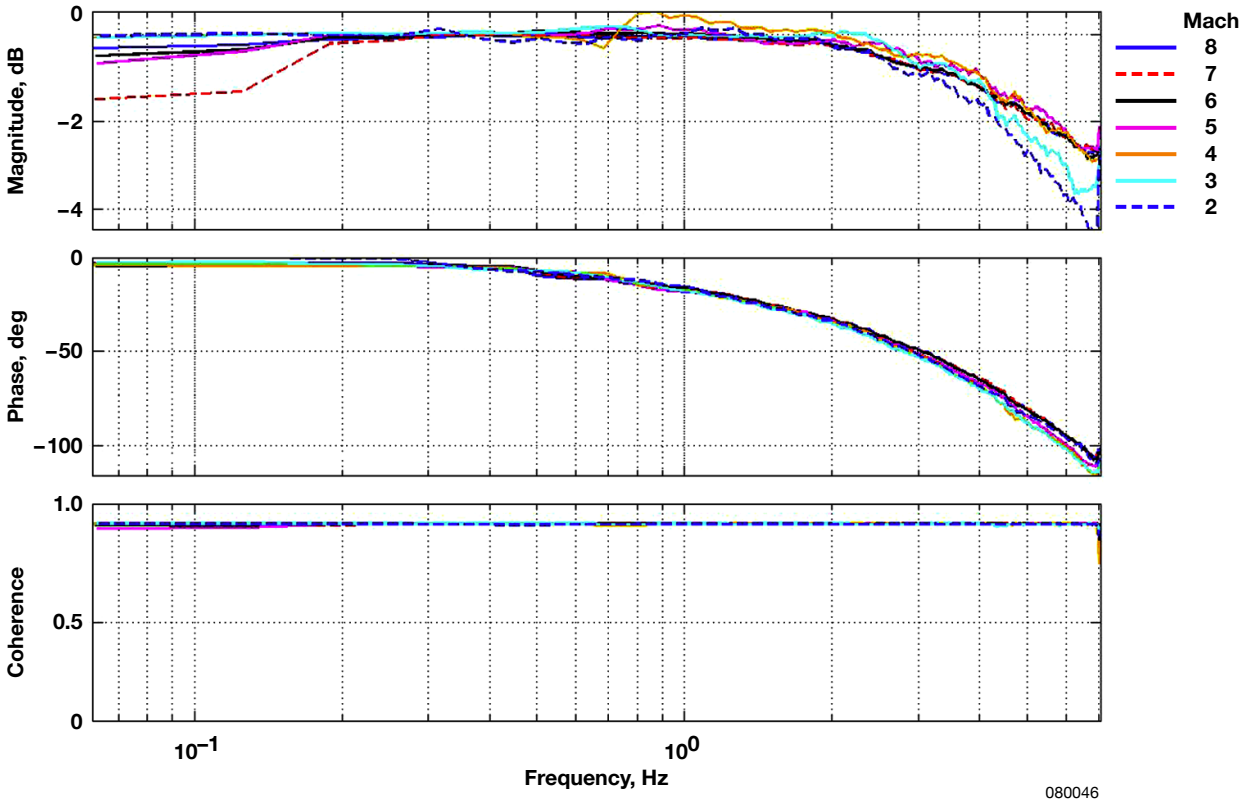

Figure 48. Flight 3 left wing frequency response curves for all parameter identification maneuvers.

Figure 49 shows the left rudder frequency responses at Mach 7, 5, and 3 flight conditions. The responses are lower in quality than those of the all-moving wings. The reason for the poor rudder response is not understood. A possible explanation is that the amplitude of the excitation commands was inadequate to achieve the desired response. Another possibility is that the aerodynamic loading on the rudders was insufficient to move the actuator outside a nonlinear region such as a free play–dead zone.

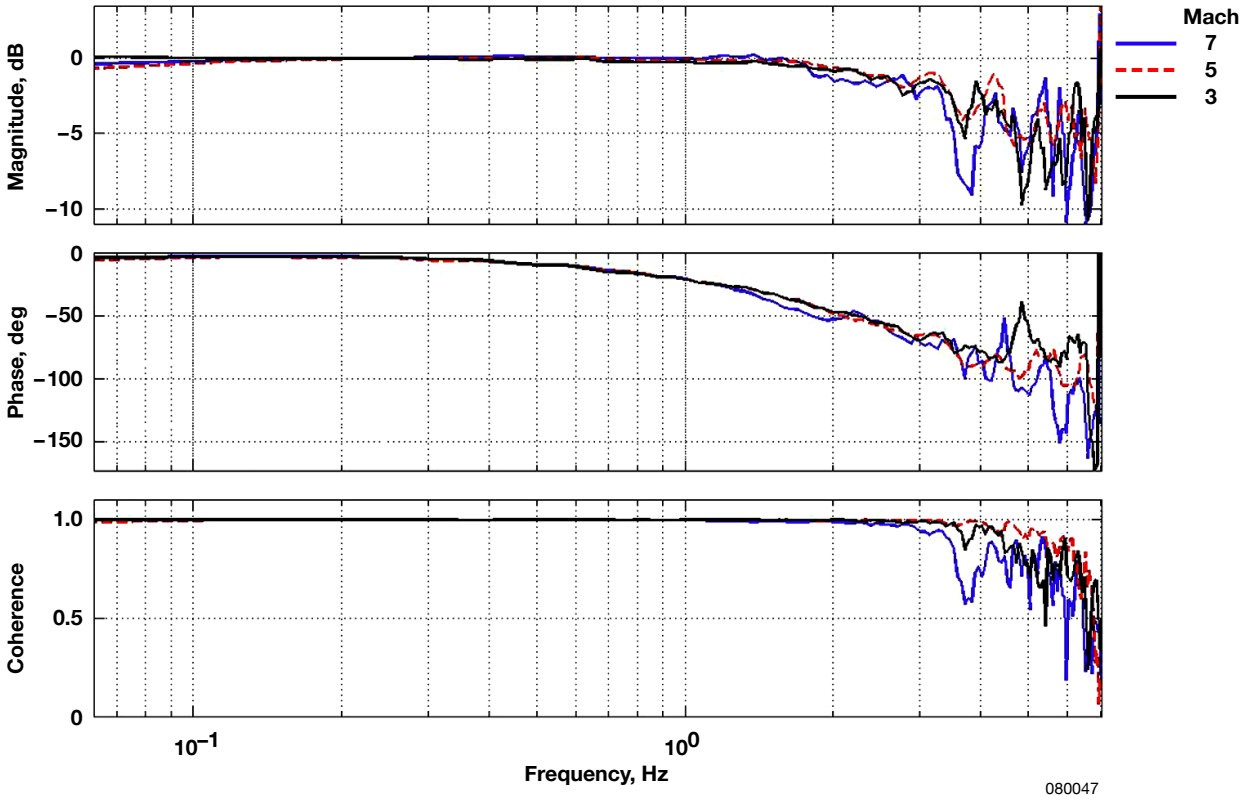

Figure 49. Flight 3 left rudder frequency response curves for Mach 7, 5, and 3.

In terms of actuator dither, figure 50 compares the left wing position from a nominal AIL simulation run with the left wing position from flight 2. The two wing positions differed in magnitude, because the in-flight vehicle elevator trim was different from simulation predictions. The flight 2 data did not show any signs of dither for all control surfaces. The data from flight 3 (fig. 51) also did not show actuator dither.

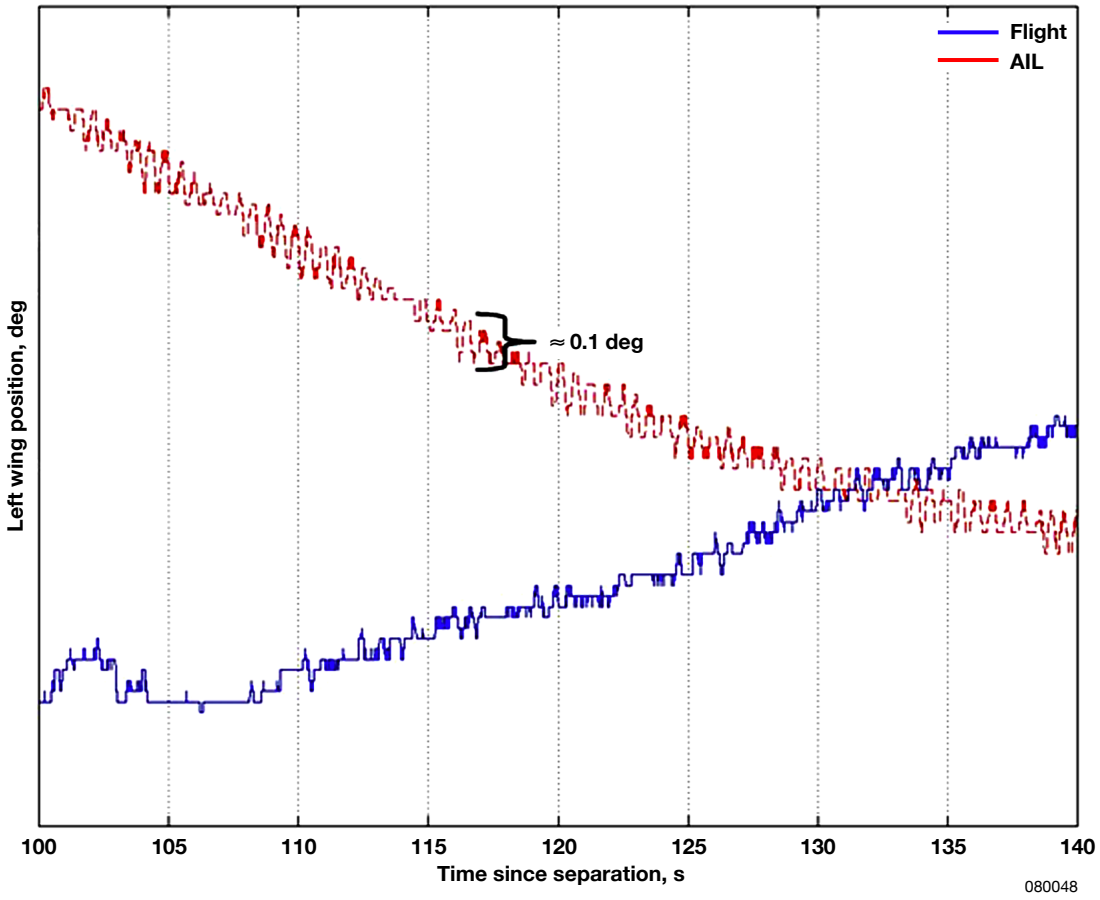

Figure 50. Left wing position (from flight 2) showing no dither compared with left wing position (from aircraft-in-the-loop test) showing dither.

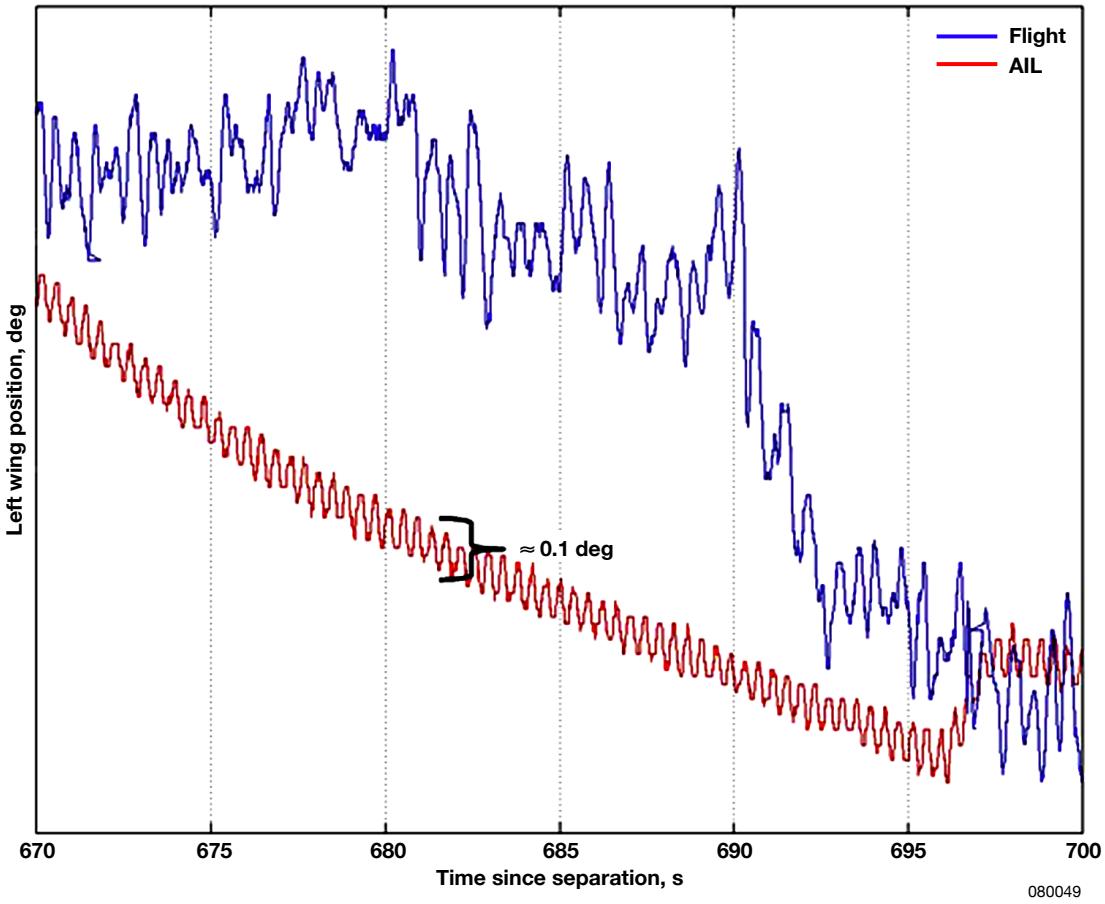

Figure 51. Left wing position (from flight 3) showing no dither compared with left wing position (from aircraft-in-the-loop test) showing dither.

4.5 Lessons Learned From Actuator Modeling and Simulation Integration

As explained in sections 3 and 4, second-order, high-fidelity, and linear models were constructed for various types of mission analyses. The use of different models is crucial to achieving accurate simulation results. An oversimplified model that is applied to all types of analyses may be adequate for one application but deficient for others. Taking this approach could produce erroneous analyses or conclusions. For example, the use of the LOADF model overpredicted the HXRV performance (7 dB and 20° of phase).

The integration of an actuator model in the simulation environment must be verified against the "truth" model. The hinge moment sign error was not detected when the high-fidelity models were incorporated into the simulation. Although the error did not affect flight 2, and the actuators appeared to perform as expected, this case is an excellent example of a model performing well in verification but lacking sufficient validation to ensure the accuracy of the overall implementation. This case is also a good example of assuming that a model is perfect or final, when it is really not. It is recommended that model performance, input, and output parameters are thoroughly evaluated and updated frequently throughout the duration of the project.

The HXRV actuator dither was a problem that was extensively studied before the first flight. The low-order actuator model available at the time was incapable of modeling the actuation system nonlinearities, which contributed to the dither within the AIL environment. After the first flight, an updated high-fidelity model, which better approximated the test data, was acquired from the manufacturer. The model was then further adjusted to match the installed actuator characteristics. The availability of a high-fidelity actuator model in the nonlinear simulation made it possible to more accurately model the control surface response and understand the causes of dither. In addition, the importance of modeling all nonlinearities present in the AIL test setup became evident, because dither was identified as the interaction between nonlinearities of the test setup and the actuation system. None of this research could have been possible without a high-fidelity actuator model.

5.0 CONCLUSION

The performance of uninstalled actuators can differ significantly from the performance of actuators installed in the vehicle configuration. Implementing a thorough actuator testing program and modeling effort for a project is invaluable for a number of reasons. The second-order, high-fidelity, and linear models can serve as useful tools for numerous types of analyses. For example, the second-order models can be used for preflight and batch mission simulation studies. The high-fidelity models can be used for final nominal and off-nominal preflight analyses, as well as for troubleshooting hardware and test configuration problems. In addition to their use in conventional control system stability studies, linear models can be used to determine the bounds of nonlinear effects such as compliance. Clearly, the advantages of using more accurate actuator models include better mission simulations and trade studies, more robust control system designs, and possible identification of subtle failure modes.

To obtain a robust set of data to use for constructing actuator models, careful test planning and access to representative flight hardware is essential. For the X-43A project, the tests that have been discussed were necessary to adequately characterize the behavior of the installed actuation system. In addition, understanding the test environment is essential. Noise caused by input-output electronics and test cable wiring, along with time delays between the inertial and simulation computers, can affect closed-loop tests. These test problems can be resolved by analyzing or measuring the nominal delays of the system, through the use of timing tests, and then comparing them with the closed-loop test delays. These nonlinearities in the test environment can also be added into the simulation for further investigation.

After the models have been constructed from the data and added into the linear or nonlinear simulation, a thorough verification and validation effort must be initiated to ensure that the models have been implemented properly. Integration problems with the nonlinear simulation such as FORTRAN model errors, hinge moment sign errors, and unmodeled aircraft-in-the-loop time delays caused problems throughout the X-43A project. The reason for these problems is that actuator model integration and checkout is not a straightforward process and requires numerous cross-checks that may initially appear to be redundant. Great care must be taken when examining the input and output signals of the models, especially when searching for sign and conversion errors.

The Hyper-X Research Vehicle flew two very successful missions and met the primary and secondary objectives. The in-flight actuator performance validated the high-fidelity models used for the preflight analysis. The test methods and modeling techniques described may appear as a large effort, but given the analysis and simulation enhancements that they provided, the project team felt that the advantages and benefits outweighed the required investment. When planned early into a project, the testing and modeling work could be performed with minimal impact to the schedule. The various types of analyses derived from these tools could provide confidence that adequate groundwork has been performed to address flight safety issues, resulting in significant increases to the overall mission success.

APPENDIX A

X-43A ELECTROMECHANICAL ACTUATOR TEST REQUIREMENTS AND MEASUREMENT ACCURACY

Table A1 of this appendix lists the test requirements for qualifying the electromechanical actuator (EMA) for use on the Hyper-X Research Vehicle. This test was performed on only one actuator. Table A2 presents the requirements for the acceptance test, which was conducted on all electromechanical actuators delivered by the manufacturer. Table A3 lists the test sensor measurement accuracy for the installed actuator tests described in the report. Figure A1 shows the dimensions of the Hyper-X Research Vehicle.

Table A1. Hyper-X Research Vehicle environmental qualification requirements for electromechanical actuators and controller.

Specification	Measurement
Altitude	120,000 ft
Thermal	–40 to +160 °F
Random vibration	12.2 *g* rms maximum, 6.5 min for vertical and lateral axes
Shock	40 *g* srs at 100 Hz to 575 *g* srs at 1,100 to 10,000 Hz (srs=shock response spectrum)
Steady state acceleration	Axial: –4.2 to +12.5 *g* for 3 min Lateral: –1.5 to +1.5 *g* for 3 min Normal: –4.0 to +4.0 *g* for 3 min
Electromagnetic compatibility	MIL-STD-461D, paragraphs 4.7.1 to 4.7.6

Table A2. Hyper-X Research Vehicle acceptance test requirements for electromechanical actuators.

Specification	Measurement
Motor dielectric strength	≤ 1 mA
Motor stator resistance	0.88 ±0.10 Ω
EMA high voltage potential-dielectric	500 Vdc 50 Vdc high energy density electronics–tachometer
EMA linearity, unloaded	≤ 0.01 in.
EMA linearity with opposing loads 500 lbf (wings), 526 lbf (rudders), 2000 lbf (cowl)	≤ 0.01 in.
Threshold, with inertial load	0.0075 in.
EMA mechanical stroke travel (wings, rudders, cowl)	2.60 in. minimum
EMA force versus rate at 125 Vdc	3.5 in/s at 500 lbf (wings), 3.3 in/s at 526 lbf (rudders), 3.1 in/s at 2000 lbf (cowl)
EMA step response at 125 Vdc inertial loads 3.896 lb•in•s^2 (wings) 0.3261 lb•in•s^2 (rudders) 3.006 lb•in•s^2 (cowl)	at 0.5° and 1.0° (wings and rudders), full stroke (cowl)
EMA frequency response with inertial loads as stated previously	≥ 7.5 Hz at –3 dB (wings and rudders only)
EMA stall force	2500 lb minimum at 125 Vdc
Static stiffness	≥ 400,000 lbf/in.
EMA brake holding force	> 4000 lbf
EMA backlash	≤ 0.005 in.

Table A3. Accuracy of sensors used for the electromechanical actuator tests.

Sensor	Accuracy
SMX 4500 laser tracker	± 0.001388°
TS-90 servo inclinometer	± 0.0033°
Digital dial indicator	± 0.012°
Load cells for hydraulic jacks	± 0.1 in-lb
External linear variable differential transformer (LVDT)	± 0.0195°

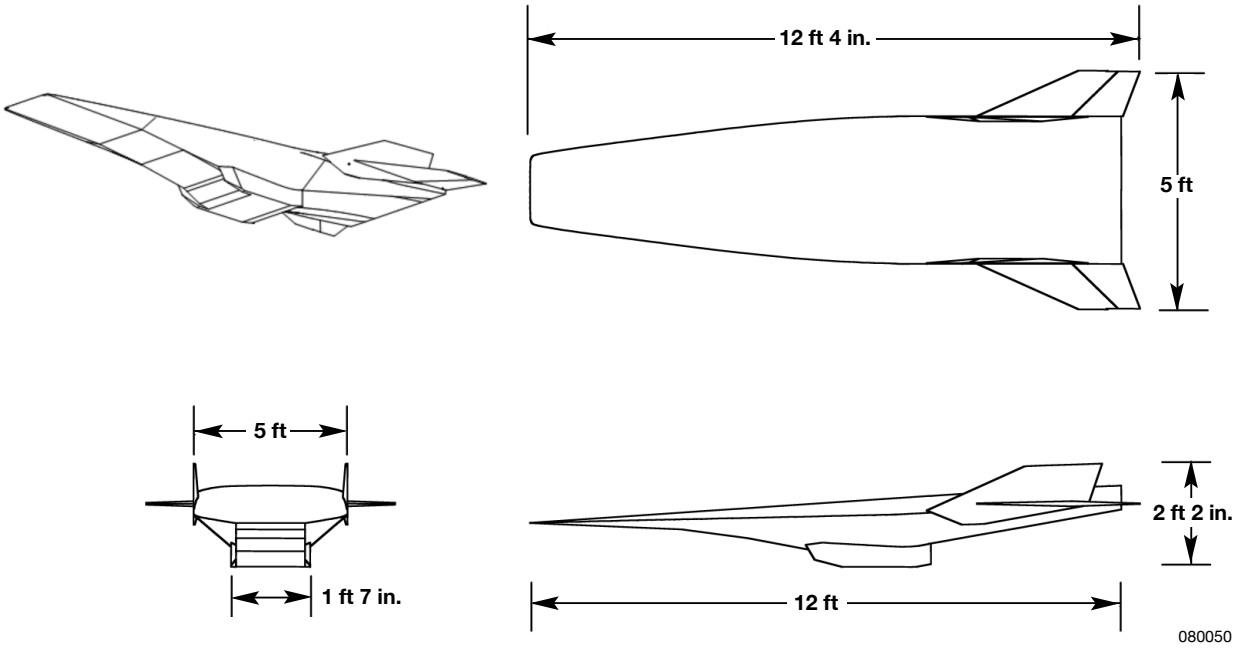

Figure A1. Hyper-X Research Vehicle dimensions (ft, in.).

REFERENCES

1. McClinton, Charles R., and Randall T. Voland, "NASA Hyper-X Overview," 2005-0101DH. Presented at the *28th Airbreathing Propulsion Subcommittee JANNAF Conference*, Charleston, South Carolina, June 12–17, 2005. (Available from the Joint Army, Navy, NASA, Air Force Interagency Propulsion Committee)

2. X-43A Mishap Investigation Board, *Report of Findings: X-43A Mishap*, Vol. 1, 2003.

3. Baumann, Ethan, "Tailored Excitation for Frequency Response Measurement Applied to the X-43A Flight Vehicle," AIAA 2006-638, Jan. 2006.

4. Cotting, Chris, Dave Bose, Stan Douglas, Mike Hannan, Chris Karlgaard, John Pomroy, Joey Powers, and Mike Pudoka, "Fault Tree Close-Out 4.1.3.7.4 FAS – Modeling and Simulation," Presented to the X-43A Mishap Investigation Board, December 6, 2001. (Unpublished; contact the NASA Dryden Flight Research Center)

5. Silvent, Edward, *Fin/FAS Compliance Test – Data Reduction*, Orbital Sciences Corporation/ T034-016, November 2001. (Unpublished; contact the NASA Dryden Flight Research Center)

6. Redifer, Matthew, Yohan Lin, and Courtney Amos Bessent, *The Hyper-X Flight Systems Validation Program*, NASA/TM-2007-214620, 2007.

7. Morelli, Eugene A., Stephen D. Derry, and Mark S. Smith, "Aerodynamic Parameter Estimation for the X-43A (Hyper-X) from Flight Data," AIAA 2005-5921, Aug. 2005.

8. Baumann, Ethan, *Research Vehicle Dither Analysis Report*, NASA X-43A Project/HX-DFRC-0325, 2003. (Internal report; contact the NASA Dryden Flight Research Center)

9. Rao, Singiresu S., *Mechanical Vibrations*, 3rd ed., Addison-Wesley Publishing Company, Reading, Massachusetts, 1995, pp. 152–157.

10. Norlin, Ken A., *Flight Simulation Software at NASA Dryden Flight Research Center*, NASA/ TM-104315, 1995.

REPORT DOCUMENTATION PAGE

Form Approved
OMB No. 0704-0188

The public reporting burden for this collection of information is estimated to average 1 hour per response, including the time for reviewing instructions, searching existing data sources, gathering and maintaining the data needed, and completing and reviewing the collection of information. Send comments regarding this burden estimate or any other aspect of this collection of information, including suggestions for reducing this burden, to Department of Defense, Washington Headquarters Services, Directorate for Information Operations and Reports (0704-0188), 1215 Jefferson Davis Highway, Suite 1204, Arlington, VA 22202-4302. Respondents should be aware that notwithstanding any other provision of law, no person shall be subject to any penalty for failing to comply with a collection of information if it does not display a currently valid OMB control number.
PLEASE DO NOT RETURN YOUR FORM TO THE ABOVE ADDRESS.

1. REPORT DATE *(DD-MM-YYYY)*	2. REPORT TYPE	3. DATES COVERED *(From - To)*
01-12-2008	Technical Memorandum	

4. TITLE AND SUBTITLE
Tests and Techniques for Characterizing and Modeling X-43A Electromechanical Actuators

5a. CONTRACT NUMBER

5b. GRANT NUMBER

5c. PROGRAM ELEMENT NUMBER

6. AUTHOR(S)
Lin, Yohan; Baumann, Ethan A.; Bose, David M.; Beck, Roger; Jenney, Gavin

5d. PROJECT NUMBER

5e. TASK NUMBER

5f. WORK UNIT NUMBER

7. PERFORMING ORGANIZATION NAME(S) AND ADDRESS(ES)
NASA Dryden Flight Research Center
P.O. Box 273
Edwards, California 93523-0273

8. PERFORMING ORGANIZATION REPORT NUMBER
H-2819

9. SPONSORING/MONITORING AGENCY NAME(S) AND ADDRESS(ES)
National Aeronautics and Space Administration
Washington, DC 20546-001

10. SPONSORING/MONITOR'S ACRONYM(S)
NASA

11. SPONSORING/MONITORING REPORT NUMBER
NASA/TM-2008-214637

12. DISTRIBUTION/AVAILABILITY STATEMENT
Unclassified -- Unlimited
Subject Category 05 Availability: NASA CASI (301) 621-0390 Distribution: Standard

13. SUPPLEMENTARY NOTES
Lin, Baumann, NASA Dryden Flight Research Center; Bose, Beck, Analytical Mechanics Associates; Jenney, Dynamic Controls. An electronic version can be found at http://dtrs.dfrc.nasa.gov or http://ntrs.nasa.gov/search.jsp

14. ABSTRACT

A series of tests were conducted on the electromechanical actuators of the X-43A research vehicle in preparation for the Mach 7 and 10 hypersonic flights. The tests were required to help validate the actuator models in the simulation and acquire a better understanding of the installed system characteristics. Static and dynamic threshold, multichannel crosstalk, command-to-surface timing, free play, voltage regeneration, calibration, frequency response, compliance, hysteretic damping, and aircraft-in-the-loop tests were performed as part of this effort. This report describes the objectives, configurations, and methods for those tests, as well as the techniques used for developing second-order actuator models from the test results. When the first flight attempt failed because of actuator problems with the launch vehicle, further analysis and model enhancements were performed as part of the return-to-flight activities. High-fidelity models are described, along with the modifications that were required to match measurements taken from the research vehicle. Problems involving the implementation of these models into the X-43A simulation are also discussed. This report emphasizes lessons learned from the actuator testing, simulation modeling, and integration efforts for the X-43A hypersonic research vehicle.

15. SUBJECT TERMS
Actuator, Characterization testing, Frequency response, Validation, Verification

16. SECURITY CLASSIFICATION OF:			17. LIMITATION OF ABSTRACT	18. NUMBER OF PAGES	19b. NAME OF RESPONSIBLE PERSON
a. REPORT	b. ABSTRACT	c. THIS PAGE			STI Help Desk (email: help@sti.nasa.gov)
					19b. TELEPHONE NUMBER *(Include area code)*
U	U	U	UU	89	(301) 621-0390